

---

Developing of a device for measuring the areal distribution  
of the forces in the contact zone of foot and underground for  
the use in leg prostheses

---

Thesis submitted by:

B.Sc. Jörg Kubisch

for the degree of

Master of Science in Mechanical Engineering

Supervising professors:

Technische Universität Ilmenau  
Dr.-Ing. habil. Thomas Fröhlich

Pontificia Universidad Católica del Perú  
Dr.-Ing. Dante Ángel Elías Giordano

Ilmenau, Germany / Lima, Perú

2020

## Aufgabenstellung für die Master-Arbeit

von Herrn Jörg Kubisch

**Thema:** Developing of a device for measuring the areal distribution of the forces in the contact zone of foot and underground for the use in leg prostheses

To control robotic prosthesis efficiently it is important to know the distributed forces acting on the foot palm. There are a lot of sensors mapping the distribution of forces acting but most of them are just sensing in one axis. When walking on instable, lose ground information about the acting transversal forces would help improve the abilities of the control. Therefore, this work is going to develop and to build a sensor network placed on the palm of a prostheses which is able to measure forces in all three room axis.

In detail, the following subtasks are to be processed:

- choosing a suitable concept
- constructing the sensor
- designing the corresponding electronic circuit
- programming the data acquisition
- building a prototype
- testing and evaluating of the built up sensor
- designing the distribution of the sensors on the foot palm
- simulation of the foot palm with the sensors

**Ausgabedatum:**

01.05.2019 – 30.09.2019

**Verantwortlicher Hochschullehrer:**

Prof. Dr.-Ing. habil. Thomas Fröhlich

**Betreuer PUCP Lima:**

Prof. Dr.-Ing. Dante Elias

**Betreuerin TU Ilmenau:**

Dipl.-Ing. Silke Augustin

Ilmenau, 29.04.19

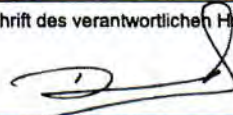
Ort, Datum



Unterschrift des verantwortlichen Hochschullehrers

Lima, 05.04.19

Ort, Datum



Unterschrift des verantwortlichen Hochschullehrers

Ort, Datum

Unterschrift des betrieblichen Betreuers

Lima, 06.04.19.

Ort, Datum



Unterschrift des Studierenden

## **Declaration**

I confirm, that the work for the following thesis was solely undertaken by myself and that no help was provided from other sources as those allowed. All sections of the paper that use quotes or describe an argument or concept developed by another author have been referenced, including all secondary literature used, to show that this material has been adopted to support my thesis.

Ilmenau, the 28.11.2019

Jörg Kubisch



## **Abstract**

The presented work demonstrates the process of designing a cheap, low cost three axis force sensor. Further it describes its integration in an array of multiple sensors to measure the distribution of forces acting on the sole of a prosthetic foot. The focus will be on easy manufacturing and common materials since the sensor will be integrated in a low cost prosthesis for lower limb amputees. Using the knowledge from bio mechanics and some basic assumptions for the later use, requirements for the project are derived. After a presentation of some state of the art sensor principles, suitable concepts are collected. Then, the concepts are compared using a comparison table to find the one that fits the requirements the best. A very compelling concept using barometers casted in silicone rubber is tested using a simple prototype to try out whether it is a good candidate or not. The tests show that the concept is capable of measuring forces but due to its disadvantageous susceptibility for temperature changes it is rejected for the further development process. The concepts are reevaluated and a new concept is chosen. Afterwards the design process is described. Beginning with the mechanical design explaining the working principle. The calculation of the dimensions is presented. After that a circuit to work with a capacitive measurement as well as a version for resistive measurement is developed and a layout for a prototype board using capacitive measurement is proposed. To prove the functionality, the capacitive system is built up as a prototype. To try the measurement behavior and to measure its repeatability a test stand is designed. It uses commercial available load cells to conduct a reference measurement. The output of the sensor is compared to the reference measurement. With various different test procedures the curves mapping the measured values to the force for normal and shear force measurement are determined. During the tests, different aspects of performance like creep behavior or hysteresis are investigated. Also the repeatability is measured various times under different loads to make reliable estimations of the precision of the measurement. Further on, a resistive force sensor which could be used instead of the capacitive sensing elements is tested regarding its curve and performance to have a comparison of the advantages and disadvantages of either designing the future sensor with resistive or capacitive sensing elements. With both concepts a repeatability of a few percent uncertainty can be achieved. Further on ways to improve future versions of the sensor are described based on the experiences made during the work with the prototype. Finally a possible way to integrate multiple sensors into a sensing array is proposed. The design as well as possible electronics to acquire the data are discussed. This way a solid basis for further developments of a sensing array measuring the force distribution is given.

## Kurzfassung

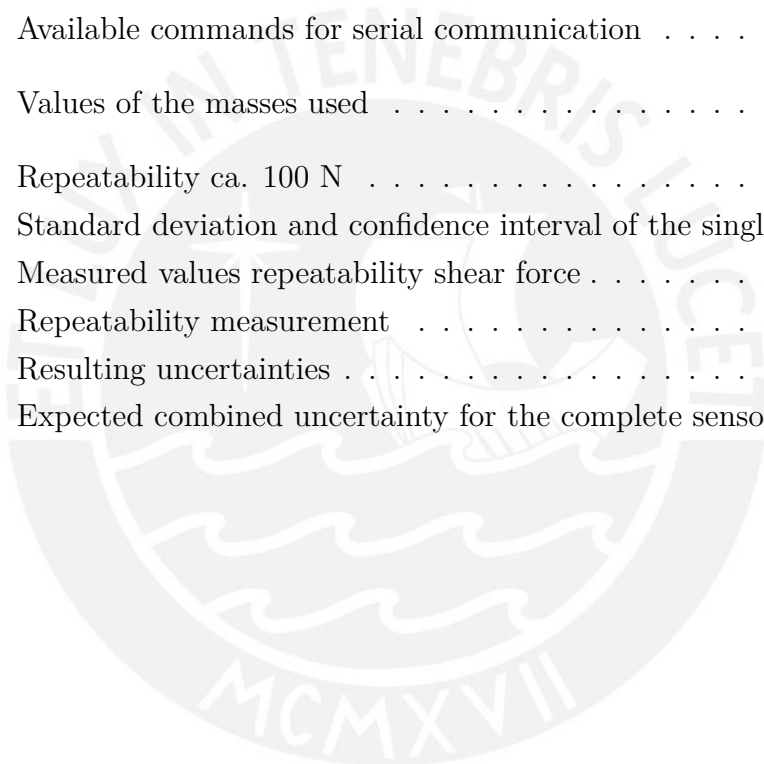
Die vorgestellte Arbeit zeigt den Prozess der Konstruktion eines preiswerten, kostengünstigen Dreiachs-Kraftsensors. Weiterhin wird eine Integration der Sensoren in ein Array, zur Messung der Verteilung von Kräften auf der Fußsohle besprochen. Der Schwerpunkt soll dabei auf einer einfachen und günstigen Herstellung, sowie der Verwendung handelsüblicher Materialien liegen, da der Sensor in ein kostengünstiges Prothesenkonzept integriert werden soll. Ausgehend von den Erkenntnissen der Biomechanik und einigen grundlegenden Annahmen für die Nutzung des Sensors, werden verschiedene Anforderungen abgeleitet. Im Folgenden wird der Stand der Technik anhand einiger aktueller Forschungsarbeiten und Sensorprinzipien vorgestellt. Daraufhin werden geeignete Konzepte gesammelt, die zur Entwicklung des Sensors eingesetzt werden können. Anschließend werden die Konzepte anhand einer Vergleichstabelle verglichen, um das bestgeeignetste Konzept zu finden. Eine sehr überzeugende Variante, bei der Barometerchips in Silikon eingegossen werden, wird mit einem einfachen Prototyp getestet, um herauszufinden, ob es sich um einen guten Kandidaten für die weitere Entwicklung handelt, oder nicht. Die Versuche zeigen, dass der Prototyp in der Lage ist, Kräfte zu messen, jedoch zeigt sich eine große Anfälligkeit für Temperaturschwankungen. Das Konzept wird deshalb nicht weiter verfolgt. Die Konzepte werden neu bewertet und anschließend ein Neues ausgewählt. Daraufhin wird der Entwurfsprozess beschrieben. Das Funktionsprinzip und die Auslegung der Abmessungen werden erläutert. Anschließend wird eine Schaltung zum Arbeiten mit einer kapazitiven Messung, sowie eine Schaltung für eine resistive Messung entwickelt und ein Layout für eine Platine zur kapazitiven Kraftmessung vorgeschlagen. Zum Nachweis der Funktionalität wird das kapazitive System als Prototyp aufgebaut. Um das Messverhalten zu testen und seine Wiederholbarkeit nachzuweisen, wird ein Prüfstand entworfen. Zur Durchführung einer Referenzmessung werden handelsübliche Wägezellen verwendet. Der Ausgang des Sensors wird mit der Referenzmessung verglichen. Mit verschiedenen Prüfverfahren werden die Kurven bestimmt, die die Messwerte der Normal- und Querkraft zuordnen. Während des Tests werden verschiedene Leistungsaspekte wie Kriechverhalten oder Hysterese untersucht. Auch die Wiederholbarkeit wird mehrmals unter verschiedenen Belastungen gemessen, um zuverlässige Schätzungen der Genauigkeit der Messung vorzunehmen. Weiterhin wird ein resistiver Kraftsensor, der anstelle der kapazitiven Sensorelemente verwendet werden könnte, hinsichtlich seiner Kurve und Leistung getestet, um einen Vergleich der Vor- und Nachteile der Konstruktion des zukünftigen Sensors mit resistiven oder kapazitiven Sensorelementen zu erhalten. Mit beiden Konzepten kann eine gute Wiederholgenauigkeit mit nur wenigen Prozent Unsicherheit er-

reicht werden. Weiterhin werden Möglichkeiten zur Verbesserung der zukünftigen Version des Sensors auf Grundlage der gesammelten Erfahrungen beschrieben. Schließlich wird ein möglicher Weg zur Integration mehrerer Sensoren in eine Sensoranordnung vorgeschlagen. Das Design, sowie die mögliche Elektrik zur Erfassung der Daten werden diskutiert. Damit wird eine solide Grundlage für die Weiterentwicklung einer Sensoranordnung zur Messung der Kraftverteilung geschaffen.



# List of Tables

6.1	Cross comparison of the features . . . . .	27
6.2	Comparison table of the concepts . . . . .	28
9.1	Available commands for serial communication . . . . .	48
11.1	Values of the masses used . . . . .	61
12.1	Repeatability ca. 100 N . . . . .	76
12.2	Standard deviation and confidence interval of the single measurement	76
12.3	Measured values repeatability shear force . . . . .	77
12.4	Repeatability measurement . . . . .	83
12.5	Resulting uncertainties . . . . .	84
12.6	Expected combined uncertainty for the complete sensor . . . . .	85



# List of Figures

2.1	The phases of human gait . . . . .	4
3.1	The importance of force feedback . . . . .	6
3.2	The importance of pressure recognition for different activities . . . . .	6
3.3	Normal ground reaction forces . . . . .	7
5.1	Basic principle of the measurement with a flexible lever . . . . .	13
5.2	Simple one axis measuring using barometers in rubber . . . . .	14
5.3	Principle of a six axis measurement . . . . .	15
5.4	Working principle of the soft pad robot foot design . . . . .	16
5.5	Structure of the sensor with doted silicon beams . . . . .	16
5.6	Built up MEMS sensor . . . . .	17
5.7	SEM image of a micro pyramidal design . . . . .	17
5.8	Structure of conductive stripes sewed together . . . . .	18
5.9	Structure of the sensor . . . . .	19
5.10	Commercial strain gauge based three axis force sensor . . . . .	19
5.11	Movement of the electrodes of the sliding electrode sensor . . . . .	20
5.12	Sketch of the electrodes of the 3D capacive sensor . . . . .	21
6.1	Basic principle of the force transducer . . . . .	23
6.2	Basic principle of the force transducer . . . . .	25
6.3	Principle of the supported sensor . . . . .	29
6.4	Principle of support material . . . . .	30
6.5	Barometer placed on the bottom plate . . . . .	31
6.6	Barometer sensor assembly . . . . .	31
6.7	Testing the sensor with different masses . . . . .	32
6.8	Drift of the barometer in silicone sensor . . . . .	32
6.9	Response of the sensor to a temperature step . . . . .	33
7.1	CAD design of the transducer . . . . .	36



8.1	Schematic of the circuit . . . . .	39
8.2	Schematic of the used Schmitt-trigger . . . . .	40
8.3	Variants of connecting the sensing element . . . . .	41
8.4	Dimensions of the sensing areas . . . . .	43
8.5	Relation between resistance and conductance to force . . . . .	44
8.6	The suggested circuit from the data sheet of the sensor . . . . .	45
8.7	The built up circuit with a potentiometer for testing . . . . .	46
9.1	Voltages while charging and discharging . . . . .	49
10.1	The force transducer with copper plate, top and bottom view . . . . .	52
10.2	Symbol for the sensing areas in the schematic. . . . .	53
10.3	The raw board top and bottom view . . . . .	54
10.4	Stocked board with the signals connected to each pin . . . . .	55
10.5	The Arduino together with the breadboard connected to the sensor . . . . .	55
11.1	Design of the test stand . . . . .	59
11.2	The mounted load cells . . . . .	59
11.3	CAD model of the adapter . . . . .	60
11.4	The designed ball bearing to reduce constraint forces . . . . .	61
11.5	The complete test stand setup . . . . .	62
11.6	Output force to voltage relation for the single load cells . . . . .	63
12.1	Construction to test different materials . . . . .	67
12.2	Force on output with 0.2 mm PS foil . . . . .	68
12.3	Force on capacitance with 0.5 mm silicone . . . . .	68
12.4	Output function with 3D-printed 0.2 mm TPU layer . . . . .	69
12.5	Sensor curve using the material 4140CEM . . . . .	70
12.6	Sensor curve using the material 4140C . . . . .	70
12.7	Comparison of the calculated sensitivity for the TPU foils . . . . .	71
12.8	Sensor curve using the material 4140CEM . . . . .	72
12.9	Force over the sum of the capacities . . . . .	73
12.10	The measured capacities for different lateral loads . . . . .	74
12.11	Shear force over the difference of the capacitances . . . . .	75
12.12	Hysteresis of the sensor with rising and falling normal load . . . . .	77
12.13	Creeping of the sensor output . . . . .	78
12.14	Creeping of the calculated force $F_c$ . . . . .	79

*List of Figures*

---

12.15	Sensor with the ball bearing as weight to prevent the transducer from lifting off . . . . .	80
12.16	Drift of the normal force measurement near the zero point . . . . .	81
12.17	Drift of the shear force measurement near the zero point . . . . .	81
12.18	The Flexiforce A101 sensor mounted on the test stand . . . . .	82
12.19	Output force relation of the Flexiforce A101 . . . . .	83
12.20	Hysteresis test of the flexiforce sensor . . . . .	84
12.21	Drift test of the Flexiforce A101 . . . . .	86
13.1	The sensor solution with two boards fixed on a rubber layer . . . . .	88
13.2	Positioning of the sensors on the foot sole . . . . .	88
13.3	Choosing the sensor using multiplexers . . . . .	89



# Contents

## Abbreviations and Symbols

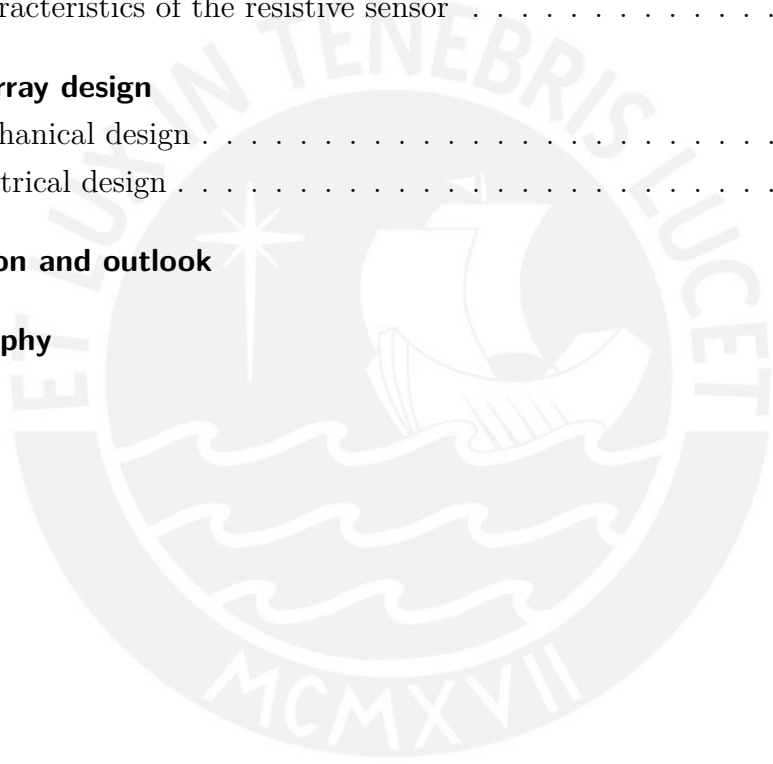
## List of Tables

## List of Figures

<b>1</b>	<b>Introduction</b>	<b>1</b>
<b>2</b>	<b>Human gait</b>	<b>3</b>
<b>3</b>	<b>Requirements</b>	<b>5</b>
3.1	General requirements . . . . .	5
3.2	Mechanical requirements . . . . .	6
3.3	Dimensions . . . . .	8
3.4	Computational Requirements . . . . .	8
<b>4</b>	<b>Basic force sensing principles</b>	<b>10</b>
4.1	Capacitive sensing . . . . .	10
4.2	Inductive sensing . . . . .	11
4.3	Piezo electric sensing . . . . .	11
4.4	Piezo resistive sensing . . . . .	11
<b>5</b>	<b>State of the art</b>	<b>13</b>
5.1	Lever in polymer . . . . .	13
5.2	Barometers in silicone . . . . .	14
5.3	Soft pad robot foot . . . . .	15
5.4	MEMS Sensors . . . . .	15
5.5	Textile based sensors . . . . .	17
5.6	Three axis resistive sensor . . . . .	18
5.7	Load cells . . . . .	19

5.8	Sliding electrode capacitive . . . . .	20
5.9	Sensor mats . . . . .	21
<b>6</b>	<b>Conceptual design</b>	<b>22</b>
6.1	Concepts . . . . .	22
6.1.1	Barometers in silikon rubber . . . . .	22
6.1.2	Transforming shear force into torque . . . . .	23
6.1.3	Flexible structure with strain gauges . . . . .	24
6.1.4	Capacitive sliding electrode . . . . .	24
6.1.5	Metal pin in polymer . . . . .	25
6.1.6	Prism structure . . . . .	25
6.2	Choosing a concept . . . . .	26
6.3	Prototype barometric sensor . . . . .	29
6.3.1	Design and assembly . . . . .	29
6.3.2	Evaluation . . . . .	32
6.3.3	Conclusion . . . . .	33
6.4	Reevaluating the concepts . . . . .	34
<b>7</b>	<b>Mechanical design</b>	<b>35</b>
<b>8</b>	<b>Electrical design</b>	<b>37</b>
8.1	Measuring capacities . . . . .	37
8.1.1	Measuring the time constant . . . . .	37
8.1.2	Measure frequency of oscillating circuit . . . . .	38
8.1.3	Measuring the impedance . . . . .	38
8.1.4	Charge balancing with a known capacity . . . . .	38
8.2	Circuit for capacitive measurement . . . . .	39
8.3	Board design . . . . .	41
8.4	Piezo resistive measurement . . . . .	43
8.5	Circuit for resistive measurement . . . . .	44
<b>9</b>	<b>Data acquisition</b>	<b>47</b>
9.1	Programming the micro-controller . . . . .	47
9.2	Program for capacitive sensing . . . . .	48
9.3	Programm for resistive sensing . . . . .	51
<b>10</b>	<b>Prototypes</b>	<b>52</b>

10.1 Building the prototype . . . . .	52
10.2 Improvement opportunities . . . . .	56
<b>11 Test stand</b>	<b>58</b>
11.1 Construction . . . . .	58
11.2 Evaluation . . . . .	60
<b>12 Conducted tests</b>	<b>66</b>
12.1 Choosing a dielectric material . . . . .	66
12.2 Characteristics of the capacitive sensor . . . . .	73
12.3 Characteristics of the resistive sensor . . . . .	82
<b>13 Sensor array design</b>	<b>87</b>
13.1 Mechanical design . . . . .	87
13.2 Electrical design . . . . .	88
<b>14 Conclusion and outlook</b>	<b>91</b>
<b>15 Bibliography</b>	<b>94</b>
<b>Appendix</b>	<b>97</b>



# 1 Introduction

To control robotic prosthesis efficiently it could be helpful to know the forces acting on the foot palm. There are a lot of sensors mapping the distribution of forces acting, but most of them are just detecting normal loads. When walking on unstable or loose ground, information about the acting traversal forces would help to improve the abilities of the control. Therefore, this work is going to develop a sensor network placed on the palm of a prosthesis which is able to measure forces in all three room axis. The general objective is building a cost-efficient sensor measuring the distributed forces in three axis. The final prosthesis should be available to a broad range of people in Peru which makes the cost factor and the simplicity really important. Since the sensor is going to be used on the foot palm of a lower limb prostheses, it has to be thin and flexible. During the work a suitable concept is going to be chosen. Afterwards a construction for putting the sensors on the palm is designed. The collection of the data will be done with a suitable micro controller which will be programmed during the work. The built up sensor prototype will be tested and its suitability will be evaluated. To achieve a low cost simple sensor the focus will be on 3D-printed parts and easy manufacturing since 3D printers are a powerful tool for development and easy available in the laboratory in Peru. Lots of solutions on the market are just for their price and bad availability in Peru simply not suitable. Therefore, a construction of a custom principle will be focused. A self made design can be easily modified later on to match the requirements and needs of the project. The built up prototype should be tested intensively to give a lot of information about its behavior in order to make a later decision whether to use the principle or not as easy as possible. The sensor has to meet certain requirements to be a useful extension for the prosthesis. The sensor has to be able to withstand high forces that can occur due to the dynamics while walking. The measurable force range should be high enough to cover the forces during slow walking. During the design a later integration into an array of multiple sensors has to be kept in mind. The sensor test will reveal the potential regarding accuracy. It should be the aim to reach an uncertainty as low as a few percent to use the sensor for a reliable qualitative estimation of the contact situation. By designing and building up a low cost prototype the potential of the chosen concept will be determined. A lot of future projects

not even in the field of lower limb prosthesis could benefit from the development of a low cost easy to assemble force sensor. The accuracy will by far not reach the performance of commercial available options but especially for the low prize a simple solution would help to support the development and prototyping process in many cases.



## 2 Human gait

To get a better understanding of the phases of the human gait and more important to be able to make some assumptions about the forces acting while walking it is useful to have a look at the theoretical basics. The kinematics and kinetics for the human movement have long been subject to research because a good knowledge about the things happening during walking is interesting for different fields of science. In medicine for example disfunctionalities can be detected by measuring ground reaction forces or gait profiles. Due to the many works regarding the topic of biomechanics there is a broad and deep knowledge about it. This can be used to define requirements for the sensor. Describing all the different methods and results would be too extensive for this work. Therefore, the following chapter will just explain shortly the sequence of walking. The human gait can be divided in several phases with different characteristics. To get an idea of the distribution and the extend of the forces during walking it is interesting to have a closer look at those phases. The won knowledge will help to define requirements for the sensor that is going to be designed. There are different modes of walking ranging from slow walking to sprinting [see Nigg, Macintosh and Mester 2000]. To designed sensor will focus on walking as declared later. Therefore, the analysis will focus on the gait cycle while walking. The measurement will take place directly on the sole of the foot. This means the ground reaction forces and their expected distribution has to be estimated in advance to establish requirements. After Perry and Burnfield 2010 the gait can be divided in the phases as shown in figure 2.1. During the swing phase the foot has no contact to the ground hence no forces are acting here. Therefore, the interesting part of the gait cycle is the stance part.

The stance phase starts with an initial contact of the heel. During the so called double support phase both feet are in contact with the ground. As the movement goes on more and more area of the foot gets in contact. During the so called standing phase the whole foot sole is in contact with the ground. It lasts about 30 % - 35 % of the total stance. The center of gravity is now over the foot and the other foot is lifted completely from the ground and enters the swing phase. During this stage of single support the reaction forces acting on the foot are the highest. The center of gravity continues to move forward thus



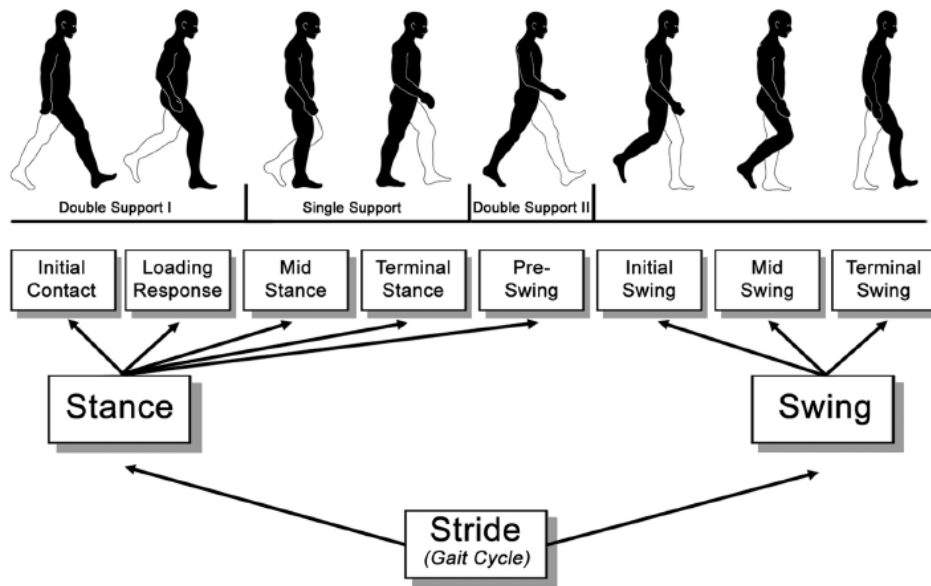


Figure 2.1: The phases of human gait [Perry and Burnfield 2010]

the pressure concentrates on the anterior part of the foot. When the heel starts to lift, the pressure is concentrated on a small area and can reach up to  $4 \text{ kg/cm}^2$  according to [Barnett 1956]. The second double support phase begins when the other foot has touched the ground again. The foot now begins to enter the swing phase itself while the other foot that has recently touched the ground enters the stance phase. Shortly before the foot lifts off the ground only the toes are still in contact. But during this phase most of the weight is carried already by the other foot so the pressure is not higher than in the previous phase. [see Barnett 1956]. After that the cycle repeats. Using this information, requirements for the sensor can be declared.

## 3 Requirements

For the development of the sensor, useful requirements have to be declared in order to have some guidelines during the process. Especially when the aim is not completely specified yet, the finding of principle solutions is one of the most important steps for the development process [VDI2222:1997-06 1997-06].

### 3.1 General requirements

The main purpose of the developed sensor will be the use in prosthetic feet. One of the goals is to build up an affordable design which can be purchased by a broad mass of peruvian citizens. This leads to a strong focus on the costs of the design. All the materials and techniques have to be low cost and accessible in Peru. The focus will be on rapid manufacturing techniques, cheap parts and common materials. The environment of use will most likely be the city of Lima. The average temperature range is from around 10 °C to 30 °C . The sensor has to work at least in the mentioned temperature range properly. The idea is to measure multiple points on the shoe sole to estimate the distribution of forces. Therefore, some requirements for density and distribution of the sensor have to be declared from which dimensional requirements for the single sensor can be derivated. To reduce the sensor number they should be placed in the areas of highest interest. Equipping the whole foot with equally spread sensors would lead to an unnecessary high number of sensors in lower interest parts. These sensors could be saved.

To get an idea of the importance of single parts, ratings by amputees could be used [Leong et al. 2016]. Different persons with amputated legs were asked about their need for sense of touch in different areas of the foot. Sketches of a foot with different areas marked were given to the test persons. Than they had to decide whether they find a sense of feel in the given area important or not in daily live situations. Figure 3.1 shows the results. The fore foot and the heal are given the most importance. But some test persons also rated the center of the foot as an important region, too. The top of the instep is not of interest for this work since it aims to build a sensor just for the palm of the foot. Figure 3.2 furthermore presents the results separated in different activities. The focus will be on

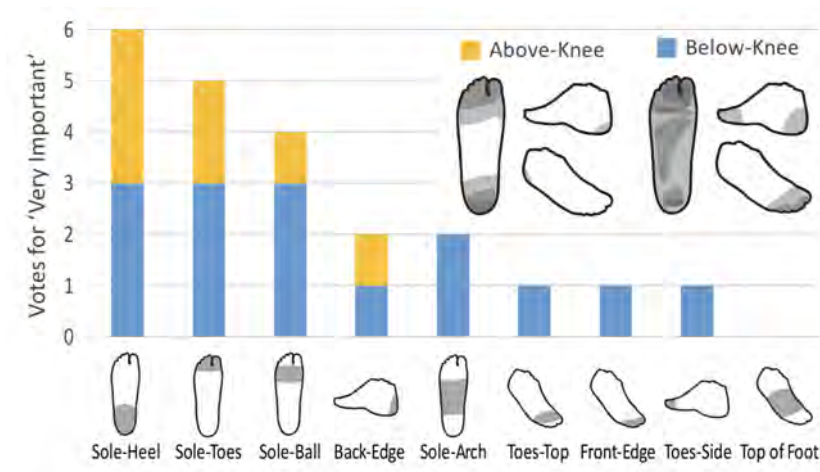


Figure 3.1: The importance of force feedback; rated by various amputees [Leong et al. 2016]



Figure 3.2: The importance of pressure recognition for different activities; rated by amputees [Leong et al. 2016]

walking. Therefore, it is clear to see that the forefoot region and the heel are the most important regions. If the human body needs a sense of feel in this region it might be important for a robotic prosthesis to measure the forces in these regions, too. Therefore, the focus will be to put as much sensors as possible in these regions. This seems to be reasonable looking at the force distribution during the stance phases (see section 2). The measurement should be possible at least while normal standing and slow walking. Because more complex and faster movements will introduce much higher forces as the measurement in figure 3.3 implies. Later on the measurement range can be enlarged if needed. Furthermore, to control such movements, faster reaction and sampling times become necessary which likely can not be achieved with low cost solutions.

## 3.2 Mechanical requirements

The aim is to measure not only the normal reaction force on the sole but also the horizontal shear forces which might be acting. A measurement in three axis is necessary. During the human movement, great ground reaction forces can occur.

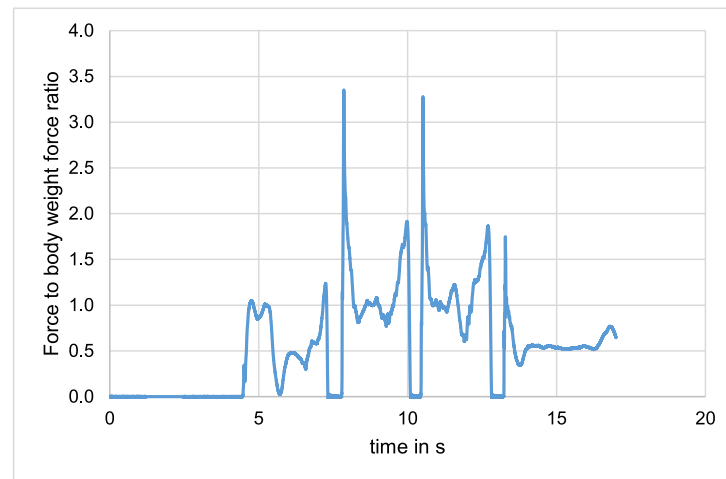


Figure 3.3: Normal ground reaction forces during different movements including small jumps

Figure 3.3 shows the ground reaction forces of a male person weighing 70.9 kg during various movements including jumps. One can see that the forces can range up to more than three times the body weight. The construction needs to withstand necessarily such great forces without damage. For the design we assume a 70 kg male human. Also the assumption is made that shear forces will not exceed 40 % of the normal load as this is normally the case during slow walking [Nigg, Macintosh and Mester 2000]. This leads to a minimum measurable force of 30 N in lateral direction. As shown in chapter 2 the actual acting lateral forces during walking are even smaller. The normal force that the sensor should be able to measure will be around 150 % of the persons weight. Assuming a 70 kg person this leads to a total force distributed on the single sensors in contact of around 1000 N. During different stance phases parts of the foot have no contact to the ground. The force distributes only to the parts in contact with the ground. At the beginning and end of the stance were only toes or heel are in contact most of the weight is carried by the other foot [see Barnett 1956]. During the phase of maximum force concentration pressure can reach more than  $4 \text{ kg/cm}^2$  as shown in chapter 2. Assuming a safety factor for dynamic loads of 2.5, this leads to a minimum measurable force of about 100 N in normal direction. Most likely the sensors do not bear all of the weight, because this would lead to a very punctual ground force distribution. The final design will integrate the sensors in the shoe sole in a way that other not measuring parts will bear some of the loads, too. But to be sure the design of the single sensor will be done assuming the worst case were the sensors alone carry all the load.

### 3.3 Dimensions

The real size of the final prosthesis has to be adapted to the size of the person wearing it. Human feet have a wide range of dimensions. To make a practical assumption for the prototype, a footprint with a shoe size equal to size EU43 is chosen. This matches the size of the average european male. This leads to a length of about 275 mm and a wide of approximately 110 mm. Note that foot size has to be adapted to the person using the prosthesis. Therefore, the final product needs to come in various sizes but the chosen values seem to be a good starting point for the design. There shall be at least four sensors in each row, which leads to a maximum width of 27.5 mm for each sensor module. The cluster of sensors themselves needs to be as slim as possible because it is going to be integrated in a prosthesis the electronics can be placed in the space normally occupied by the human foot. Therefore, the size of the electronics is not as critical as it would be if the whole sensor had to be integrated in a shoe sole.

### 3.4 Computational Requirements

The data extracted by the sensor shall be in a format usable by state of the art computational systems. The same applies to the used method of data transfer. During the time of the development of this work there was neither information available about the system receiving the data in the future prosthesis system. Nor about its requirements on the used bus and data format. Therefore, the focus will be on the extraction of the measured values. For the communication of the sensor with other devices a serial connection will be used. This is by far not the option with the best performance but it is easy to use. Once the surrounding systems are designed the serial connection can be replaced by an interface with higher bandwidth without influence on the sensor performance. One aim should also be to secure that peripheral devices such as power sources needed are few and simple. Therefore, the aim will be to build a sensor which can work with low voltages. So it can be powered by the same voltage source as the controller collecting the results. As shown in section 3.2 the normal forces range from 0 N to around 100 N per sensor during the walking movement. The shear forces do also have a great variance. This means the sensor has to be able to detect small forces to notice the first contact but also to measure the high forces when standing or walking to provide useful data. During the walking phase there are two interesting parts. The first contact has to be detected sensitively. Here the exact force is not that important as long there can be a clear discrimination made between contact and no contact. The forces rise fast after the first contact since more

weight is put on the foot in order to lift the other. Once there is a lot of weight on the foot it is important to know the values of the forces more exactly in order to get information about the pressure distribution. This means for the sensitivity of the sensor that it has to be high when there are no or low forces acting to register even a slight contact. On the other hand it has to be more exact and needs a higher resolution when higher forces are acting. Since the sensor has to be cheap and simple the resolution and the accuracy will not be able to compete with commercial solutions. But the purpose is to build an affordable design so the accuracy is good enough if it reaches a few percent. Main focus will be on a qualitative mapping of the forces. Looking at the human body very high measurement speeds are achieved. Among the different nerve cells sensing the pressure and contact forces one of the fastest and the ones considered to estimate contact forces are the so called Meissner's corpuscles. Depending on the sensed intensity they send with a frequency of 100 Hz up to more than 500 Hz [Dahiya and Valle 2013]. Using low cost materials and parts the sensor will most likely not reach those sampling rates. For palms with multiple sensors the speed issue is supposed to be come more problematic with rising sensor density. Therefore, sensor speed will not be in the focus of the development.



## 4 Basic force sensing principles

In various fields measuring of the contact forces is important and useful. In orthopedics the contact forces while walking can give information about eventual posture errors of the patient. In the automotive sector sensor mats can be used to analyze new tires or improve the comfort of the seats XSensor Technology Corporation 2019. Just to give a small hint of the variety of uses. The following section will give a short overview of the basic principles that can be used to measure forces acting. The advantages and disadvantages are mentioned. Force sensing in general can only be done indirect by translating the force signal in another physical dimension that can than be measured. There are also very complex ways of measuring forces for example in electromagnetic compensated balances where the acting force is compensated by a controlled magnetic field. These concepts are not suitable for a small, easy and cheap concept thus they are not further mentioned in this work. So the following principles are not all possibilities available at the moment but a selection of concepts related to the task.

### 4.1 Capacitive sensing

Capacitive force sensors measure the change of capacity between two plates. When the elastic, dielectric layer between them is deformed the resulting capacitance change can be used to calculate the acting force. Lots of commercially available pressure sensors use this concept. It has the advantage that no special materials are needed. The dielectric material just has to be a good isolating one. Of course materials with a good linearity or a high dielectric permittivity can increase the sensor performance. This makes it possible to build simple and cheap sensor chips. But the electronics needed to measure the capacities can bear some trouble since it is not possible to measure the capacity directly. Also the sensor is likely to be influenced by external electrical fields because they could easily induce voltages. Therefore, it is necessary to think in ways to reduce this error source. Also miniaturization can be problematic since smaller sensor areas cause smaller capacitances which are harder to measure exactly.

## 4.2 Inductive sensing

Inductiv sensors use the change of inductivity due to the approximation of a ferromagnetic counterpart. If the approximation is due to the deformation of an elastic material the acting force can be estimated. Another way to use magnetic fields for force measurement would be using inverted magnetostriction. If a ferromagnetic material is deformed it changes its permeability. This change would influence the induction of a voltage in a coil if excitation and measurement coil are connected magnetically via the deformed material. This principle is not that easy effected by external fields. But it might be complicated to build up a small sensor. Miniaturized coils only introduce very weak magnetic fields, which makes the measurement of a change challenging.

## 4.3 Piezo electric sensing

The piezoelectric effect is found in various materials. If those materials are exposed to mechanical stress they accumulate charge that can be measured. This effect has its origin in the crystalline structure and can be found in various materials like quartz and even some biological ones like human bones. Those materials can be used as a transducer to convert an applied force into a measurable electric signal. The effect can also be inverted causing a material to expand or shrink when a voltage is applied. The use as sensor as well as actuator is very versatile. Therefore, a lot of research was focused on this effect in the last decades leading to a high variety an advanced materials with high efficiency. The main advantage of this principle are that the measured signal is a voltage signal which can be measured very accurate and fast. But on the other hand special materials that show a strong piezo electric effect are needed. These materials are often very expensive as the need rare resources. The output voltages are usually very low so they need to be amplified. To achieve good results the used amplifier needs to be precise which could make it kind of expensive.

## 4.4 Piezo resistive sensing

Some materials change their conductivity under mechanical stress. This effect is called piezo resistive effect. If the conductivity is a function of the applied force those materials can also be used as transducers. Measuring the resistance of a known probe can give information about its deformation. Strain gauges for example use this effect. The advantages of using this principle are the low costs of the needed material. A lot of resistive



force and pressure sensors are used in high quantity which makes them cheap. Also the complexity of the circuit does not rise a lot when more sensors are used to achieve a higher spacial resolution. Disadvantages might be the influence, temperature has on the measurement. Depending on the used material temperature can be a huge error source since it does effect the conductivity a lot. A solution might be to connect the sensors in bridges which might lead to a more complex circuit. Measuring the temperature to correct the temperature influence could also help. Anyway the principle relies on a precise resistance measurement.



## 5 State of the art

The following chapter will present the actual state of the art for contact force measurement and sensors for collecting gait information. All of the presented works use the previously mentioned basic principles. Analyzing the different solutions the reader gets a basic idea of the variety of different ways to implement force sensing in actual working sensors. Since there is a wide spectrum of tasks a broad variety of concepts and designs has developed. As already mentioned the focus will be on small and low cost principles hence only them are interesting for the presented work.

### 5.1 Lever in polymer

Robots need sensors to give them feedback when they are in contact with their environment. Therefore, a lot of ideas have arisen during the last years in order to build cheap and reliable sensors to control the robot movement when walking or manipulating. The work of Tiwana et al. 2011 presents an interesting principle for measuring shear forces. A small lever is casted into a polymer cap. By measuring the capacity between the lever and some fixed plates its bending state can be estimated. The capacity changes when the levers bend because the width of the gap between the lever and the electrodes varies (see

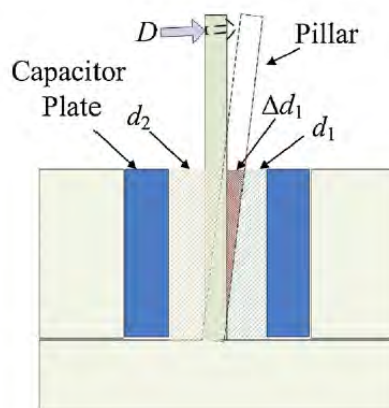


Figure 5.1: Basic principle of the measurement with a flexible lever [Tiwana et al. 2011]

figure 5.1). Knowing the stiffness of the polymer cap and of the lever the acting force can be calculated from the resistance measurement. The aim of the presented work was to design a sensor for controlling manual manipulation tasks. Therefore, the forces applied are much lower than the ones expected on a foot. Anyway with some modifications the force range could be extended so that wider force ranges are conceivable. The presented sensor is capable of measuring just in one axis [see Tiwana et al. 2011]. Some modifications or a joint of more than one sensor would be necessary to measure shear forces as well as normal ones at the same time.

## 5.2 Barometers in silicone

Yaroslav Tenzer, Leif P. Jentoft and Robert D. Howe 2012 describe in their articles a very interesting way of measuring forces acting on a surface. Small barometer chips are casted in silicone rubber. A force on the silicone leads to an increase in pressure inside the silicone which can be measured by the barometers. Other works also show, that it is possible to build sensors that could measure forces and torques in multiple axis. This principle is highly interesting because of its simple design and because of the low prices for the needed parts. MEMS barometer chips are used in nearly every modern mobile phone. Other devices like smartwatches or GPS trackers have them integrated, too. The extremely high number of produced chips leads to a very low price. Modern models come with an integrated data preprocessing and temperature compensation. Via different bus options one can retrieve directly the measured pressure and temperature. The used rubber materials also have good damping properties so that the build up sensor is very resistant to impacts and overload [see Y. Tenzer, L. P. Jentoft and R. D. Howe 2014].

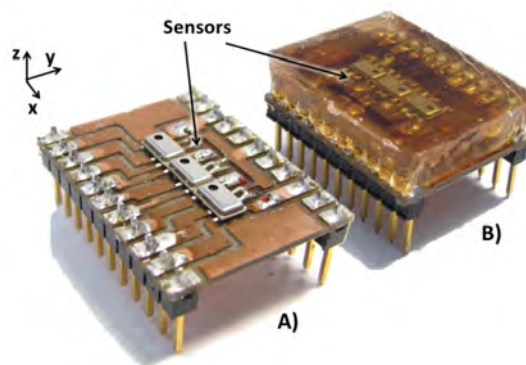


Figure 5.2: Simple one axis measuring using barometers in rubber[Y. Tenzer, L. P. Jentoft and R. D. Howe 2014]

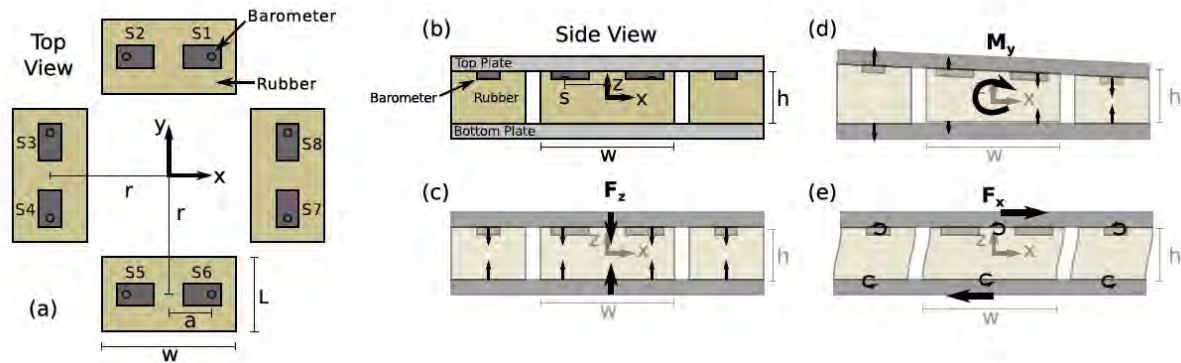


Figure 5.3: Principle of a six axis measurement [Guggenheim et al. 2016]

### 5.3 Soft pad robot foot

A more advanced version of the concept of barometers in silicone mentioned in section 5.2 is used by a cheetah imitating robot of the Massachusetts Institute of Technology. The sensor consists of a soft silicone pad guarded by a more durable outer hull. A force acting on the pad leads to an increase of pressure inside the pad. The pressure change can be measured using barometric sensors [see M. Y. Chuah and S. Kim 2014]. Later works use hall sensors and magnets instead. Nine magnets, positioned directly on the silicone are displaced as the silicone deforms due to the pressure change. An array of five hall sensors detects the displacements of the magnets. With this information it is possible to calculate the direction and absolute value of the acting forces [M. Chuah 2013]. The determination of the force is very complex and with normal analytics nearly impossible to solve. Therefore, an artificial neural network was designed and trained to interpret the inputs. Although the results were quiet good, the complexity of designing and training the network leads to a lot of work which makes this concept kind of unattractive for this work. To train the network a huge number of data sets is necessary. The amount of data would be even multiplied by the number of the used sensors in the array. Nevertheless, it is worth mentioning because it gives a good outlook on possible future developments. The physical design of sensors becomes simpler because modern computational systems allow more complex calculating to work with costly operations to calculate the outputs.

### 5.4 MEMS Sensors

Micro-electrical-mechanical systems (MEMS) are becoming more and more important. There are also recent projects for building miniaturized force sensors. For example the

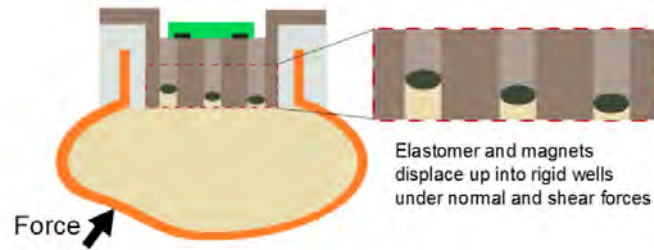


Figure 5.4: Working principle of the soft pad robot foot design [M. Chuah 2013]

ones mentioned by Takahashi et al. 2013 in their article. [see Takahashi et al. 2013]. Their work presents a small powerful sensor for measuring the contact forces acting on the shoe of an athlete.

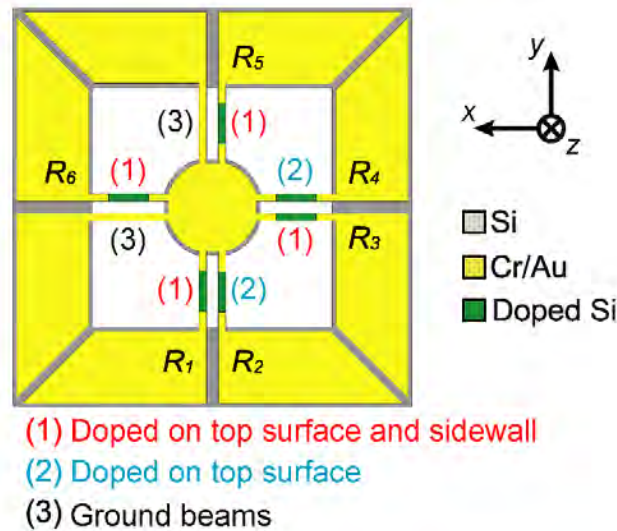


Figure 5.5: Structure of the sensor with doped silicon beams [Ishido et al. 2015]

Interesting is the design as a spike. Lateral forces are converted in a moment at the base. The described sensor is built of beams with a piezo resistive layer formed by doped areas to measure its deformation. Various of those beams are used to determine the forces and moments acting in all six axis.

Another interesting concept is the design of small pyramids structures. With integrated piezo resistive materials in the walls the deformation of the pyramid can be estimated. Knowing the characteristics of the material the applied normal and shear forces can be calculated [see Polster and Hoffmann 2009].

The examples show that there are different options to build very small sensors which are able to measure forces in multiple axis. As the example of the integration in a runners shoe

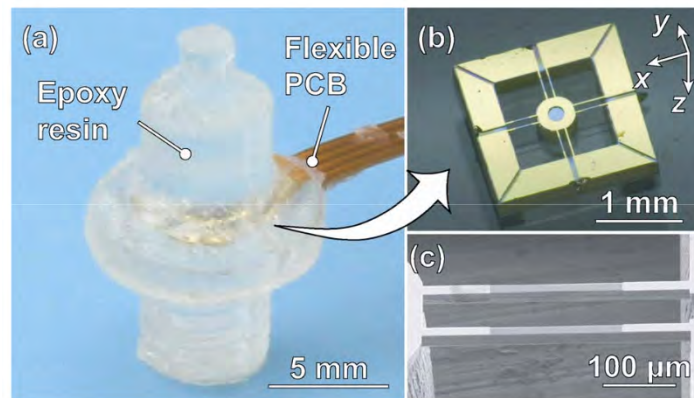


Figure 5.6: Built up Sensor a) integrated in an epoxy resin b) the sensing structure c) SEM image of the beams [Ishido et al. 2015]

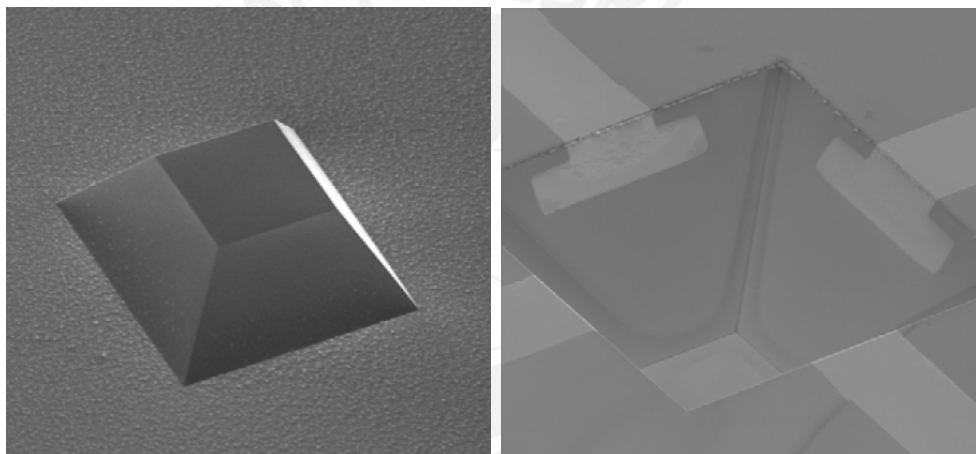


Figure 5.7: SEM image of a micro pyramidal design; edge length about 0,1 mm left: top view; right: image with the integrated electrodes [Polster and Hoffmann 2009]

showed the bearable forces can be very high depending on the design. But the problem is that to build up such small structures special techniques and machinery is needed like for example etching equipment [see Ishido et al. 2015]. This equipment was not available to design the presented work. Therefore, using techniques of fabrication MEMS devices would cause significant costs and it would cost a lot of time to build up the necessary know how.

## 5.5 Textile based sensors

To design flexible sensor matrices, the sensors could be embedded in textiles. As shown in figure 5.8 thin piezoresistive or capacitive sensing layers can be sandwiched between

conductive lines to form a flexible network of sensors. Each point can be addressed by choosing the right column and row. This way easy and cheap slip on solutions for prosthesis can be build [Leong et al. 2016]. Some of those designs lead to a good performance with cheap and common materials. Some of the works use even conductive thread to sew the conductive lines directly into the fabric.

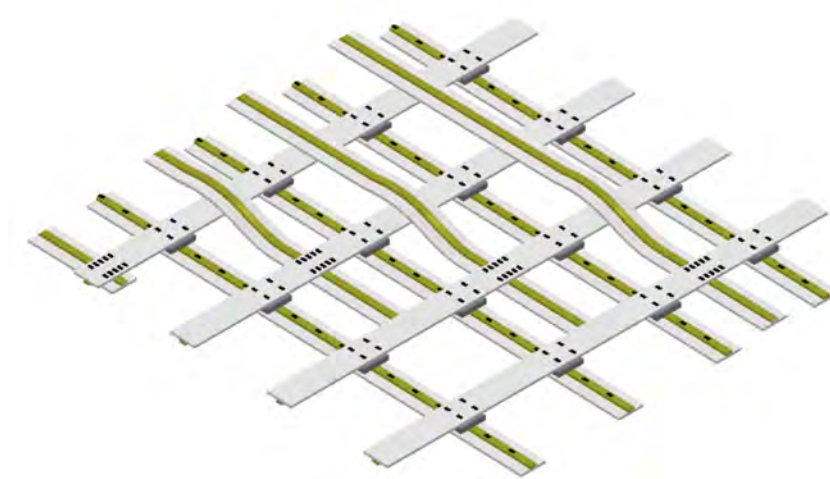


Figure 5.8: Structure of conductive stripes sewed together to form a network of pressure sensors at the junction points [Danilovic 2013]

Each of the actual works only measure the normal pressure acting on the surface. During the research there was no solution found capable of detecting also shear forces. It can be assumed that building a three axis textile sensor would be not that trivial. Which means that principle would loose most of its advantages. Nevertheless, it is interesting and with high potential for future low cost medical devices and therefore mentioned in this work.

## 5.6 Three axis resistive sensor

To build a small three axis force sensor quantum tunneling composite Ting et al. 2013 used a quantum tunneling composite material which acts like a very good piezo resistive material. The material is placed as a thin layer between electrodes. The four upper electrodes are connected to a spheric cap acting as a transducer. It converts the shear forces into a torque at its base. Resulting reaction forces on the four electrodes can be evaluated by measuring the resistance between each upper electrode and the bottom one. From the four measurements the acting shear and normal forces can be calculated. The principle is interesting for the way it works with the shear forces by transforming them into normal loads at the base. The material its self is new and not common in use

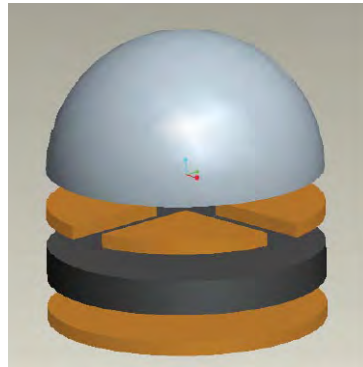


Figure 5.9: Structure of the sensor [Ting et al. 2013]

which makes it hard to get in Peru and kind of expensive. Using other piezo resistive materials as a thin layer like this would cause such small resistance changes that they could be hardly even measured. Therefore, the design like this might not work, but the force transducer principle could be used anyway in a modified way.

## 5.7 Load cells

To measure forces and moments in multiple axis there are a lot of different commercial load cells available. In industry they are common in use because of their robustness and variety in design and specifications. Most of them use strain gauges to estimate the forces and moments acting. The structures are mostly milled out of a solid metal block which gives them a good linearity and repeatability. There are designs available for very high forces.



Figure 5.10: Commercial strain gauge based three axis force sensor [ME-Messsysteme GMBH 2019]

But since they are normally made out of metal they are relatively heavy. Building them out of polymers for example would cause strong nonlinear and unpredictable side ef-



facts that would make the measurement very imprecise. Buying a commercial three axis solution might be expensive. Nevertheless, a structure with strain gauges could be an interesting principle to think of in the design phase.

## 5.8 Sliding electrode capacitive

When using a capacitive principle it is good to measure differential capacities, which means the sensors are arranged in a way that a change in force leads to a rising value on the one side and a falling one at the other side. This way external effects that might cause a drifting are suppressed if they affect both measurements in the same way. Such designs are complicated to achieve if the aim is to build a sensor with a low height. For robotic surgery there is already a device to measure normal and shear forces that implements a difference measurement at least for the shear force measurement.

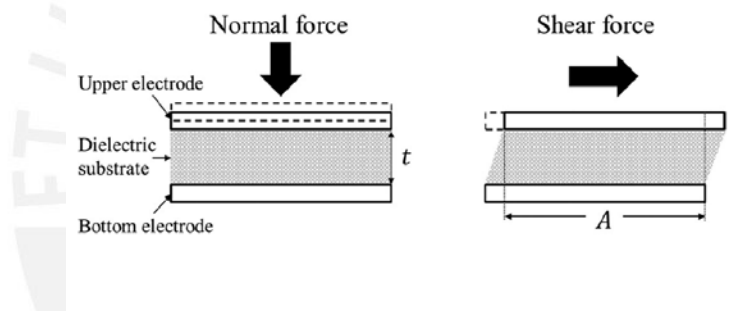


Figure 5.11: Movement of the electrodes of the sliding electrode sensor [U. Kim et al. 2015]

The principle is shown in figure 5.11. There are several electrodes over a bigger bottom electrode separated by a dielectric layer. Normal forces compress the material uniformly and all capacitances between the top electrodes and the bottom one rise. If there is a shear force the electrodes shift relatively to one another. The electrodes on the outside are not completely covered by the bottom electrode. A lateral movement will thus change the covered area and the capacitance between top and bottom electrode. The electrodes on the opposite site face contrary change. The difference between those capacitances indicates the acting shear force. The electrodes covered completely will not change capacitance when a shear force acts because their covers area does not change. Figure 5.12 shows the used shape and distribution of the electrodes. Since the big plate (red rectangle in figure 5.12) is not connected there is at least one additional excitation electrode needed.

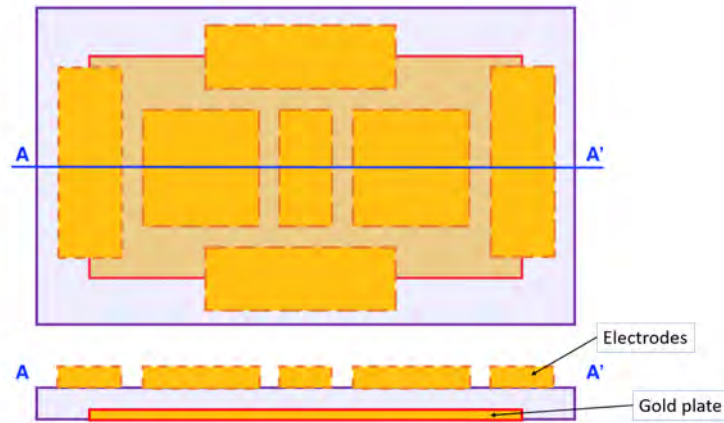


Figure 5.12: Sketch of the electrodes of the 3D capacitive sensor

## 5.9 Sensor mats

To measure the pressure in the contact zone of two objects sensor mats are a good option. A lot of different companies have developed a broad variety of different models for nearly every possible use. There are possible applications from optimizing the comfort of seats up to measuring the pressure in the contact zone of tires. Modern sensor mats are thin and flexible. They can map the pressure life with high frame rates. For example the model LX100:25.50.05 from X-Sensor which would fit the measurement quite well if it was just to measure normal pressure on the foot sole. They can work with resistive measurement [XSensor Technology Corporation 2019] or capacitive [see *plasticelctronic* 2019]. But those solutions only offer a measurement in normal direction. Shear forces are not measured. One of the main goals of this work is to measure the forces in normal direction as well the shear forces. Therefore, sensor mats are no option. Although they are an interesting and powerful tool for pressure analysis.

# 6 Conceptual design

In chapter 5 various concepts for measuring forces were shown. To construct a sensor, a suitable concept has to be chosen first of all. The following chapter will show the process of choosing the concept. It will try to make clear why the final concept was picked out of the presented ones. According to VDI2222:1997-06 1997-06 the principles have to be collected and presented in a simple way to find the best solution. Primarily different ideas are shown and discussed. Afterwards the thoughts leading to the final decision are explained.

## 6.1 Concepts

Since the sensor has to be cheap and small while capable of measuring more than 100 N of force lots of the cheap commercial available sensors are not suitable especially the plastic based hobby solutions because they work only with low forces. Most of the sensors based on strain gauges are way too expensive. They are extremely accurate but this accuracy is not needed for the use in context of this work. The focus therefore will be put on lightweight, small and cheap concepts that could be eventually completely built up with the equipment already available.

### 6.1.1 Barometers in silikon rubber

The principle of barometers casted in silicone rubber as described in section 5.2 could be used for the desired task. There are several works showing that three axis force sensors can be built up easily with good results. Unfortunately all the shown concepts were only designed and tested for small forces of a few newtons (see [Guggenheim et al. 2016]). To make the concept suitable for the task it has to be modified to support higher loads. This could be achieved by using a durable case carrying most of the load and a soft infill translating the deformation into a measurable pressure. Alternatively sensors for higher pressure ranges could be used. But since they are not produced in quantities as high as the barometric sensors they are not that cheap. Modifying the structure to use

barometric sensors with a measurement range of around 70 kPa to around 120 kPa will reduce the prize for each unit significantly. To improve the accuracy the sensors could be also arranged in a pyramidal structure [see Reeks et al. 2016] The rest of the case structure would remain the same. The rigid support hull might cause also some problems on the other hand because it slows down heat conduction and could therefore cause a bet heat behavior.

### 6.1.2 Transforming shear force into torque

To measure forces in three axis a solid block acting as a transducer for shear forces can be designed. Figure 6.1 shows the basic principle how the rigid transducer works.

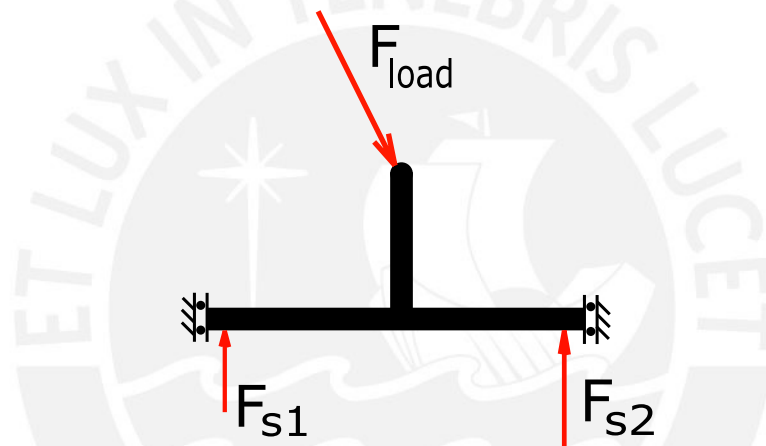


Figure 6.1: Basic principle of the force transducer

The block is supported by at least three force sensing elements. A normal force will be distributed equally on the elements while a shear force on the top will introduce a momentum. This Momentum leads to a rising load on one side and a declining one on the other side. This way the acting forces on the tip can be calculated based on the values of the force sensing elements. The elements can either capacitive or piezo resistive. [van\_\_electrodes] This method allows the use of only one dimensional sensing elements. The top element of the sensor just needs to be rigid enough to neglect the influence of its deformation. Its advantages are its simple design which allows an easy build with low cost materials. It is robust. Possibly thin single axis force sensors could be just bought and integrated to measure the reaction forces. This reduces the work needed for development. But there are also some disadvantages. To convert the shear forces in torques a certain distance between the sensor plain and the attack point of the forces is needed. This means that the sensor necessarily needs a certain minimum height to work properly. The lower

the height the lower the momentum introduced by a shear force which also lowers the achievable resolution. This stands in contrary with the desire to design the sensor as slim as possible. Also its relatively big structure might reduce the speed in which heat enters. This makes its response to a heat change slow and therefore harder to compensate.

### 6.1.3 Flexible structure with strain gauges

Another possible way could be to built up a flexible structure equipped with strain gauges. A principle like it is used in commercial load cells (see chapter 5.7). The design of the structure could be adapted to the shape of the foot sole. Advantages of this design would be that there is a lot know how already available because a lot of different sensors working with this principle are already on the market. If the design is chosen well, the strain gauges can be connected in a bridge circuit which allows a very good temperature compensation. But it also bears some disadvantages. To achieve a good linearity the flexible material has to be chosen well. Most commercial load cells use metals not only for their good linearity but also for their heat conduction properties. If plastic parts were used, the calculation of the force from the sensor data would be very complex. If the structure is designed as a single peace covering the whole sole of the foot there would be also problems with high cross talk between the measurement points.

### 6.1.4 Capacitive sliding electrode

For robotic surgery a sensor using a capacitive measurement to detect the horizontal and vertical movement of an electrode placed on an elastic dielectric substrate was presented by Mancillas 2018. The functionality was described in chapter 5.8.

Sensors working with this principle are already available. But as they are designed for robotic surgery their measurable force range is very small around a few newtons [see Mancillas 2018]. If stress caused by a shear force becomes bigger the transverse contraction will not be small enough to ignore it. Than it will be really complicated to distinguish between normal and shear forces. It will be complicated to find a proper dielectric material. Increasing the size would also reduce the transverse contraction since the tension is reduced but the size is already restricted by the requirements. On the other hand this principle can lead to a very thin device since it just needs electrodes and a thin dielectric layer in between.

### 6.1.5 Metal pin in polymer

Advancing the principle introduced in section 5.1 a design for multi axis measurement can be achieved. The bending lever could be replaced by a round one which has mostly the same areal inertia for both main axis. This lever can now be surrounded by four electrodes in a ring shaped distribution. The bending state can be estimated in the same way as it was done in the single axis version. Most likely the output will not be linear. Because of that, calibration and curve approximation could be complex. The normal force can be measured by a single axis sensing element directly beneath the structure.

### 6.1.6 Prism structure

Multi component forces could be measured also by equipping a prism like structure with thin force measuring elements. The way normal and shear forces change the measured forces by the single elements is shown in figure 6.2. From the single measurement the acting forces can be calculated. Torque introduced on the element would effect the measurement. This means the final design should also implement a solution to minimize this effect. This will make the design more complicated as it seems on the first sight on the basic principle.

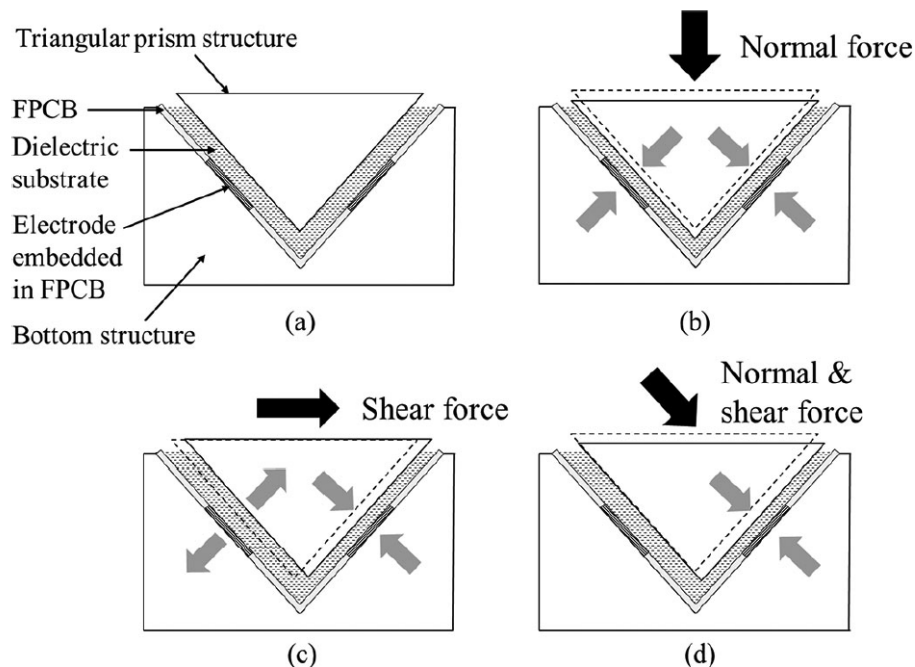


Figure 6.2: Basic principle of the force transducer [U. Kim et al. 2015]

## 6.2 Choosing a concept

To choose a suitable concept the former mentioned concepts have to be compared. From the requirements which are further explained in chapter 3 different features of importance were considered. The previously mentioned concepts are compared regarding the features to find the concept which will most likely fulfill the requirements the best. The features of importance are:

- **Weight** Describes the mass of the built up sensor. Lower weight leads to higher comfort for the person wearing the prosthesis equipped with the sensor.
- **Area** The area is restricted by the requirements. In the case of the concept choosing it is not possible to know the exact size of the final construction but there are some concepts that tend to a higher need for space which might cause difficulties to build it small enough. This feature describes more the general tendency of how difficult it will be to build a sensor with a small area.
- **Height** Also the height should be as low as possible since it makes the integration of the sensor into the prosthesis more easy.
- **Complexity** This feature describes the complexity of the concept itself as well as the fabrication. A more complex concept will be more susceptible to errors and its fabrication costs might be higher.
- **Materials** Some of the concepts require special materials or parts. Common materials found in every day life are easy to obtain and cheap. Therefore a design which uses few or no specialized materials is favorable.
- **Data acquisition** This feature describes the complexity of the calculation needed. The simpler the force can be calculated from the measured values the faster is the measurement. Also it might require more advanced programming and micro controller to process complicated models
- **Force range** Although the needed force range is already given in the requirements there are some concepts which might work good for lower forces but cause trouble with higher forces. Concepts which are already proven to work with even higher forces will most likely cause fewer problems when measuring forces at the top end of the force range and are therefore favorable in this point.

According to VDI2223:2004-01 2004-01 a comparison table can be used to make the decision. But first the weightings for the different features according to their importance have to be estimated. VDI2223:2004-01 2004-01 suggests a cross comparison in this case. The cross comparison table for the selected features can be seen in table 6.1. Each feature is compared in its row with the other ones one by one regarding its importance. If the feature in one row appears to be more important than the feature in the actual column the value two is inserted. If the importance is equal the value is one and if the column feature is of more importance the actual cell gets a zero. The sum of each row now gives a value for the individual importance of the feature among the others. To get not too high weightings the outcome is divided by two. This operation does not affect the outcome because it just divides the final result by two for all the concepts.

Table 6.1: Cross comparison of the features

	weight	area	height	complexity	materials	data aquisition	force range	resulting weights
weight		0	0	2	0	2	1	3
area	2		2	2	1	2	2	6
height	2	0		2	1	2	1	4
complexity	0	0	0		2	1	2	3
materials	2	2	2	2		1	0	5
data aquisition	0	2	2	2	2		0	4
force range	1	2	2	2	2	2		6

The resulting weights from table 6.1 can now be used to design a comparison table for the different concepts. The scores for every feature are given from one to four. The higher the score the more favorable the outcome of the concept is regarding the actual feature. Then the given points are multiplied with the weighting factors and summed up. Note that the scores are assumptions made on the state of knowledge during the planning phase. Technical parameters are just estimated to make a decision with low afford. The results are shown in table 6.2. One can see that two concepts are equal and have more points than the others. So the decision was going to be made between those two. The barometers in silicone concept was very interesting but it was not clear if the concept would really work with the high forces needed for this project. There was only few information available and it was unsure if the concept can be applied to higher forces.



In order to evaluate the prospects of the concept more detailed a simple prototype was manufactured and tested.

Table 6.2: Comparison table of the concepts

feature	weigth	Barometer in silicone	transform to mo- mentum	structure with strain gauges	sliding elec- trode	metal pin in polymere	prism struc- ture
weight	3	3	4	2	3	1	3
area	6	2	2	1	1	1	2
height	4	3	1	2	4	2	2
complexity	3	3	4	2	2	3	1
materials	3	3	3	2	3	3	3
data aquisition	1	4	3	2	2	2	3
force range	3	1	2	4	1	3	3
sum		58	58	46	51	46	53

## 6.3 Prototype barometric sensor

The chosen principle seemed to be good for the task. But little was known about its behavior and the facts in the decision table are often just assumptions. To make sure the concept works it will be best to design some simple tests. Therefore a simple prototype was designed to test the general behavior of the concept. To achieve fast results its design is easy and just maps the basic behavior. Other requirements than its measure range are not assumed very important for the first try.

### 6.3.1 Design and assembly

The pressure measured by the barometers inside the silicone rubber is proportional to the acting force  $F$  [Guggenheim et al. 2016].

$$p = \frac{F}{A} \quad (6.1)$$

Since the area  $A$  is restricted by the requirements the pressure would be too high for simple barometric chips if forces up to 100 N are acting. To make the concept work with higher forces a structure made of two materials was used. The silicone is supported by a more rigid material on the outside which takes most of the load (see figure 6.3).

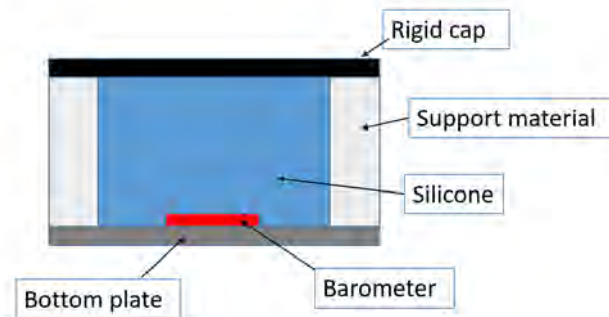


Figure 6.3: Principle of the supported sensor

The behavior can now be assumed to be like a composite of two resorts. Each spring represents either the outer hull or the soft infill. The load is supported in the following way:

$$F_{load} = k_{support} \cdot x + k_{silicone} \cdot x \quad (6.2)$$

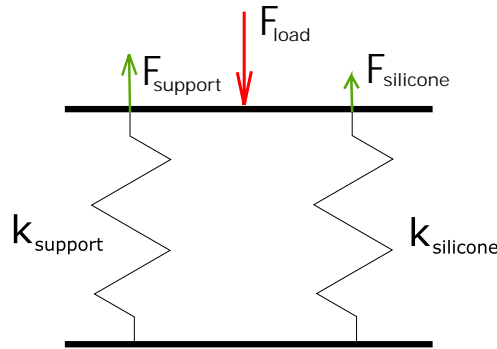


Figure 6.4: Principle of support material; Each material supports a fraction of the load proportional to its stiffness

The displacement  $x$  is equal for both springs. This leads to the equation for the force acting on the silicone.

$$F_{silicone} = \frac{k_{silicone}}{k_{silicone} + k_{support}} \cdot F_{load} \quad (6.3)$$

And with the pressure  $p$  inside the silicone shown in equation 6.4 one can see that the additional pressure to the environmental air pressure  $p_{environment}$  can be reduced using a stiffer support material.

$$p = \frac{F_{silicone}}{A_{silicone}} + p_{environment} = \frac{k_{silicone}}{k_{silicone} + k_{support}} \cdot \frac{F_{load}}{A_{silicone}} + p_{environment} \quad (6.4)$$

As silicone molde Silikast L20 from Silika was used. Its modulus of elasticity was assumed to be around 280 kPa [see Yaroslav Tenzer, Leif P. Jentoft and Robert D. Howe 2012]. As support material TPU95A was chosen. It can be 3D printed which makes it easy to fabricate the support ring. Its elasticity module is around 26 MPa and therefore way higher than the one of the silicone [Technical data sheet TPU95A 2017]. In order to fulfill the requirements the outer diameter of the prototype is set to 26.5 mm. The inner diameter filled with the silicone mold is set to 18.5 mm. This leads to the stiffness  $k_{support} \approx 1.7 \cdot 10^7$  N/m and  $k_{silicone} \approx 6.9 \cdot 10^4$  N/m. The expected sensitivity will be.

$$\frac{\delta p}{\delta F} = \frac{k_{silicone}}{k_{silicone} + k_{support}} \cdot \frac{1}{A_{silicone}} \approx 15 \frac{\text{Pa}}{\text{N}} \quad (6.5)$$

As barometer a small and cheap chip was selected. The BMP180 was chosen since it is cheap and of good availability. The producing company Bosch already announced the end of the product life cycle but in Lima it was still sold in huge amounts. Later versions of Bosch Barometers like the BMP280 are even better for the task [see Data sheet BMP280

*Digital pressure sensor* 2018]. If the concept was chosen the used sensor will be changed to one, still produced. The BMP180 has a pressure range from 70 kPa to 120 kPa. It can also measure temperature [see *Data sheet BMP180 Digital pressure sensor* 2013]. Assuming that the normal air pressure ranges between 900 hPa and 1100 hPa there is a usable additional pressure for the measurement of around 10 kPa. To make the soldering more easy a premounted BMP180 will be used. The boards are sold by *Adafruit*. The board is glued to a 3D-printed ABS plate (figure 6.5). Afterwards a ring made of TPU95 from a 3D-Printer is placed on top of the bottom plate as shown in the left picture of figure 6.6. The Ring is than filled with the silicone rubber. To make sure the rubber enters the sensor case the curing was done in a vacuum chamber. Although the pressure only reached -30 kPa the results where good. For an equal force distribution the sensor was covert with a rigid cap formed by a money coin.

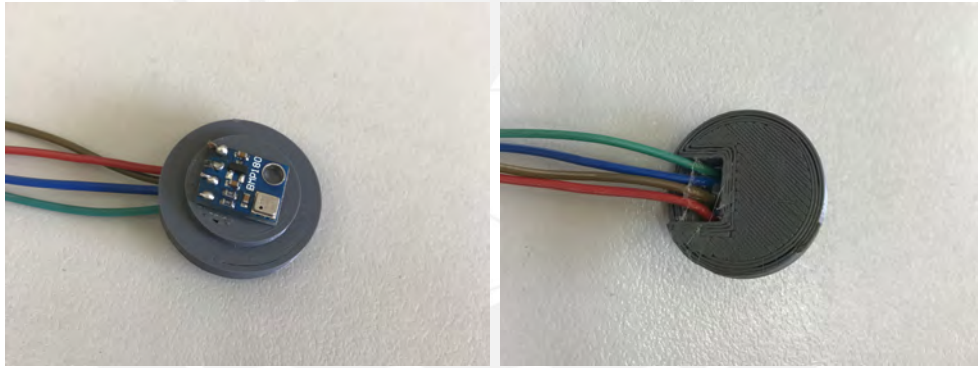


Figure 6.5: Barometer placed on the bottom plate

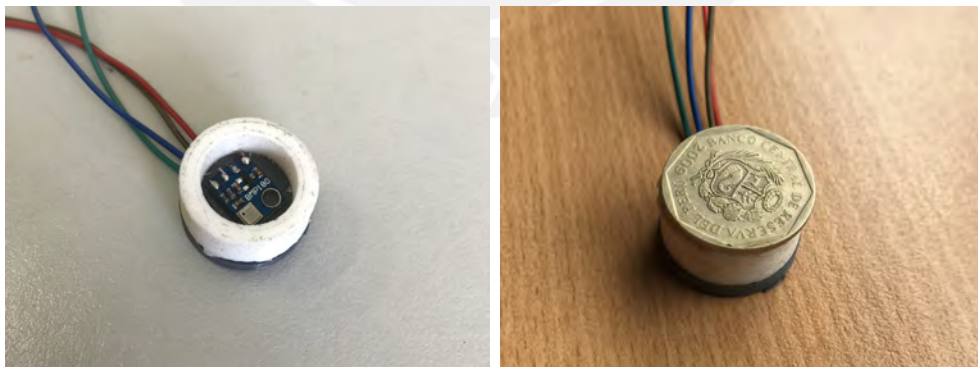


Figure 6.6: Barometer sensor assembly without the silicone cast (left) sensor assambled with coin as cap (right)

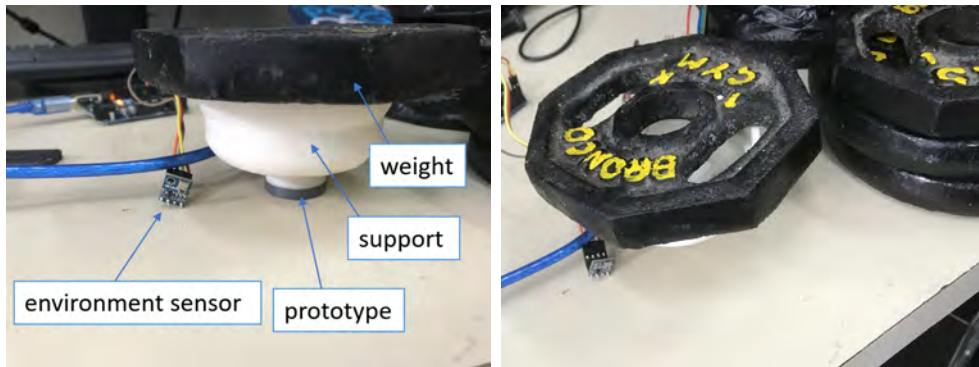


Figure 6.7: Testing the sensor with different masses

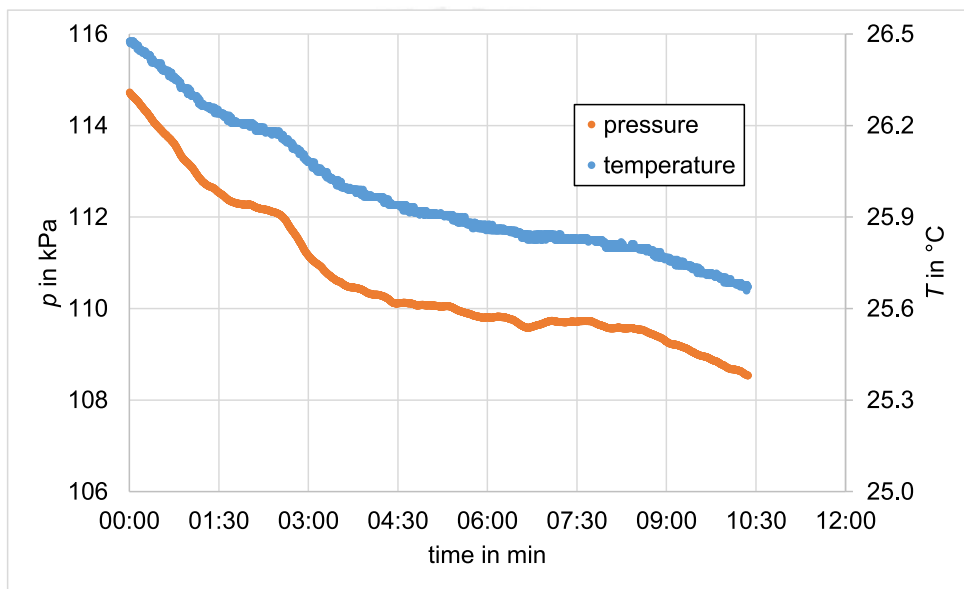


Figure 6.8: Drift of the barometer in silicone sensor; constant load of 10 N

### 6.3.2 Evaluation

The sensor showed good response to applied forces. The sensibility was around 20 Pa/N which is actually higher than expected. A reason for this could be the 3D-printed structure of the support ring which is not as stiff as completely homogeneous material would be. As shown in figure 6.8 temperature has a strong impact.

Under relatively constant environmental temperature a linear compensation was sufficient to manage the temperature influence and get stable outputs.

Figure 6.9 shows the response to a temperature step while under constant load. The step was introduced by putting the sensor in a refrigerator until it stabilized. Afterwards it was put outside again. This way a step from around 8 °C to 22 °C was achieved. As one can clearly see in the graph, the response of the sensor is really slow. At first

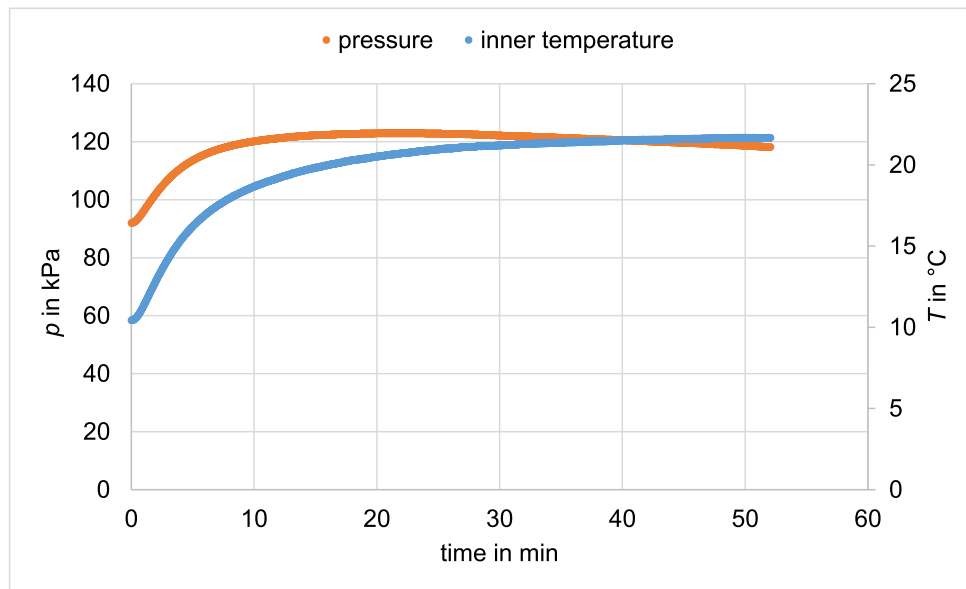


Figure 6.9: Response of the sensor to a temperature step. Initial outside temperature was about 4 °C. load ca. 1 kg

the measured value sinks a little. This could be explained by the design of the sensor. Although the thermal expansion of the used elastomers should be similar they are not equal. The heat enters from the outside and reaches the outer hull at first. When it starts to expand the pressure on the inside sinks. Shortly after the inside begins to warm up, too. The expansion of the material inside the barometers leads to a strong increase of measured value. This behavior leads to two serious problems. At first the slow response to temperature changes makes it necessary to measure the outside temperature with at least one external sensor close to the force sensor. The second problem is caused by the limited range of the barometers which are used. The step shown in figure 6.9 consumes nearly half of the usable range of the barometers [see *Data sheet BMP180 Digital pressure sensor* 2013]. To work with varying temperature and the desired loads, the barometers would have to be exchanged or a significant loss in resolution is caused.

### 6.3.3 Conclusion

The concept works to measure forces with a good resolution. The outer hull enables it to work with much higher forces than the original designs. But there is a slow and strong impact of temperature which, although it could be compensated by measuring the outside temperature and some algorithms, would cause some serious afford during the following development process. To avoid a huge loss in resolution the barometers would have to be replaced by pressure sensors with a much wider range. But one of the big advantages of

the concept was the low price. Other pressure sensors with a wider range are a lot more expensive. The concept would lose its price advantage in that case. To stick with the BMP sensors would mean a lot of work on temperature compensation and unpredictable trouble. Therefore it was decided to rework the concept in order to choose another one.

## 6.4 Reevaluating the concepts

With the won knowledge by the tests of the prototype the concepts were evaluated again. Since the design with the barometers which was tested shows a complicated and slow behavior it is not favorable anymore. The newly won knowledge would cause a worse rating on the ease of data acquisition and complexity for the barometers in silicone prototype. This leads to fewer points in the rating for this principle. The principle using a transducer to convert the shear loads into a torque which was equally valued in the comparison table will be focused instead.



## 7 Mechanical design

The mechanical design will be the same for both used measuring concepts. The principle was introduced and chosen in chapter 6.2. A cantilever transforms the shear forces in a torque at the base while normal forces are acting directly. From measuring the reaction forces at the base of the transducer the loads at the top can be reconstructed. For an easy calculation a model which implies that the transducer is totally rigid will be assumed. Of course it deforms in reality but if it is solid enough, the deformation will be very little and can therefore be ignored. There are three unknown forces, two lateral and one normal force. This means that there are at least three measurement points needed to build up enough linear independent equations. To make the readout easier a design with four sensors, two of them on each symmetry axis, is chosen. This also helps to reduce cross talk. [see Guggenheim et al. 2016]. From figure 6.1 one can see that the reaction forces can be calculated, knowing the height of the transducer  $h$  and the distance of the sensors from the middle axis  $d$ , as follows:

$$\begin{aligned} F_{s1} &= F_z/4 + F_x \cdot \frac{h}{d/2} \\ F_{s2} &= F_z/4 - F_x \cdot \frac{h}{d/2} \end{aligned} \quad (7.1)$$

The sliding of the transducer due to lateral shear is very small since the ratio of height to area of the dielectric layer is small, too. To achieve easier to handle equations lateral shift will be neglected. This assumption allows the use of linear bearings in the calculation model (see figure 6.1) and the resulting equations 7.1. For a three dimensional problem the equations are:

$$\begin{pmatrix} F_{s1} \\ F_{s2} \\ F_{s3} \\ F_{s4} \end{pmatrix} = \begin{bmatrix} \frac{h}{d/2} & 0 & \frac{1}{4} \\ -\frac{h}{d/2} & 0 & \frac{1}{4} \\ 0 & \frac{h}{d/2} & \frac{1}{4} \\ 0 & -\frac{h}{d/2} & \frac{1}{4} \end{bmatrix} \begin{pmatrix} F_x \\ F_y \\ F_z \end{pmatrix} \quad (7.2)$$



And finally solving for the acting forces:

$$\begin{pmatrix} F_x \\ F_y \\ F_z \end{pmatrix} = \begin{bmatrix} \frac{d}{h} & -\frac{h}{d/2} & 0 & 0 \\ 0 & 0 & \frac{d}{h} & -\frac{h}{d/2} \\ \frac{1}{4} & \frac{1}{4} & \frac{1}{4} & \frac{1}{4} \end{bmatrix} \begin{pmatrix} F_{s1} \\ F_{s2} \\ F_{s3} \\ F_{s4} \end{pmatrix} \quad (7.3)$$

Depending on the used sensing method (capacitive or resistive) there will be different equations to determine the acting force  $F_i$  from the measured value. It will be very complicated to measure the single components of the equation. Also only the force measurement not the single parts are of interest. Therefore, in practical use the system will be treated as a black box and its transfer function will be determined experimentally. Nevertheless the dimensions especially the height of the transducer are chosen considering the mentioned equations. The sensibility for the shear forces can be adjusted by changing the relation between height and sensor distance from the axis of the transducer. The dimensions are supposed to be as small as possible. To make the prototyping fast and easy the transducer is printed with a 3D Printer and made of PLA. The dimensions for the capacitive version are given by the size of the electrodes in chapter 8.3. As width there is a slightly smaller value assumed to make sure the transducer is fully covered by the sensing electrodes. The width should be  $w = 25$  mm. This leads to a value  $d = 6.25$  mm. The height will be set in a first try to be  $h = 8$  mm. The design of the transducer is shown in figure 7.1. It is



Figure 7.1: CAD design of the transducer

very important to design the tip round. If it was flat an eccentrically acting force would produce a moment proportional to the eccentricity. This moment would cause a bias in the measurement of shear force. A round tip does not allow the transmission of torques to the transducer and reduces this way the bias.

# 8 Electrical design

The following chapter will describe the development of the circuit as well as the data acquisition. For handling the prototypes an Arduino Uno was chosen as an easy to handle computational base. The Arduino already comes with a broad library which supports various features and methods useful for the desired task. Also it is relatively cheap and was easily available in Lima. The Arduino Uno works with an Atmega 328 Atmel Chip with clock rate of 16 Mhz.

## 8.1 Measuring capacities

There are several ways of measuring capacities. To realize the sensor a robust way has to be found which also only needs cheap and few components. The measurement of capacitances can just be conducted indirectly which means that another quantity is measured and from that measurement the capacity is calculated.

### 8.1.1 Measuring the time constant

If a capacity is loaded the voltage changes over time following the formula:

$$U(t) = U_1 \cdot e^{-t/\tau} \quad (8.1)$$

Assuming that the initial charge was zero and the voltage jumps immediately to  $U_1$ . With:

$$\tau = RC \quad (8.2)$$

The voltage reaches  $U(t = \tau) = 1/e \cdot U_1 \approx 0.63 \cdot U_1$ . If the resistance is known, the capacity can be calculated as follows:

$$C = \frac{1}{\tau R} \quad (8.3)$$

### 8.1.2 Measure frequency of oscillating circuit

Another option would be to build up an oscillating circuit with known parameters except for the capacitance to be measured. The natural frequency of an ideal oscillating circuit is given by the following equation.

$$\omega_0 = \frac{1}{\sqrt{LC}} \quad (8.4)$$

With  $C$  as the capacitance and  $L$  as the inductivity. One can see that the natural frequency depends on the capacitance. Therefore, measuring the natural frequency can be used to obtain a value for  $C$ . Excitating the circuit and measuring its natural frequency can lead to good results. But a high quality frequency generator is needed. Therefore the concept is not suitable for the desired task because the aim is to build a principle that is as simple as possible.

### 8.1.3 Measuring the impedance

If a capacity with its serial resistance is exposed to an alternating current its impedance could be described as follows.

$$Z = \frac{1}{j\omega C} + R \quad (8.5)$$

with  $\omega$  as the frequency of the current. Connecting the unknown capacity with its serial resistance to an alternating current voltage bridge the capacitance can be calculated from the bridge voltage.

### 8.1.4 Charge balancing with a known capacity

Figure 8.1 shows one easy way to measure capacities. A known capacity ( $C_{ref}$ ) is charged with an known voltage. Once the voltage reached its stationary value switch  $S_2$  is opened. Meanwhile switch  $S_1$  connects the unknown capacitor ( $C_{measure}$ ) to ground to make sure it is completely unloaded. After  $S_2$  is opened switch  $S_1$  changes so it now connects the two capacities. This leads to an equalization of load between them. For an ideal capacitor the voltage over the capacity  $U_C$  is:

$$U_C = \frac{Q}{C} \quad (8.6)$$

with  $Q$  as the load and  $C$  as the capacity. So the electrical load of the fully charged  $C_{ref}$

is:

$$Q = U \cdot C_{ref} \quad (8.7)$$

Because  $S_2$  is open when the capacities are connected the load cannot change. The voltage which will be measured by the voltmeter therefore is:

$$U_{measure} = \frac{Q}{C_{ref} + C_{measure}} \quad (8.8)$$

If the loading voltage and the reference are known the unknown capacity can be calculated. Although this method is theoretically very easy. [jon 2014] shows that it can be used to

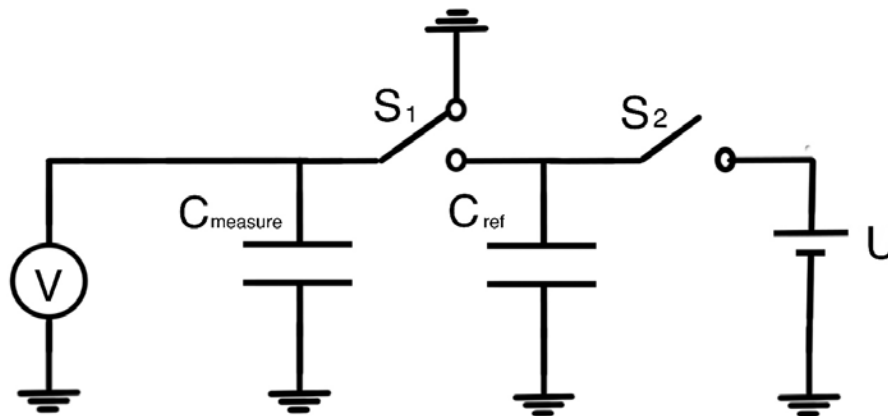


Figure 8.1: Schematic of the circuit

build easy and cheap proximity sensors just using the on board hardware of the Arduino. the method might be inaccurate because no switch and especially no transistor is free of a leakage current. With small capacities and the resulting small loads the voltage would sink rapidly and even a very small delay in the measurement would no longer be neglectable.

## 8.2 Circuit for capacitive measurement

The best way for measuring seems to be the estimation of the time constant. In order to measure the time a Schmitt-trigger will be used as shown in Figure 8.2

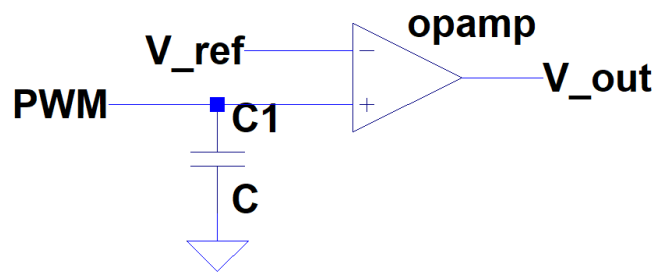


Figure 8.2: Schematic of the used Schmitt-trigger

The reference voltage will be set to a value of approximately  $U_{ref} \approx 0.63 \cdot U_{out}$ . The Arduino will repeat sending voltage steps to the entrance pin. This is achieved by setting up a PWM Signal (see section 9.2) When the voltage rises to high level the capacitor is charged. This leads to a rising voltage on the entrance of the amplifier. If the voltage on the capacitor is higher as the reference voltage, the voltage on the entrance of the opamp (operational amplifier) becomes positive. Since the opamp is set to be in permanent saturation the output voltage jumps immediately from low to high level. The capacities are going to be relatively small. Therefore, the main objective of the measuring circuit must be a low bias on the measurement. The bias current of the opamp slows the charging down. Therefore, an opamp with an ultra low bias current has to be chosen. Also, there will be a focus on short wires between the capacity and the input pin to reduce the error by the wire capacities. Since there are four capacities for each sensor there has to be the possibility to select them one by one. There are basically two options where to put a switch for selection. Either between the capacity and the opamp. This has the advantage that only one chip is needed. But for measuring capacities as small as the ones used in this work (see section 8.3) the error produced by the multiplexer in the measurement would be tremendous. Therefore the only opportunity is to use single opamps, one for each measuring area and demultiplex just the output signals afterwards. To save space in the sensor area the demultiplexer will not be placed on the board but near the controller where space is not that critical. To change between the single measurement channels a CD4067B 16 channel multiplexer was used.

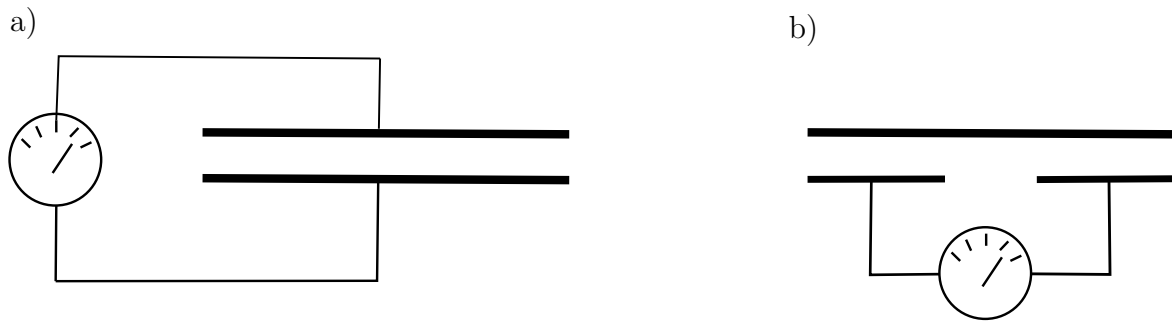


Figure 8.3: Variants of connecting the sensing element

### 8.3 Board design

At first shape and design of the measuring areas has to be chosen. First thing is the connection schematic which is chosen. There are two different options. One is, connecting the upper electrode and the lower one to the measurement circuit (variant a in figure 8.3) another possibility would be to use only electrodes at the bottom. One as excitation and one as receiving electrode (variant b in figure 8.3). Variant b has the advantage that all electrodes that have to be connected are in the same layer. Its therefore possible to design the whole circuit on one board. This helps to reduce the height of the sensor [see Mancillas 2018]. The first variant is more complicated to build up, but there is no extra excitation electrode needed. This results in a small sensor area with equal capacitance. The sensor area is more important in this case, because the smaller the area, the more sensors can be integrated on the sole. The next thing is to decide about the form of the electrodes. One could be rectangular. But as one can see this does not use the available area very efficient. Using triangular shapes would lead to a higher sensor area and therefore to a higher capacitance. The area of one sensor element can than be calculated as follows:

$$A = h_0 \cdot \tan(\alpha) \cdot l^2 \quad (8.9)$$

To make the calculation more easy it is supposed that the height  $h_0$  is small and the length  $l$  is nearly half the width of the sensor  $w$ . Than the equation looks as follows.

$$A \approx \tan(\alpha) \cdot \left(\frac{w}{2}\right)^2 \quad (8.10)$$

The conflict when choosing the size arises of the desire to build the sensor as small

as possible. But with a smaller active area the capacitance decreases which makes the measurement more difficult. To make a decision the theoretical capacitance of an ideal capacitor with parallel plates is calculated.

$$C = \epsilon_r \cdot \frac{A}{b} \quad (8.11)$$

With  $b$  as the thickness of the dielectric material between the plates and  $\epsilon_r$  as the relative permittivity. Since the permittivity is influenced by the material but never smaller than the permittivity in vacuum the calculations are done with the value  $\epsilon_0$  to make sure the capacitance is big enough for every chosen material.

Inserting equation 8.11 in 8.10 leads to:

$$C = \epsilon_0 \cdot \frac{\tan(\alpha) \cdot (w/2)^2}{b} \quad (8.12)$$

The series resistance used to slow down the charging of the capacitor should not be higher than  $20 \text{ M}\Omega$  to make sure the isolating resistances between the wires on the board are significantly higher. As explained in chapter 9.2 one of the integrated timers working with  $16 \text{ Mhz}$  frequency is used to measure the delay for charging. The resolution of this time measurement should be higher than the final sensor resolution. This leads to a minimum time for the charging process. It appears to be a good value to decide to have at least 1000 time steps. To have a resolution of  $0.1\%$ . To trigger the output signal the capacitor has to be charged at least for the time interval  $\tau$ .

Calculating the time needed for 1000 counting steps one can get the minimum time  $t_{min} = 1000 \cdot \frac{1}{16\text{Mhz}} = 6.25 \cdot 10^{-5} \text{ s}$ . This leads together with equation 8.2 to the following inequation:

$$\tau = C \cdot R \geq t_{min} \quad (8.13)$$

Based on this the following dimensions were chosen as displayed in figure 8.4. As angle for the triangular shapes  $35^\circ$  was set.

As one can see in the sketch in figure 8.4 the tips of the triangles are cut off making them look more like a trapezium. This was done to make sure there is enough space between the areas to prevent cross talk between the measuring areas. The area of one sensor area is than  $A_{sens} \approx 100 \text{ mm}^2$  For a dielectric layer with a thickness of  $0.25 \text{ mm}$  this leads to a minimum theoretical capacitance of around  $C \approx 3.6 \text{ pF}$ . The real capacitance will be higher because the calculation was done with  $\epsilon_0$ .

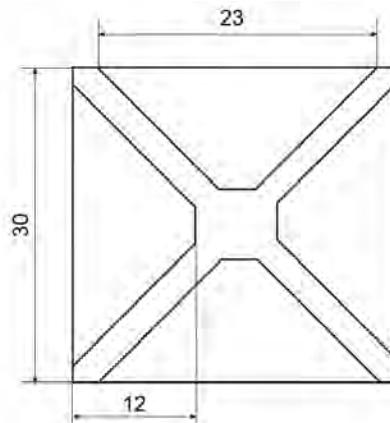


Figure 8.4: Dimensions of the sensing areas

The board was designed with the software Autodesk Eagle. The circuit is shown in the appendix. A double layer board was used to generate some kind of shield for electrical fields on the bottom side. Underneath the sensor areas there is a big area connected to ground potential blocking electrical fields. The used opamps are of the type INA121 from Texas Instruments it is important that they have a very low input current. The wires connecting the capacitive areas with their resistance and the measuring opamp have an effect like antennas which means they receive external fields and introduce them as noise into the circuit. In order to minimize this error source those wires have to be as short as possible. Therefore the opamps and the resistors are placed as close as possible to the corresponding capacitive area. By using SMD devices and a more advanced routing mill the board layout could be designed much smaller. But the designed prototype is for the proof of function and to run some basic tests. To reduce the afford easy to solder trough hole parts and a generous arrangement with wider spaces between the parts was chosen. The sensor has to be calibrated in order to match the measured capacities to the forces. This means that the exact values for the capacities are not interesting as long they can be measured repeatable. The resistors used do not need to be very precise since a different, but constant resistance just leads to a linear offset which would be eliminated while calibration.

## 8.4 Piezo resistive measurement

Another possible idea was to measure the reaction forces by piezo resistive sensors. The main challenge here is to find small ones which also support an adequate force range. A good and cheap option was the FlexiForce A101 from TechScan. It is capable of measuring



forces up to 44 N. Other sensors of a similar size often do not have a force range as big as the requirements demand. For example the FSR400 from Interlink Electronics has even smaller dimensions with a diameter of only 5 mm but it can only be used for forces up to 20 N [see *FSR 400 Series Data Sheet* 2019]. Also its dimensions of 7 mm in diameter make a small design possible. One of the main benefits is also its curve. Its conductance rises linear with a rising force. Which means:

$$F \sim \frac{1}{R} \quad (8.14)$$

As you can see in the curve in figure 8.5 this gives the Sensor a very rapid change in resistance for lower forces. In chapter 3.4 one of the mentioned requirements was a good sensitivity on the lower end of the force range. The characteristics of this sensor match the requirements very good in this sense.

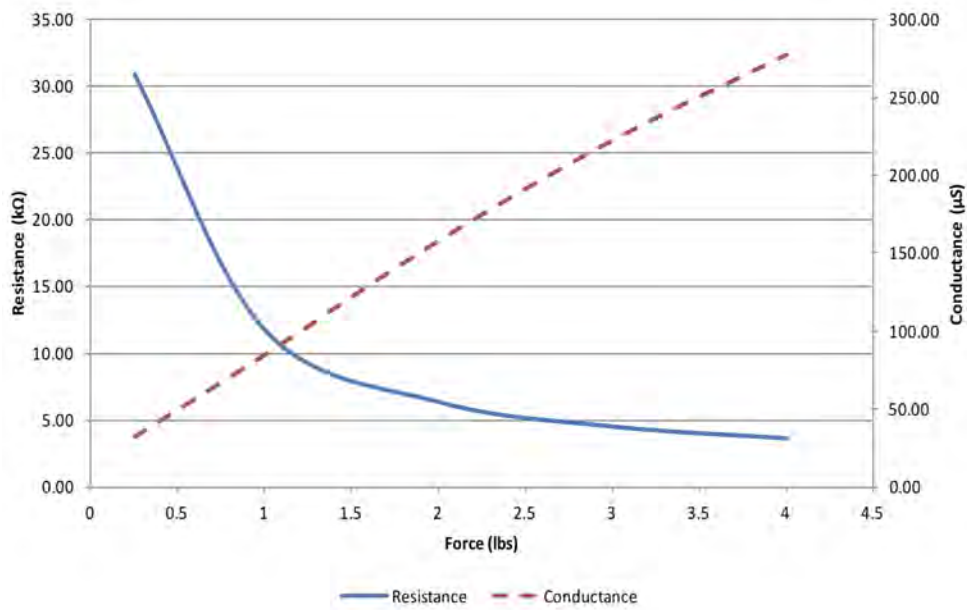


Figure 8.5: Relation between resistance and conductance to force from *Data sheet FlexiForce Standard Model A101* 2019

## 8.5 Circuit for resistive measurement

To achieve a linear output the data sheet suggests a circuit example similar to an inverting amplifier as seen in figure 8.6 [see *Data sheet FlexiForce Standard Model A101* 2019]. Since

this circuit is already tested for the sensor and recommended by the fabricator it will be used slightly modified for this work, too.

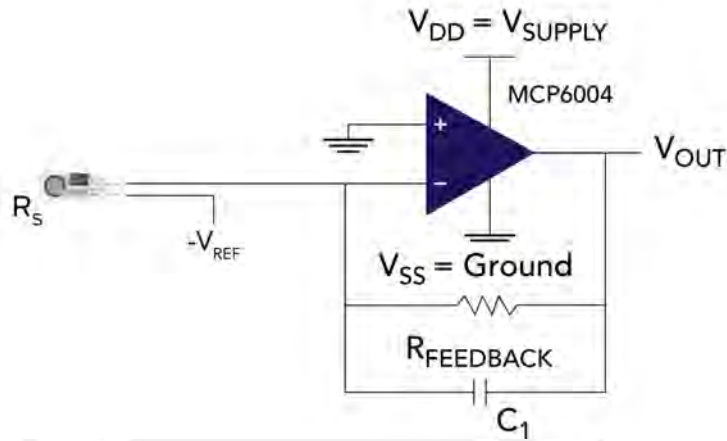


Figure 8.6: The suggested circuit from the data sheet of the sensor [*Data sheet FlexiForce Standard Model A101 2019*]

To achieve a negative drive voltage without an extra power source, the ground of the measurement circuit will be virtual. This means that the poles that are connected to a negative voltage in the example circuit will now be connected to ground. While the ground pins of the circuit will be connected to a small positive voltage. This leads to a negative potential between the positive input of the opamp and the input of the sensor. The maximum output voltage of the Arduino is 5 V [Arduino AG 2019]. To achieve a good signal to noise ratio the voltage output of the circuit should be as high as possible. A rail to rail amplifier with its low output voltage swing is needed to drive output voltages close to the supply voltage. Also a low noise and power consumption is mandatory. The AD8606 from Analog Devices seems to be a good choice. The output voltage can be calculated as follows:

$$U_{out} = -U_{ref} \cdot \frac{R_{feedback}}{R_{sensor}} \quad (8.15)$$

where  $U_{ref}$  is the reference voltage and  $R_{feedback}$  is the resistance of the feedback resistor. One can clearly see that when the resistance of the sensor is greater than the feedback resistance the voltage is lower than the reference and when the sensor resistance is higher the voltage is amplified. This means the feedback resistor has to be chosen well in order to measure the whole range of resistances which reaches from around 50 k $\Omega$  down to as low as 1 k $\Omega$  on full load. The opamp works best within the middle of its output range where there is a reserve to the minimum as well as to the maximum output voltage. This

way output voltage swing and sudden voltage fluctuations do not affect the output. It may therefore be good to design a variable reference voltage using a PWM signal which is smoothed by a low pass filter. This way the controller can set different reference voltages by changing the pulse wide of the signal. Also the capacitor placed in the feedback loop to eliminate high frequency noise has to be chosen in order to support the needs of the application. To estimate the behavior of the circuit a simulation with the software LtSpice was made (see appendix). It was found that  $10\text{ k}\Omega$  is a good value for the feedback resistor. The capacitance in the feedback circuit is suggested to be  $47\text{ pF}$  when an  $100\text{ k}\Omega$  resistor is used. Since the feedback resistor used in this circuit is far smaller and the cut off frequency can be lower, a bigger capacitance is chosen. Tests revealed that  $100\text{ nF}$  seem to produce a low noise and are working well in this setup. The used parts are inexpensive and the Arduino possess six analogue inputs which can be used for measurements. Every FlexiForce sensor will be connected to its own amplifier circuit. To make sure the circuit works properly it was built up and connected to a variable resistance as shown in figure 8.7. The results where very close to the calculation and observing the outputs using an oscilloscope showed good noise to signal ratios. After the test the variable resistor was exchanged for a connector to use the board with the force sensor.

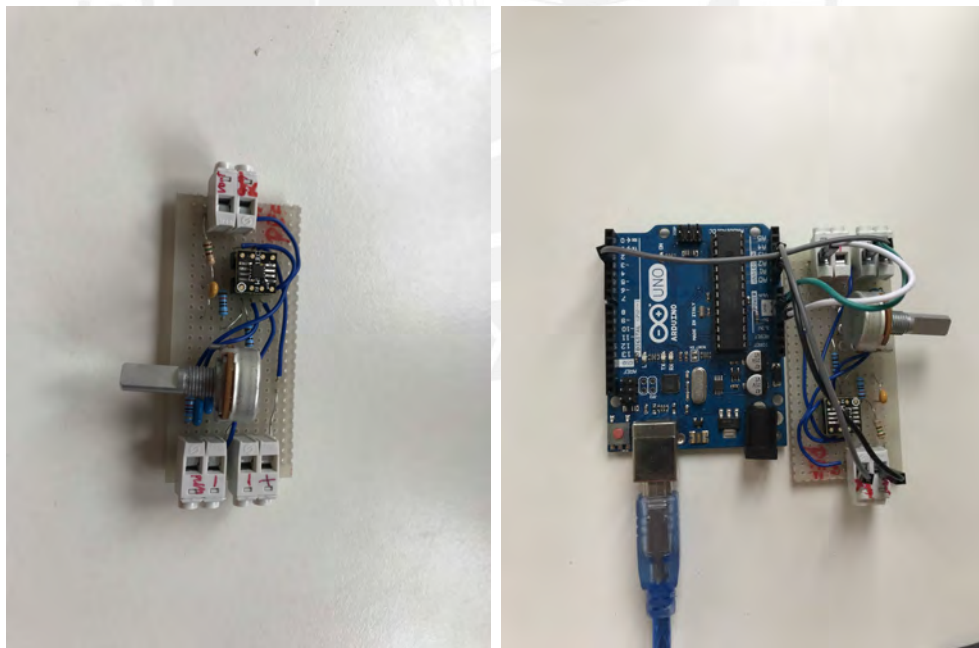


Figure 8.7: The built up circuit with a potentiometer for testing

## 9 Data acquisition

To build up a working prototype, the measurement has to be conducted and the values have to be processed. The following sections will explain the steps that were taken to achieve values and to process them. As earlier mentioned in the requirements, the data bus will not be focused and a slow but easy to handle serial connection was used. The main processing of the data like filtering will be done using MATLAB on first hand since it is easy to visualize data and to modify the code. Later on the final processing could be implemented in the micro controller itself. As development platform the Arduino Uno is used.

### 9.1 Programming the micro-controller

The Arduino can be programmed in a C based language. The designed programs to run the sensors can be seen in the appendix. The following section will briefly explain the basic routines and functions in order to understand the procedure. The techniques for capacitive and resistive measuring differ, which means they need different programs. Nevertheless the frame stays the same and only the crucial parts were changed. This way the programming effort can be reduced because most parts like the sending of the data stay the same. Just the measurement routine and the calculation of the values had to be designed twice. The program starts with a setup where the serial connection is prepared and the communication with the BMP180 sensor, used as temperature sensor, is initialized. To avoid overfull buffers, the program than waits in a loop until it receives a start signal via the serial connection. There are two modes of measurement implemented. One continuous mode where the micro controller sends the value measured for each channel one after another and repeats this continuously. The program can also change into a passive mode where it waits for a command indicating the desired channel. Then it measures the value and returns only the requested measurement result. Afterwards it waits again for a signal. This method is slower but it helps to prevent overfull buffers when the receiver is driven manual or by a slow software which cannot handle the data fast enough. Table 9.1 shows the available commands which can be processed by the program.

Command [char]	Description
'0'	channel 0 (passive mode)
'1'	Start the continuous measurement / channel 1 (passive mode)
'2'	Pause the continuous measurement / channel 2 (passive mode)
'3'	changing format of sent data / channel 3 (passive mode)
'4'	setting the delay for the measurement / channel 4 (passive mode)
'5'	setting the number of measurements
'p'	Change to passive mode
'a'	Change to active mode

Table 9.1: Available commands for serial communication

The channels 0 - 3 are declared to be the channels representing the results of the four force measurements and channel 5 returns the measured temperature. The data can be send via the serial connection in two formats. One option is to send the data as strings. This way they can be plotted directly to the monitor by using for example the serial monitor of the Arduino IDE. If the data is send to a program processing it, binary sending can be chosen. In this mode the bytes representing the values are send directly. This has the advantage that the number of sent bytes is much smaller. But on the other hand the receiving program needs to know which data type to expect in order to decode the information. The basic steps done by the program in the main loop are the following. At first there it checks for incoming commands. If there is anything in the incoming buffer the program reads it out and processes the command. Afterwards the measurement depending on the selected channel is done. The output values are calculated and send via the serial connection. Afterwards the channel number for the next loop iteration is calculated and the bits to control the multiplexer are updated. Finally the program waits for the set delay time. This step is crucial because it controls the measurement rate, prevents overload of the serial connection and gives the multiplexer time to switch properly before the measurement. Then the process is repeated in the next iteration.

## 9.2 Program for capacitive sensing

For the measurement of the capacity the time needed to charge the capacitor voltage until it reaches the reference value is measured. The circuit needs an rectangular excitation voltage as input and gives a digital signal indicating the moment when the reference voltage is surpassed.

The rectangular input signal can be generated using one of the internal timers of the Arduino. Timer 2 seems to be a good choice. Using Timer 0 would not allow using

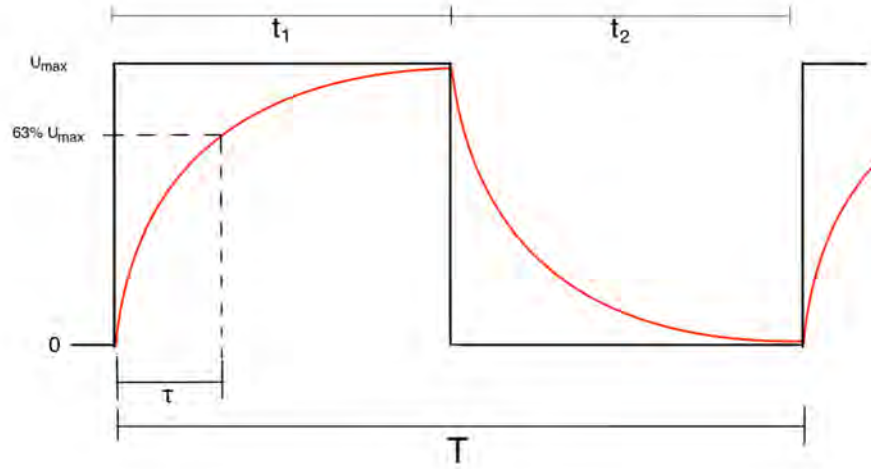


Figure 9.1: Sketch of the voltages while charging and discharging; black: input, red: Voltage on the capacitor

prescalers, since this timer also controls the delay function which might be influenced. Timer 1 is the only Timer with a 16 bit counting register. Its high resolution is more useful for measuring the charging time. The maximum frequency of the PWM signal can be calculated to assure the complete discharge of the capacitor between the measurements. Technically the voltage reaches the step voltage after  $5\tau$  with  $\tau = C \cdot R$ . After this time period the difference between the current value and the static end value is lower than 0.7 %. The measurement is finished after the time period  $\tau$ . It is not necessary to fully charge the capacitor. Therefore, the charging interval can be shorter. To make sure it is long enough it will set to be:

$$t_1 \approx \frac{1}{3}t_2 \quad (9.1)$$

For the PWM generation phase correct mode was chosen. There is no advantage in this case compared to fast PWM mode using this mode would bring according to the knowledge collected during this work the same effect. Just the values for the prescale and the compare registers would have to be calculated a new but in a similar way. In figure 9.1 one can see that the period is:

$$T = \frac{1}{f} = t_1 + t_2 \quad (9.2)$$

And with equation 9.1 one receives:

$$f = \frac{3}{4t_2} \quad (9.3)$$

For complete discharge the discharge time should be  $t_2 > 6\tau$ . With equation 8.2 this leads to:

$$f > \frac{1}{8\tau} = \frac{1}{8R \cdot C} \quad (9.4)$$

When using the phase correct PWM mode the timer counts upwards. The output is set when the timer register value reaches the timer compare register (OCRA2). It continues counting till it reaches the value  $N_{top}$  stored in the OCRA register and than counts back down. The output is reset when the value in the compare register is passed. From zero the counter starts to increment again. The frequency in this case is:

$$f_{pwm} = 16 \text{ Mhz} \cdot \frac{1}{2N_{top} \cdot prescale} \quad (9.5)$$

where *prescale* represents the prescale factor. There are various options to choose.

The time measurement is done using interrupts. One interrupt is attached to pin 3 which drives the excitation signal. On the rising flank when the charging of the capacitors starts the function "start" is called by the interrupt. This function resets the TCNT1 register which is the counting register of timer 1. This timer was previously in the setup adjusted to run without prescaling. One increment in the value of the TCNT1 register hence represents 4  $\mu s$  of time passed. The output signal of the sensor is connected to pin 2 of the board. An interrupt activated by a rising flank is attached to it, too. The rising flank indicating that the reference voltage was reached triggers the function "stop" which copies the value of the TCNT1 register to a global variable. The value read from the TCNT register ( $n_{time}$ ), representing the time needed, can now be used to calculate the capacity of the selected channel using the following equation.

$$C_{meas} = \frac{n_{time} \cdot 1000}{f_{clock} \cdot R} = \frac{n_{time} \cdot 1000}{16 \text{ Mhz} \cdot 5 \text{ M}\Omega} \quad \{C_{meas}\} = \text{pF} \quad (9.6)$$

To calculate the mean value of multiple measurements the functions "start" and "stop" can be extended by a counting variable called "turns". The variable is reseted at the beginning of the measurement to zero. Every time the "stop" function is called by the interupt the measured time is now added to the sum of previous measurements and "turns" is incremented by one. The main program meanwhile waits for a fixed period of

time. Afterwards the mean value of the passed measurements can be calculated from the sum value  $n_{total}$  by.

$$n_{time} = \frac{n_{total}}{turns} \quad (9.7)$$

### 9.3 Programm for resistive sensing

To do the resistive measurement the program needs to be changed. Here the aim is not to measure time periods between two signals as it was the case with capacitive sensing but to measure voltages. Before the actual measurement can start the PWM signal, used to set the input voltage for the circuit, has to be adjusted. To achieve a higher frequency of the signal fast PWM mode is used. This way the low pass filter produces a smoother output because the frequency is further away from the cut off frequency of the filter. The pulse wide can be set by changing the value in the OCRA register which is the output compare register. The output is turned out when the timer register TCNT, which is incremented constantly, reaches the value of the OCRA. Finding the right pulse width is done iteratively. The output voltage is measured and then compared to a desired voltage range of 2.5 V to 3.5 V. Note that in the program all the voltages are stored in mV to have more exact values because the double precision is only 8 bit on the Arduino uno platform. If the voltage is outside the boundaries the value in the OCRA register is reduced or respectively elevated. This is repeated until the output voltage lies in between the boundaries. Than the actual measurement can start. The two voltages needed, can be measured directly by the integrated ADC (Analog-digital converter) of the Arduino. It has a resolution of 10 bit. Note that the accuracy could be improved by using a better external ADC with a higher resolution. To achieve good results anyway the measurement is repeated several times and the average value is calculated. Important is to know that the Arduino uses only one ADC to measure its inputs. If the selected input pin changes the program needs to wait a little time. If the measurement pin changes constantly without a short delay the results are useless and nonsense because the changing of the connected input needs a little time. Therefore, the two voltage measurements are done first for one pin and than all measurements for the second pin. Knowing the output voltage  $V_{out}$  and the reference voltage  $V_{ref}$  as well as the feedback resistance  $R_{feedback}$  the sensor resistance  $R_{meas}$  can be calculated.

$$R_{meas} = R_{feedback} \cdot \frac{V_{ref}}{V_{out} - V_{ref}} \quad (9.8)$$



# 10 Prototypes

To test the functionality of the chosen concept a prototype was designed following the determinations made in chapter 8.3. The following section will describe the built up prototype and the design process. The capacitive version is compelling because it does not need bought sensors and can be adapted easily to different needs. Therefore, the prototype will use this concept. During the development there was no mayor disadvantage of the concept compared to the resistive alternative noticed so it should work out good. Later on the expected results for a similar resistive version will be discussed.

## 10.1 Building the prototype

The mechanical transducer was designed using the Inventor Autodesk 2019 CAD software. Than it was 3D-printed. To make sure the spherical top is smooth, it was polished using sand paper. A 0.1 mm copper plate was cut out to fit the bottom of the transducer. On one edge the plate has a bridge to connect it later to the electric circuit on the board. The plate and the transducer were glued together as shown in figure 10.1



Figure 10.1: The force transducer with copper plate, top and bottom view

For the board design the software Autodesk Eagle was used. The layout and the schematic can be seen in the appendix. For easy mounting through pin devices were chosen. This

leads to a way bulkier design but the main purpose of the prototype was to show the functionality. Later on designs can be optimized to occupy far less space than this first version. The used amplifiers were of the type INA121 from Texas Instruments. Testing them revealed that they need a reference voltage which is approximately in the middle between the two potentials of the supply voltage. Therefore, an extra conductive line was introduced providing all the amplifiers with a reference voltage. Note that reference voltage in this case does not mean the voltage reference for the measurement but a voltage required by the chip that was named reference voltage in the data sheet, too. The amplifiers are used to just switch between minimum and maximum output. It is therefore enough to simply connect the reference pin to the 3.3 V output of the Arduino. To achieve maximum amplification the gain adjust pins were connected by a shortcut. To build up the sensor areas of copper, forming the bottom electrode of the measurement capacitor, are needed. The easiest way to produce them was to design a device with the desired areas as its footprint in Autodesk Eagle. By surrounding normal connection pads with filled shapes the pads can be shaped to form the needed areas. The designed device can be integrated in the schematic like any other component. It can then be placed on the board layout. During the fabrication the areas will be milled out directly together with the other pads and tracks. Each electrode has its own connection. To improve the readability of the schematic a symbol for the sensing areas was designed. It is shown in figure 10.2.

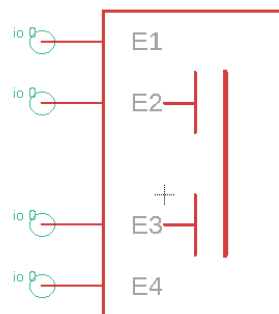


Figure 10.2: Symbol for the sensing areas in the schematic.

During the design a pin to connect the upper electrode was placed on the board. After some trials it was found more useful to solder the electrodes bridge directly to the board. The board was designed as a double layer board. By connecting the not used spaces to the ground potential the bottom layer works as a shield to reduce the influence of external fields on the measurement. That is why no tracks cross the sensing area on the bottom layer. This way a closed copper area with ground potential is achieved. The sensing areas

are a few millimeters wider than the transducer to make sure the upper electrode is fully covered. The tracks connected directly to the sensor areas can easily couple in interference fields. To minimize their influence on the measurement the conductive tracks connecting the sensing areas to other components have to be as short as possible. Therefore, no chips with multiple amplifiers were chosen but single amplifier chips were connected to each area and placed as close as possible to it. Also the resistors connected were placed directly into the pads of the footprint of the sensing element. This causes a design rule check error because the software detects two elements in one hole. But this error can be ignored since the sensing element is on the board and nothing is soldered into the holes as it is normally the case. Pads to connect additional ceramic capacitors were placed for testing purposes and to have the possibility to adjust the offset capacitance. Also the possibility to connect an extra capacitor and amplifier was foreseen to potentially extend the prototype for a difference measurement in normal direction. Although it was not used later on. To connect the board to the voltage source and the controller pinhead connectors were used. The reference voltage which is compared to the voltage on the capacitor is produced by a voltage divider directly on the board. It will be connected to a digital output of the Arduino. A electrolyte capacitor needed to filter noise will not be placed on the board to be able to change it easily. Also the multiplexer needed to choose between the outputs will not be placed on the board. The produced board is shown in figure 10.3.

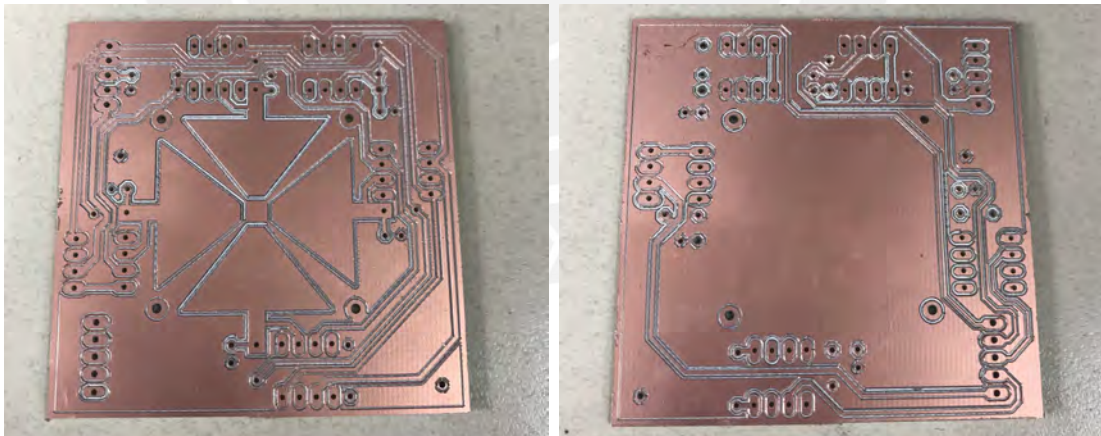


Figure 10.3: The raw board top and bottom view; dimensions 62 mm x 62 mm

The components were placed and soldered by hand. To fix some broken tracks beneath the amplifiers wire bridges had to be added at some points (see figure 10.4). Also the lines for conducting the charging current were damaged at some points. The easiest solution to fix this problem was to solder connectors directly to the resistors and connect them via cables. All the components that are needed but not placed on the board, like

noise filtering capacitors or the multiplexer are placed on a bread board that was placed next to the Arduino (see figure 10.5). This way the debugging and testing was easier because connections can be made fast and easily. There was also a BMP180 sensor on a breakout board placed next to the sensor to measure the environment temperature. Different materials had to be tested and changed frequently. Therefore, the dielectric layer was not glued to neither of the components. The sensor works anyway since the normal load holds down the top electrode and presses all the layers together.

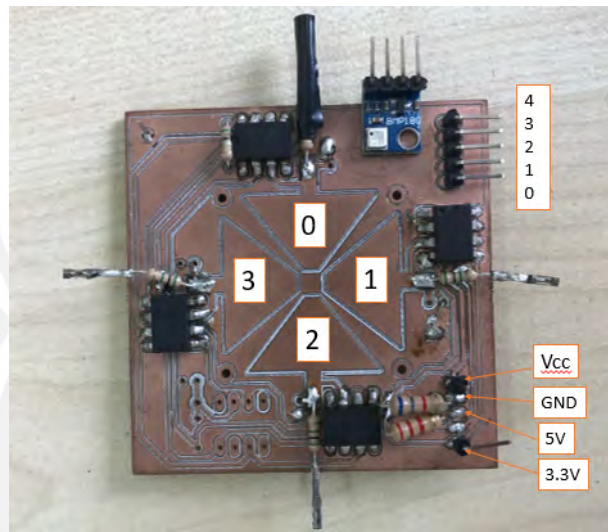


Figure 10.4: Stacked board with the signals connected to each pin

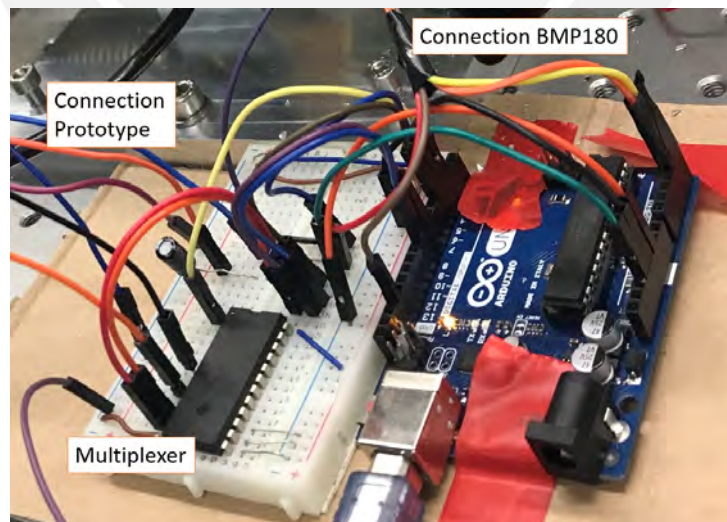


Figure 10.5: The Arduino together with the breadboard connected to the sensor

## 10.2 Improvement opportunities

After testing the board there are a few points that were not optimal and need to be improved in a future version. During testing it was noticed that the used INA121 amplifier works not fast enough. It is usually designed for measurement tasks not for fast reaction times. Observing the output voltage with an oscilloscope one can see that the flanks are not steep enough. Flanks that are not steep enough are not detected repeatable as rising flanks and lead to errors or rising uncertainties. Anyway two of the used amplifiers worked well and produced sufficient steep flanks so that the testing could be done using those two. With two sensing areas the prototype can still measure one shear force direction and the normal load. The areas 1 and 3 worked while the output of 0 and 4 was not steep enough and unpredictable. During this work it could not be completely clarified what exactly influenced the behavior of those two chips because they had also some unexpected irregularities in their output. Further developments need to change the amplifier necessarily. It is highly recommended to use a comparator instead of the INA121 amplifier. But it is still important that the chip has a high entrance impedance to make sure the bias current at its input is really low. It is also expected that steeper flanks on the output signal would increase the stability of the time measurement. During the assembly it was noticed that some of the tracks especially the ones carrying the PWM signal (see layout in appendix; label 'PWM') were too thin for the used milling machine to process them. The line turned out to be very fragile at some points and were accidentally damaged during the soldering. So the resistors had to be connected to the controller directly using wires. The input pins were connected on both layers to conductive tracks. But the fabricated boards had no conductive inlay in the drill holes, so the pins had to be soldered on the top as well as on the bottom layer. They are not designed for that and so soldering was very complicated. Looking on figure 10.4 it is visible that there was some trouble soldering the input pins which are on different sites of the board. During the assembly it turned out that the bottom electrodes do not need to be that much bigger than the transducer. It is very easy to place the electrode in a way that it is aligned with the bottom sensing areas. The surplus area of sensing area is a source of error that can be avoided or at least minimized by better fitting areas. This would improve the accuracy also. To reduce the impact of external electrical field even further a conductive shield could be designed that encloses the whole circuit. If it is made of a thin conductive foil it would be flexible and would not disturb the mechanical movement of the transducer. To build this the board has to be smaller and isolated to avoid short cuts when there is contact to the shield. In order to reduce the size of the peripheral electronic devices small SMD parts can be used.

This was not done for the prototype because soldering those tiny parts requires a lot of skill or even a machine doing this work. But for later designs that are integrated in an array of multiple sensors reducing the chip size will be indispensable.



# 11 Test stand

To evaluate the prototype a test stand was designed. It had to be able to measure forces in at least to axis in order to evaluate the sensor performance on normal load as well as on shear load. The following chapter will describe the build up construction and show the results of the measurements made to evaluate the performance of the test stand. The measured values from the sensor are compared to a reference measurement.

## 11.1 Construction

Figure 11.1 shows the design of the test stand. The sensor is mounted directly on top of two load cells which are used as force reference. Since the load cells have a distance between them, there will be higher influence of side load on the measurement of the single cells. This can not be avoided because of the nature of the construction. In section 11.2 this influence will be measured so that the measured values can be corrected.

The load cells are of the model SHBxR fabricated by Vishay and can measure a force in one direction each. They support a side load of 150 % of the maximum measurement force. That is why they can be safely stacked together with different measurement directions as shown in picture 11.2. To introduce the force to the sensor a plate made of aluminum is placed above it. Weights can be connected via a string and a deflection roller to generate a shear force. The normal force is also generated by weights which are supported by a metal plate lead by a linear guide. To avoid constraint forces caused by the small lateral shift of the contact point due to deformation of the load cells the linear guided support plate has to be separated by a ball bearing. The ball bearing itself can be seen in figure 11.4. Figure 11.5 shows the bearing integrated between the two aluminum plates in the complete set up test stand. To fix the sensor an adapter was mounted on the end of the upper load cell (see figure 11.2). The actual prototype is bigger than the final design. That is why an adapter plate needed to be designed in order to mount it (figure fig:adapter). It is important to support the board beneath the active sensing area to avoid a bending of the board when forces are acting on the sensor.

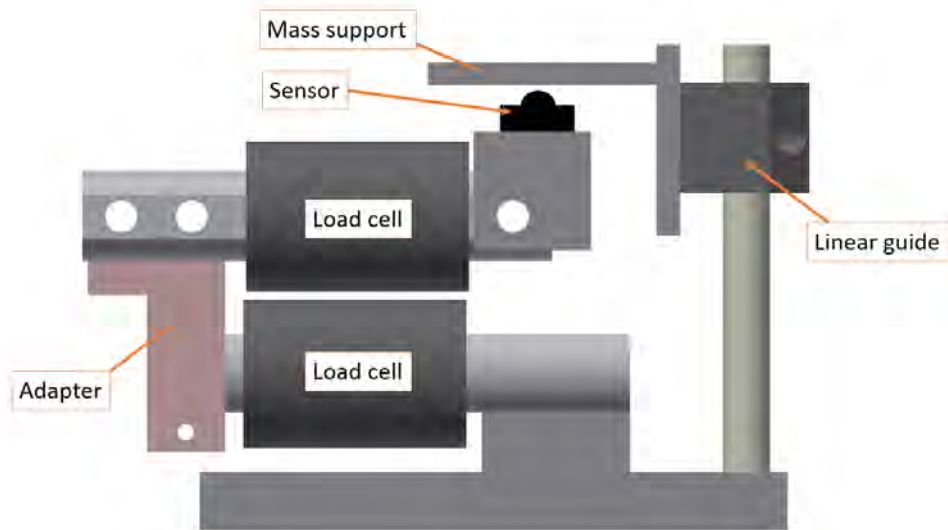


Figure 11.1: Design of the test stand

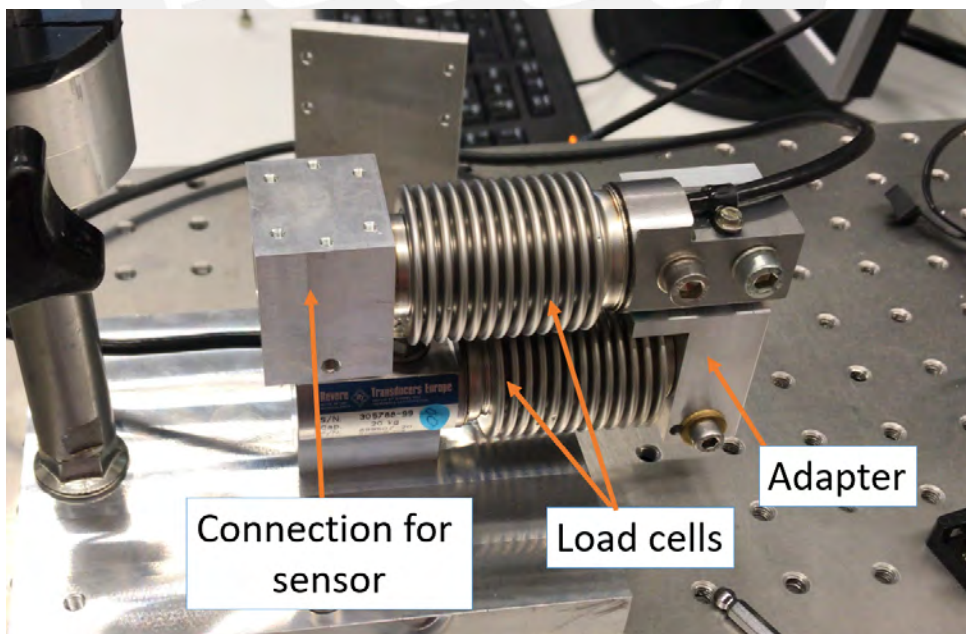


Figure 11.2: The mounted load cells



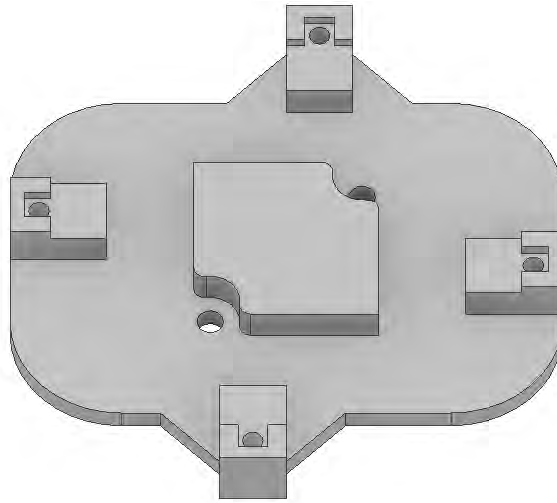


Figure 11.3: CAD model of the adapter

## 11.2 Evaluation

To evaluate the behavior of the test stand, several tests were conducted. At first the test weights needed to be calibrated in order to know their exact mass. To do this the masses were measured in an "ABBA" cycle using a Sartorius LC 6200 S balance and a class E2 1kg weight. Table 11.1 shows the results for the available weights and their uncertainties. Afterwards the outputs of the load cells were tested by putting the weights directly onto the single load cells without the guided plate. This way the acting force is known since it is directly introduced by the weights and can be calculated knowing the gravitational acceleration  $g$ .

$$F = mg \quad (11.1)$$

According to DIN 1305:1988-01 a value of  $g = 9.80665 \text{ m/s}^2$  was assumed. Figure 11.6 shows the output for both cells. The measurement was done using a DMP40 precision amplifier from HBM connected in six wire connection to the bridge. The supply voltage was set to 2.5 V in order to reduce the effects of self heating. The output of the DMP40 is given in mV divided by the supply voltage in V.

The behavior is linear. So the measured cell outputs can be translated into a force value

$$F_{x;z} = \beta_{x;z} \cdot V_{x;z} \quad (11.2)$$

The factors were estimated from the measurement by linear regression (see figure 11.6).



Figure 11.4: The designed ball bearing to reduce constraint forces

Number	Mass in g	95 % confidence interval in mg
1	497.518	3.3
2	504.392	3.3
3	994.845	4.4
4	1989.236	7.2
5	1993.901	7.2
6	4998.710	16.8
7	482.337	3.3
8	1001.020	4.4
9	1000.930	4.4
10	1001.385	4.4
11	1001.285	4.4
12	1007.319	4.4
13	1003.450	4.4
14	1003.625	4.4
15	4999.525	16.8

Table 11.1: Values of the masses used

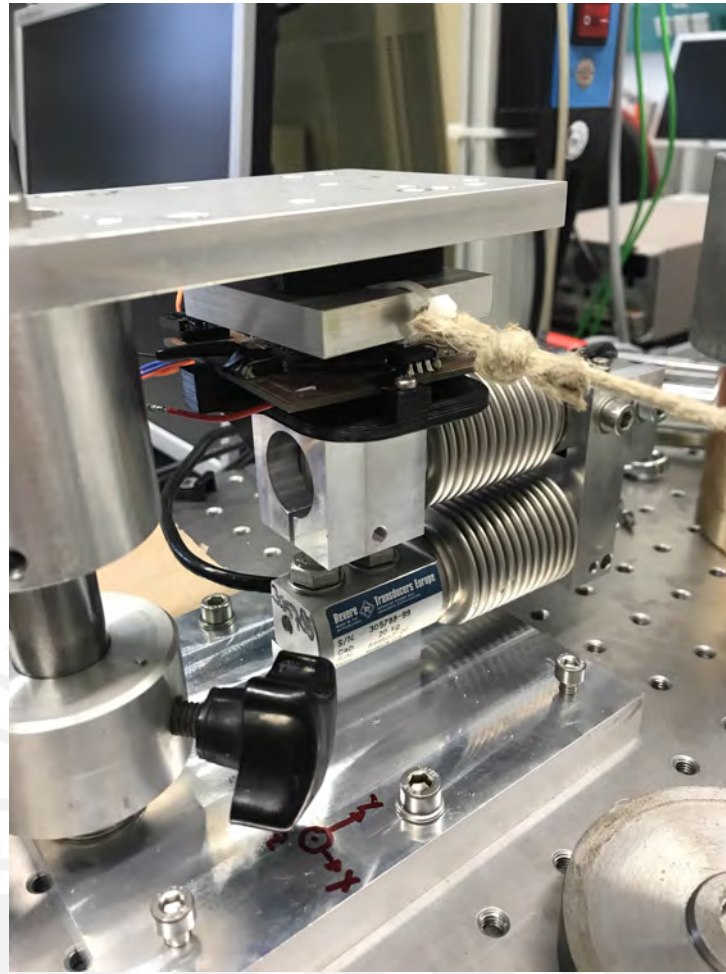


Figure 11.5: The complete test stand setup with shear force coupling and the ball bearing between the aluminum plates.

The estimated factors are:

$$\begin{aligned}\beta_x &= 98.746 \text{ N/mV} \\ \beta_z &= 98.704 \text{ N/mV}\end{aligned}\tag{11.3}$$

Afterwards the conjunction of the two cells was tested. They were mounted as shown in figure 11.2 and again directly loaded with masses. The repeatability was tested by repeatedly putting and removing the weights number 6 and 15 while measuring the output. The two cells together show an influence of the side load. To know the forces acting in each axis the output of the load cells  $\vec{V} = \begin{pmatrix} V_x \\ V_z \end{pmatrix}$  has to be corrected. The corrected output

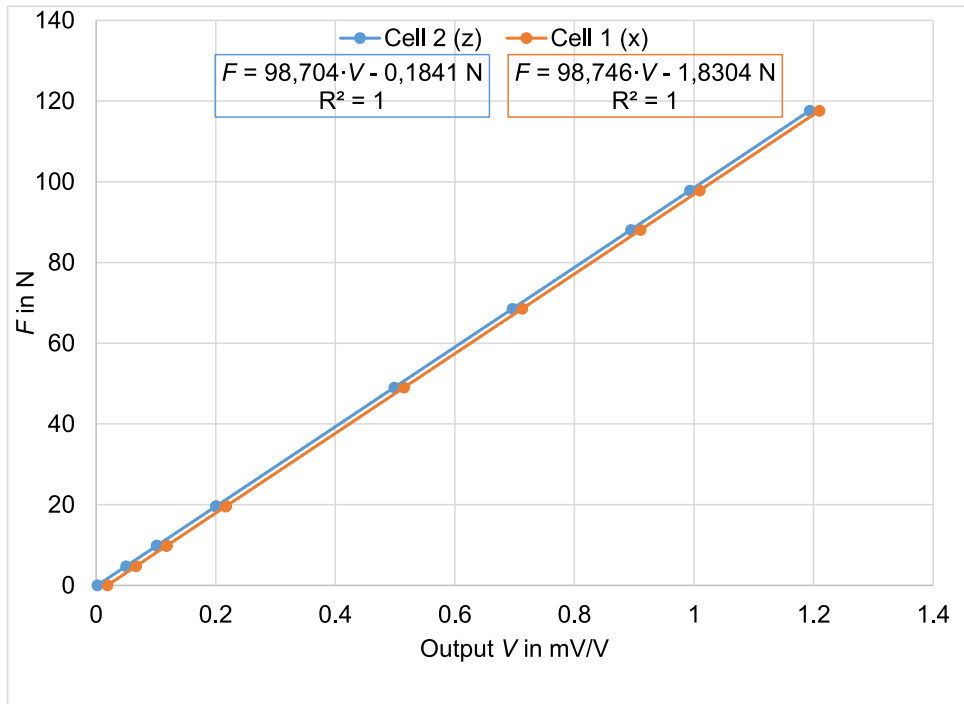


Figure 11.6: Output force to voltage relation for the single load cells and the equations calculated using a linear regression

will be called  $\vec{V}_{cor} = \begin{pmatrix} V_{xcor} \\ V_{zcor} \end{pmatrix}$  It is connected to the measured output by the following equation:

$$\vec{V}_{cor} = \begin{bmatrix} c_x & c_{xz} \\ c_{zx} & c_z \end{bmatrix} \vec{V} \quad (11.4)$$

To get the components of the correction matrix  $\vec{C}$ , the equation is transformed.

$$\vec{V} = \vec{C}^{-1} \cdot \vec{V}_{cor} = \begin{bmatrix} \gamma_x & \gamma_{xz} \\ \gamma_{zx} & \gamma_z \end{bmatrix} \vec{V}_{cor} \quad (11.5)$$

Now forces in only one axis were applied. Knowing that the force is either acting in x or in z direction one component of the corrected output should be zero. The resulting

equations are:

$$\begin{aligned} \text{for } \vec{F} = \begin{pmatrix} F_x \\ 0 \end{pmatrix} &\rightarrow \begin{pmatrix} V_x \\ V_z \end{pmatrix} = \begin{bmatrix} \gamma_x & \gamma_{xz} \\ \gamma_{zx} & \gamma_z \end{bmatrix} \begin{pmatrix} V_{corx} \\ 0 \end{pmatrix} \\ \text{for } \vec{F} = \begin{pmatrix} 0 \\ F_z \end{pmatrix} &\rightarrow \begin{pmatrix} V_x \\ V_z \end{pmatrix} = \begin{bmatrix} \gamma_x & \gamma_{xz} \\ \gamma_{zx} & \gamma_z \end{bmatrix} \begin{pmatrix} 0 \\ V_{corz} \end{pmatrix} \end{aligned} \quad (11.6)$$

The corrected output can be calculated using the factors  $\beta_{x;z}$ . The friction in the deflection roller for the shear force will be ignored since it is very small in comparison to the forces that were used during the tests (shear force 50 N)

$$V_{corx.y} = \beta_{x.y} F_{x.y} \quad (11.7)$$

This allows the calculation of the factors using the resulting equations.

$$\begin{aligned} \text{for } \vec{F} = \begin{pmatrix} F_x \\ 0 \end{pmatrix} &\rightarrow \gamma_x = \frac{V_x}{V_{corx}}; \gamma_{zx} = \frac{V_z}{V_{corz}} \\ \text{for } \vec{F} = \begin{pmatrix} 0 \\ F_z \end{pmatrix} &\rightarrow \gamma_z = \frac{V_z}{V_{corz}}; \gamma_{xz} = \frac{V_x}{V_{corx}} \end{aligned}$$

The inverse of the calculated matrix gives finally the correction matrix.

$$\begin{bmatrix} \gamma_x & \gamma_{xz} \\ \gamma_{zx} & \gamma_z \end{bmatrix}^{-1} = \begin{bmatrix} c_x & c_{xz} \\ c_{zx} & c_z \end{bmatrix} \quad (11.8)$$

The measured values are with a confidence interval of 95%:

$$\begin{aligned} \gamma_x &= 0.9880 \pm 0.00344 & \gamma_{zx} &= 0.0039 \pm 0.00036 \\ \gamma_{xz} &= -0.0427 \pm 0.00021 & \gamma_z &= 1.0140 \pm 0.00339 \end{aligned}$$

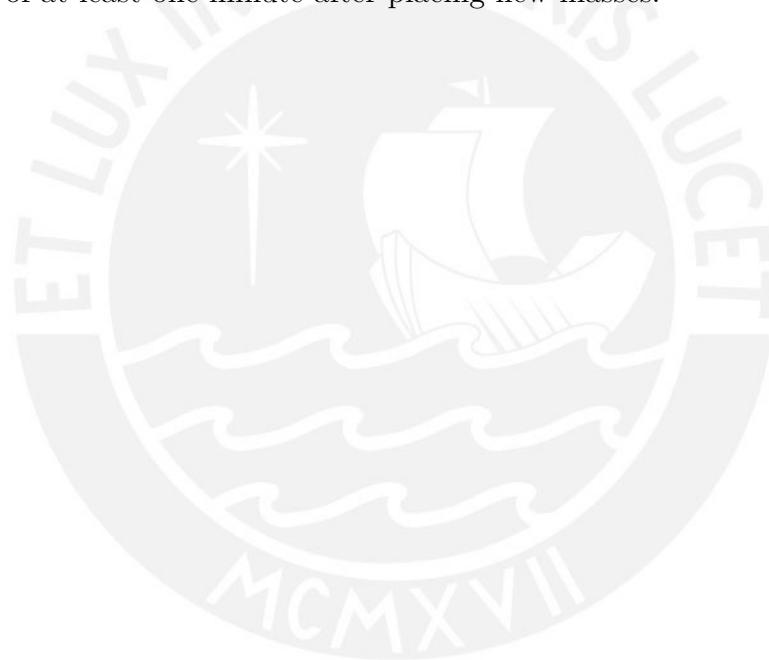
$$\begin{aligned} c_x &= 1.0120 & c_{zx} &= -0.0039 \\ c_{xz} &= 0.0427 & c_z &= 0.9861 \end{aligned}$$

Knowing the conversion factors and the correction matrix the acting forces can be calcu-

lated easily from the measured values as follows.

$$\vec{F} = \begin{bmatrix} c_x & c_{xz} \\ c_{zx} & c_z \end{bmatrix} \begin{pmatrix} V_x \\ V_z \end{pmatrix} (\beta_x \quad \beta_z) \quad (11.9)$$

The linear guide contains a sliding bearing. Due to its friction there is a creeping behavior. When masses are put on the table the force slightly changes. At the beginning the drifting speed is faster and it gets slower by the time. Because the measurements of the reference force and the sensor values can not be done completely simultaneously this creeping causes a small error. It turned out to help a lot to hit the bearing carefully a few times with a small hammer. This way the stick slip effect is overcome and the force settles way faster. Nevertheless to be sure the creeping is at a very low level the measurement was conducted with a delay of at least one minute after placing new masses.



# 12 Conducted tests

The following chapter will describe the tests done to specify the sensors behavior and to evaluate its suitability for the task. All the tests with the capacitive prototype were done using only two sensing areas, because the other two did not work properly as described previously in section 10.2. Because of the design with four sensing areas were two opposite ones are needed to measure each shear force component the sensor is still capable of measuring in one lateral direction. The measurement for the other axis works the same. That is why similar results are expected and a conclusion can be made also by measuring two dimensional loads in the tests.

## 12.1 Choosing a dielectric material

Lots of the sensor behavior depends on the dielectric material placed between the electrodes. Since technical data in means of linearity and permittivity are not really accurate for most plastics and rubbers, a suitable material is going to be chosen by testing various materials and comparing there behaviors. To find a material the selection was done in two steps. At first different materials were collected and tested to find a suitable group of materials. This group later on will be tested more exactly. The chosen materials for the first trial were:

- Polyethylene foil (PE)
- Thermoplastic polyurethane (TPU) thin 3D print 0.2 mm and 0.4 mm
- Silicone mold hardness shore A20 thin mold 0.2 mm - 0.8 mm
- Polyesterol foil (PS) 0.2 mm . 0.3 mm . 0.6 mm

The testing of the materials behavior will be done by putting weights on the sensor prototype. The capacities are measured for both sensor areas and compared to the force. Each result was the mean value of 50 single measurements. The resulting curves are then compared. The loads ranged from 0 N to around 50 N. Most of the tested materials show

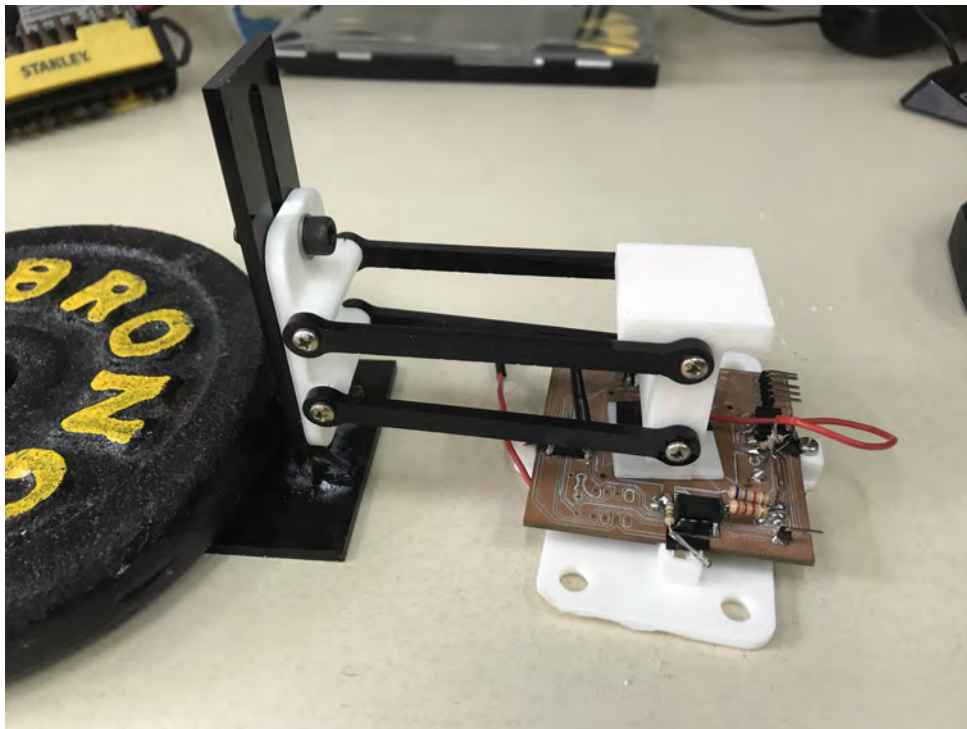


Figure 12.1: Construction to test different materials

a similar behavior. The functions can be approximated very good using an exponential function (as expected [1D-capa]).

The curves differed in the capacitance change over force. A material that produces a higher change in capacitance is favorable since it leads to a higher resolution. The graph in figure 12.2 shows an example for a too low change in capacitance on force. For higher loads the capacitance change on rising force is very small and leads to a bad resolution. Another unfavorable output showed the silicone for example as one can see in the graph in figure 12.3. The output can be approximated really good when lower forces are acting. But the function is too steep for higher forces. The change in capacitance between 10 N and 18 N is smaller than the uncertainty of the measurement. It would be impossible to distinguish between higher forces. For a lower force range this material might be good but it is not suitable for the task of this work.

Finally TPU was found to be a good material to use. Its output curve can be seen in figure 12.4. On the range of 0 N - 55 N the capacitance change is around 20 pF. Also the repeatability of the measurements appears to be good. Other materials e.g. the PE foils showed a big variation between single measurements. TPU as dielectric layer is a good trade-off between repeatability and capacitance range. That is why for the further investigations the focus will be on TPU as dielectric layer.



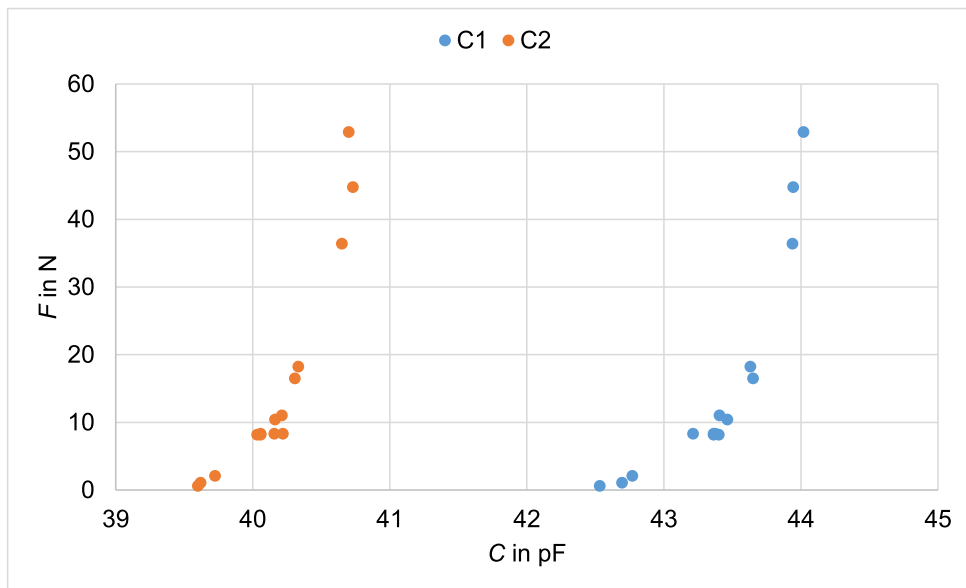


Figure 12.2: Force on output with 0.2 mm PS foil

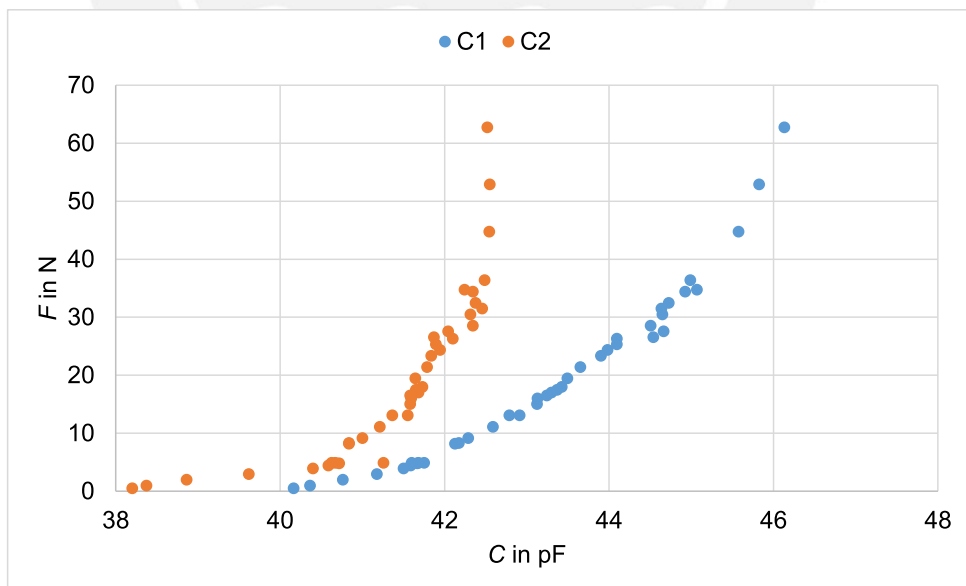


Figure 12.3: Force on capacitance with 0.5 mm silicone

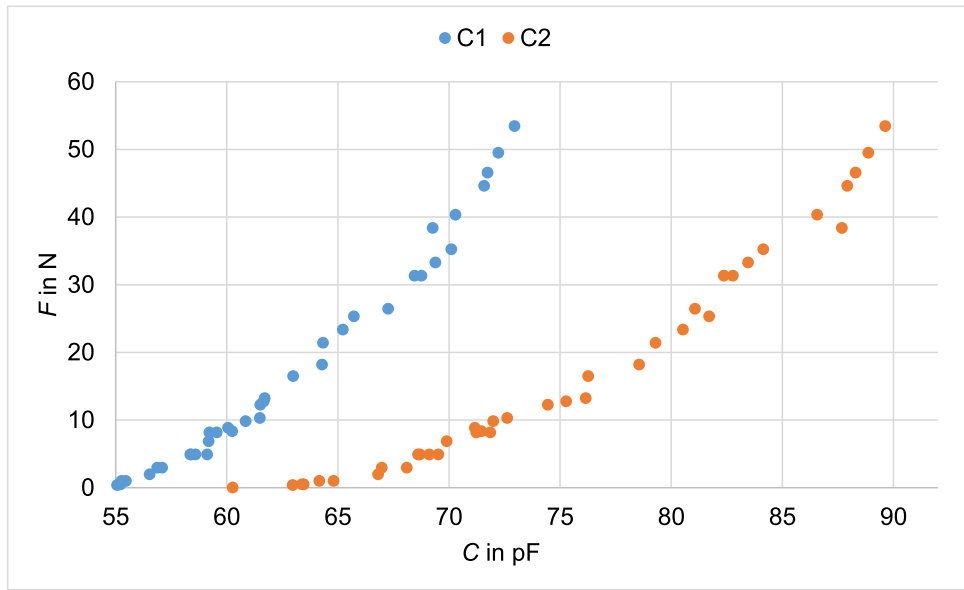


Figure 12.4: Output function with 3D-printed 0.2 mm TPU layer

The used TPU layer in the first trial was 3D-printed. This leads to a very inhomogeneous structure. Every printed piece behaves different and the trapped air also influences the results. To avoid errors from inhomogeneous materials, special TPU foils were ordered. The ordered samples are produced by the company Saxonymed. They are normally for the use in medical applications. The thickness of the tested samples ranges from 0.15 mm to 0.4 mm. The different types also differ in hardness. By testing those samples the best fitting foil should be found. The samples were at first cut in small quadratic pieces which could then be inserted between the sensor electrodes. The procedure of taking the curves was repeated for the TPU foils. The test force was stepwise increased up to a value of around 110 N. But this time the tests were already conducted on the test stand described in chapter 11. As approximation function the following was chosen:

$$C_{regression} = a \cdot F^b \quad | \text{with} : \{C_{regression}\} = \text{pF}; \{F\} = \text{N} \quad (12.1)$$

The outputs were similar but again differed in the change of capacitance. The comparison of the figures 12.5 and 12.6 shows that increasing the thickness does shorten the capacitance range as it was expected.

All the sensor curves were approximated using the function shown in equation 12.1. For all the materials the mean quadratic error of the regression was less than one percent. Differentiating the reversed function, that was found using the regression tool, one receives

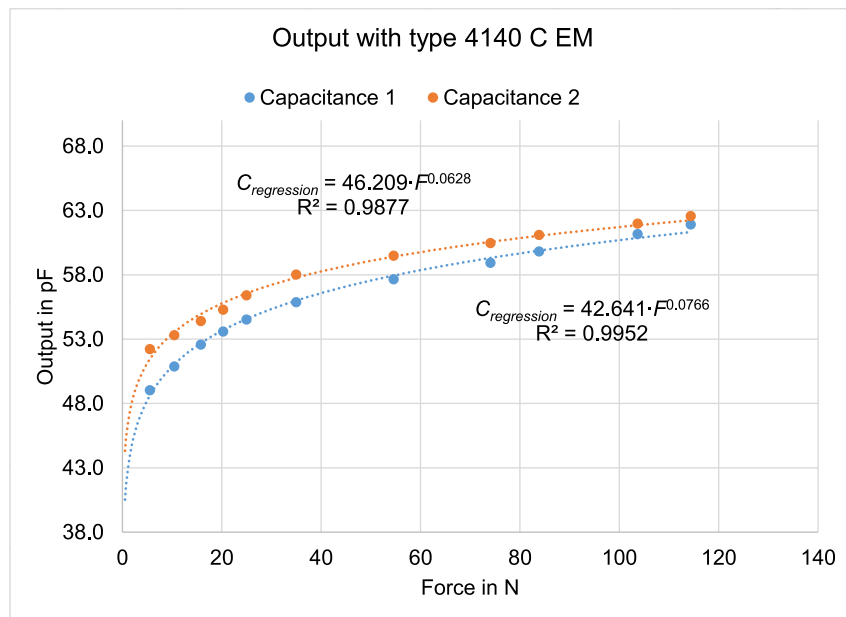


Figure 12.5: Sensor curve using the material 4140CEM; thickness: 0.2 mm; hardness: Shore A 93; small dots represent the regression curve

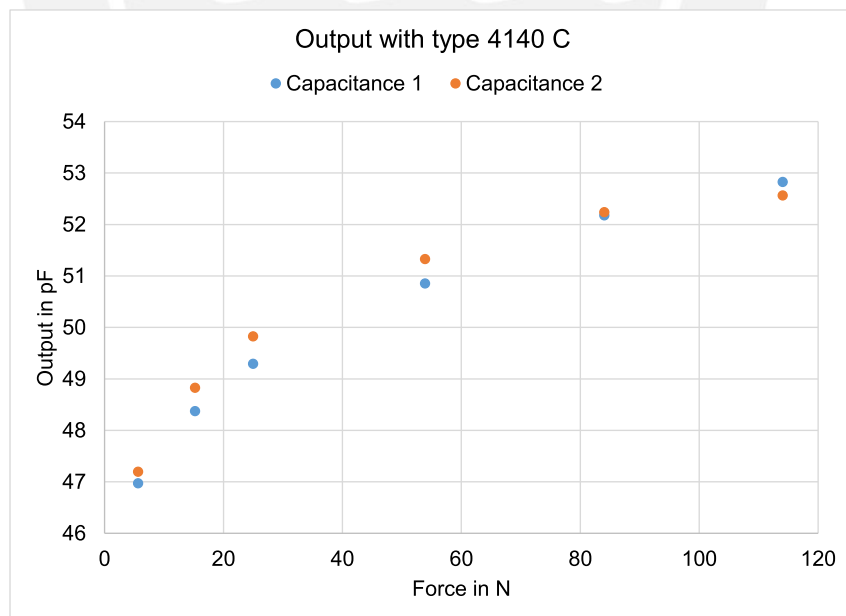


Figure 12.6: Sensor curve using the material 4140C; thickness: 0.4 mm; hardness: Shore A 93; small dots represent the regression curve

an expression for the theoretical sensibility with the used material depending on the force as shown in equation 12.2. The graph in figure 12.7 shows the resulting curves for all the tested materials.

$$\text{sensibility} \rightarrow \frac{dC}{dF} = a \cdot b \cdot F^{b-1} \quad (12.2)$$

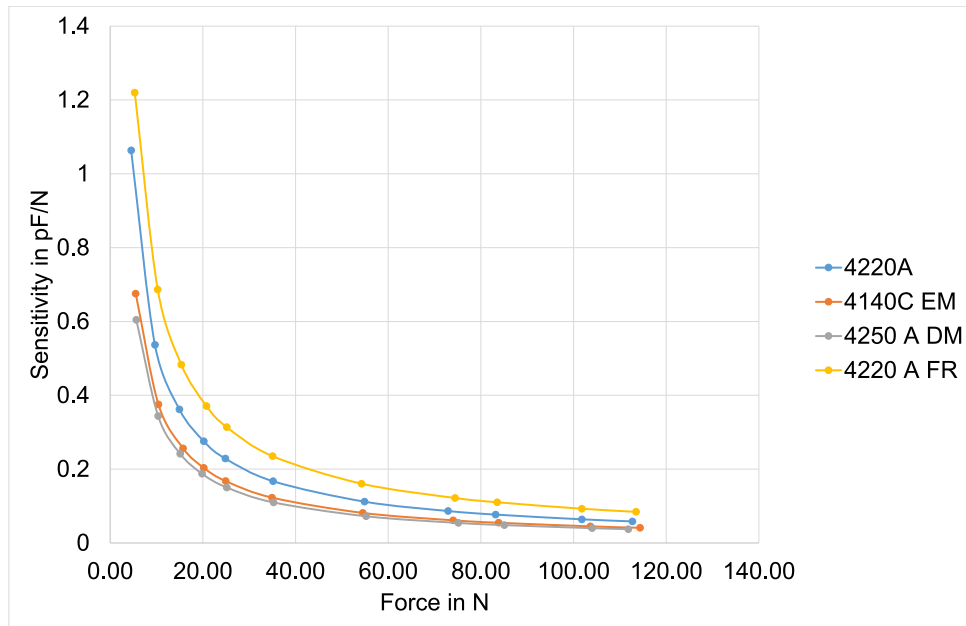


Figure 12.7: Comparison of the calculated sensibility for the TPU foils

The foil type 4220 A FR has the highest sensibility for all applied forces. But as to see in figure 12.8 the output does not match the regression function very well. Most likely the behavior changes due to the small thickness. The type 4220 A foil is of the same material but thicker. Its thickness is 0.25 mm. It has the second largest sensibility and the output with this foil fits the regression curve way better. That is why the foil type 4220 A was chosen to be used.

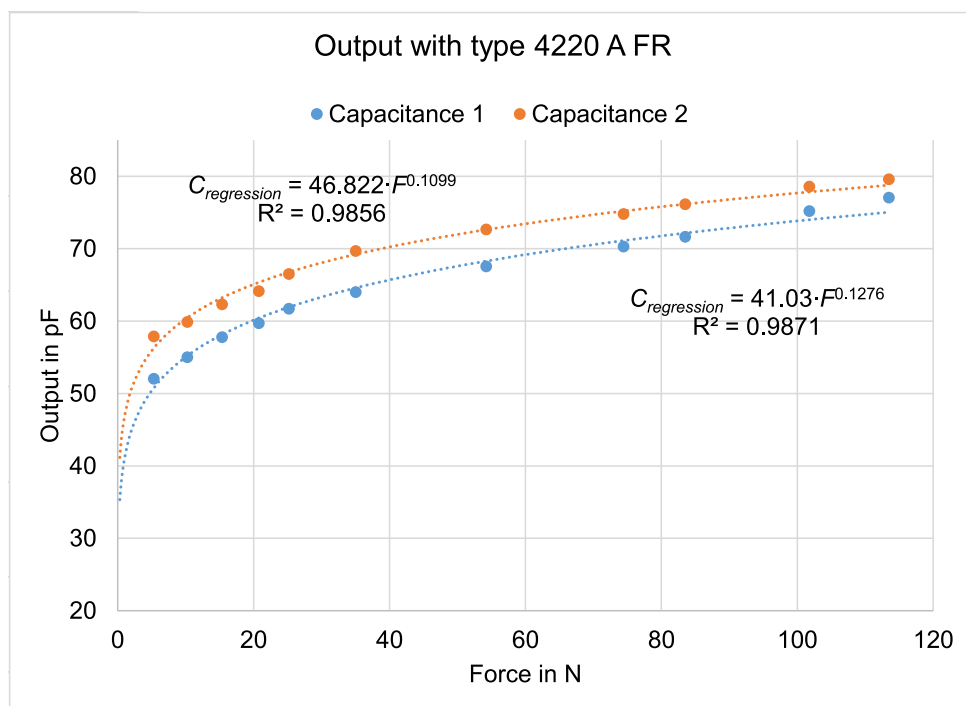


Figure 12.8: Sensor curve using the material 4140CEM; thickness: 0.15 mm; hardness: Shore A 86; small dots represent the regression curve

## 12.2 Characteristics of the capacitive sensor

After the material for the dielectric layer was chosen the sensor performance was evaluated. In the following the tests to characterize the behavior of the sensor and the results are discussed. At first the sensor curve has to be determined. Again masses were put to generate a normal load on the sensor element. The output and the measured reference force are compared in the diagram in figure 12.9. For the calculation of the normal force the sum of the capacities is used. Shear loads will cause the difference to change but the sum is supposed to stay the same. This way it is possible to distinguish between the force components.

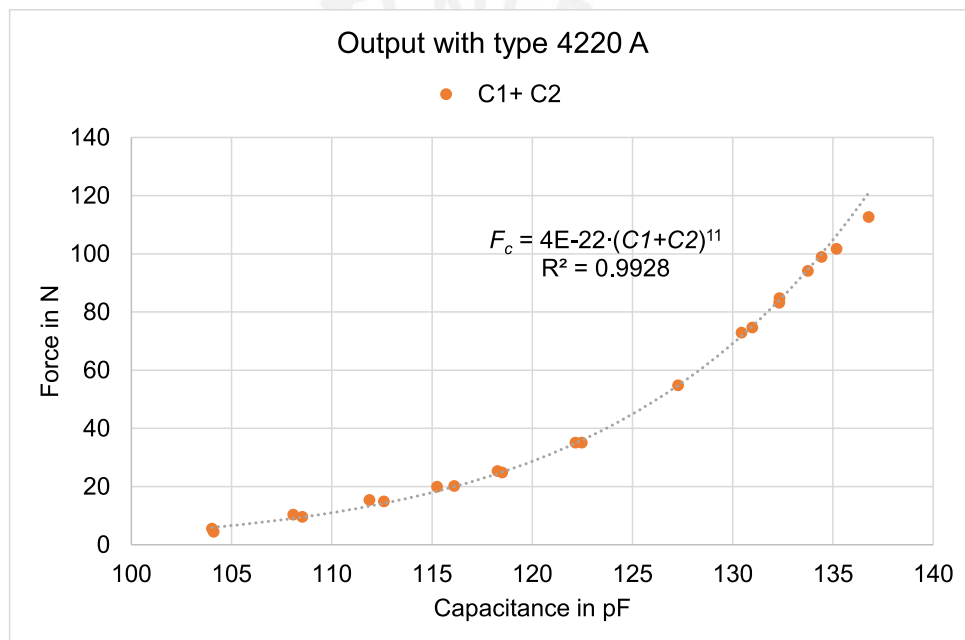


Figure 12.9: Force over the sum of the capacities and the regression using a potential function

The acting force is calculated using the equation:

$$F_c = a_z \cdot (C_1 + C_2)^{b_z} \quad (12.3)$$

For the test the following coefficients were estimated.

$$a_z = 3.866 \cdot 10^{-22} \frac{\text{N}}{\text{pF}^2} \quad b_z = 11$$

The contact between the sensor and the test stand is a punctual. Laterally acting force

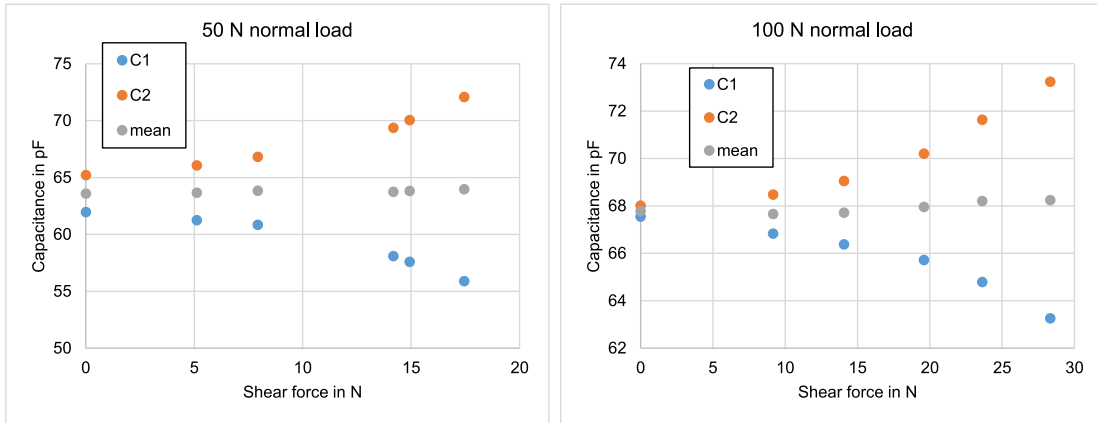


Figure 12.10: The measured capacities for different lateral loads; the gray dots mark the mean value

can only be transmitted via friction. This means the response to shear loads can not be measured without a normal load. Therefore a constant normal load was put onto the sensor during the measurement of the shear force response. Apart from that the procedure was the same. To verify that the found equation does not only work on one point the measurement was repeated with a different normal load.

The gray dots in figure 12.10 marking the mean value show that the shear force has no impact on it. It is also visible that the shape of the function describing the variation of capacitance due to shear load is the same for both loads. One function for regression can be used. Eventually the factors have to be adjusted according to the measured normal load. This will not be researched further on this work since the purpose of the tests presented here is to proof the general functionality. As one can see in figure 12.10 the output produced by force follows a quadratic form. To calculate forces from the measured capacity difference the square root operation can be used. The following equation was used to map the forces on the measured capacitance differences.

$$F_c = a_x \cdot \sqrt{C_2 - C_1} \quad (12.4)$$

Figure 12.11 shows the results of the regression for a normal load of 50 N. The function fits the measured values very good. The following factor was used.

$$a_x = 4.936 \frac{\text{N}}{\sqrt{\text{pF}}}$$

In order make the function work for a varying normal load is has to be supplemented by a dependency for the actual mean value (indicating the normal load) and a offset compensation (offset difference varies depending on the normal load). The complete

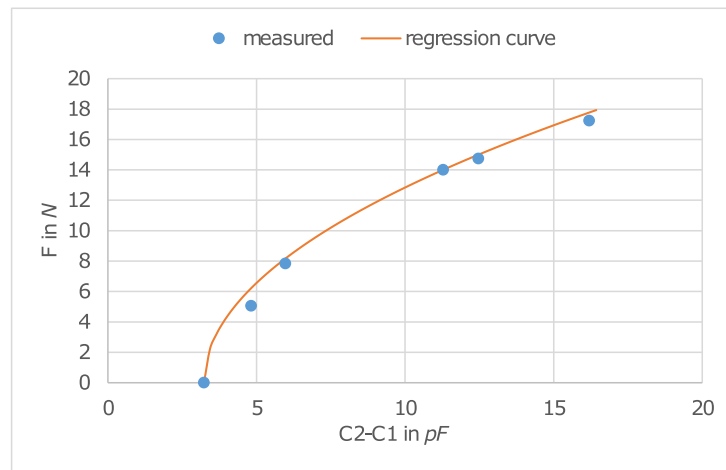


Figure 12.11: Shear force over the difference of the capacitances (dots) and the output of the function used to calculate the force (line); normal load 50 N

equation is then:

$$F_c = a_x(C_{mean}) \cdot \sqrt{C_2 - C_1 - C_0(C_{mean})} \quad | \quad \text{with : } C_{mean} = \frac{C_1 + C_2}{2} \quad (12.5)$$

The functions for  $C_0(C_{mean})$  and  $a_x(C_{mean})$  were not estimated but this could be easily done by taking the shear load curves with different normal loads and comparing the coefficients of the resulting functions.

To get information about the stability of the measurement it was repeated with the same load and the outputs were registered. From the variation of the measured force compared to the reference force the standard deviation  $S$  can be calculated.

$$S = \sqrt{\frac{\sum_{i=1}^n (x_i - \bar{x})^2}{n - 1}} \quad (12.6)$$

Note that the sensor had to be disassembled after the estimation of the output curve. This changed the offset values of the capacities. The curve stays the same but because the calibration was not repeated there is a force offset. As one can later see this does not effect the repeatability. The measurement was done by placing the weights and waiting around three minutes to allow the test stand to settle and to reduce the creeping influence. After the values were recorded the weights were removed. After around two minutes the procedure was repeated. To predict the accuracy of the single measurement conducted with the sensor the 95% confidence interval  $CI$  for the single measurement was calculated. The calculated values for the interval are of that size that with a certainty of 95 % the



expected value lies inside that boundaries.

$$CI_{95\%} = S \cdot t^* \quad (12.7)$$

Table 12.1: Repeatability ca. 100 N

temp. in °C	$F_z$ in N	$(C1 + C2)$ in pF	$F_c$ in N
25.9	103.41	136.379	117.18
25.7	103.74	136.241	115.88
25.5	103.31	136.722	120.46
25.8	104.77	136.578	119.07
25.1	104.83	136.732	120.56
25.4	104.01	136.762	120.85
25.9	104.45	136.781	121.03
25.1	104.03	136.796	121.18
25.4	104.95	136.912	122.32

The results of the repeatability have a mean force offset of  $\bar{\Delta F} = 15.67$  N. The standard deviation of the force difference  $\Delta F$  is  $S_{\Delta F} = 1.85$  N. Looking at the decreasing sensitivity with rising force it is to assume that the repeatability will improve if lower forces are measured because uncertainties in the capacitance measurement will not effect the result that severe. Therefore, the test was repeated with lower normal loads. The results proof that assumption.

From table 12.2 it is clear to see that a reduction of the force range would result in a better accuracy of the measurement. But even four percent are a good value for a low budget version like the presented one.

The repeatability was also determined for the shear force measurement. A constant load of 50 N was applied on the z axis. The measured values are displayed in table 12.3. This result shows that the sensor measurement matches the reference force when it is not disassembled after calibration which is obviously not the case in real use because the layers will be glued together. The deviation is  $S = 0.278$  N this results in a confidence interval for the single measurement  $CI_{95\%} = 0.628$  N.

Table 12.2: Standard deviation and confidence interval of the single measurement for different loads

$F_z$ in N	$S$ in N	$CI_{95\%}$ in N
100	1.85	4.27
40	0.5	1.15
5	0.155	0.36

Table 12.3: Measured values repeatability shear force

$F_x$ in N	$F_z$ in N	$C2 - C1$ in pF	$F_c$ in N
10.43	55.29	10.61	9.39
10.30	55.49	10.88	9.73
10.47	55.45	11.19	10.11
10.40	55.39	11.11	10.02
10.06	55.52	10.93	9.80
10.24	55.42	11.12	10.03
10.31	54.00	11.05	9.95
10.27	55.11	10.76	9.59
10.11	55.45	11.07	9.97

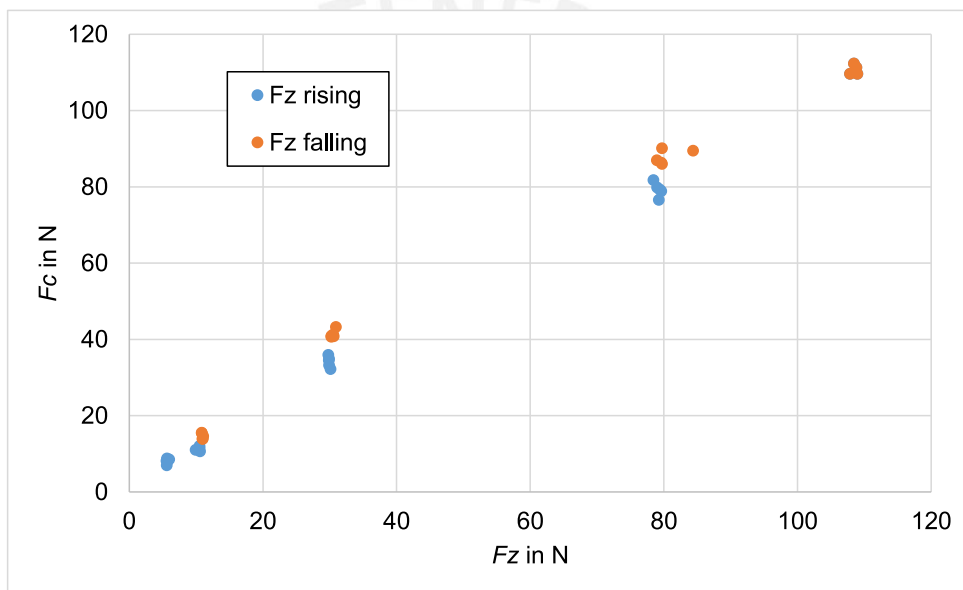


Figure 12.12: Hysteresis of the sensor with rising and falling normal load

The sensibility and also the accuracy of the shear force measurement could be augmented by increasing the height of the transducer. Till which point this makes sense would have to be researched in further work on the prototype. Sensors using polymers tend to show hysteresis effects when acting forces change. Therefore, the sensor was tested on its hysteresis. In four cycles the force was step wise increased up to 100 N and the decreased step wise. Between every step there was a delay of around three minutes. The results are shown in figure 12.12.

One can see, that initial and and value do not significantly drift during the measurement. Between the first measurement and the last nearly two hours have past. So a good time stability is shown. The hysteresis is clearly visible. The difference between rising and falling curve is of multiple newtons and bigger than the confidence interval estimated.

The influence of the hysteresis is significant and can influence the measurement. More detailed research on the hysteresis of this sensor is recommended because the performance could be improved here. During the tests a drift of the output values especially on high forces was noticed. Therefore a further research to estimate the drift behavior was conducted. The Arduino was connected to a computer and made to send the measured values in continuous time intervals. The chosen measurement was 4.5 s per sample. The measurement was started with no load on the test stand. After a while the normal force was increased to 100 N. Finally after 15 more minutes the load was removed again. This way the creeping behavior in both directions can be mapped. In the resulting curve one can see the drifting in the loading step. Even after minutes of time the drifting can still be noticed and during the measured period the drifting on the loading step resulted in a change of measured output of more than ten Newton while the reference measurement indicated a drift of the force that is small in comparison (see figure 12.13).

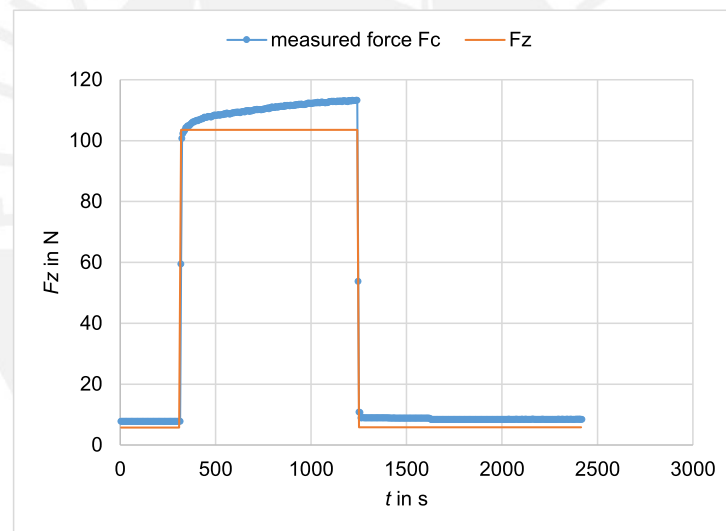


Figure 12.13: Creeping of the sensor output compared to the normal load  $Fz$  measured by the reference

There is also creeping behavior on the unloading step but due to the scaling it is not clearly visible in the measurement. Figure 12.14 shows a second measurement made to show the creeping on the unloading step. After some minutes waiting the preload of about 100 N was released and the values from the sensor as well as the values from the reference were noted. One can see that the extent of the creeping is lower than it is on the loading step. This is plausible and was expected. Nevertheless the creeping is after five minutes still noticeable. Interesting for the evaluation of the sensor is also the drift of the zero point. It was not possible to measure the exact zero point drift, because the layers are

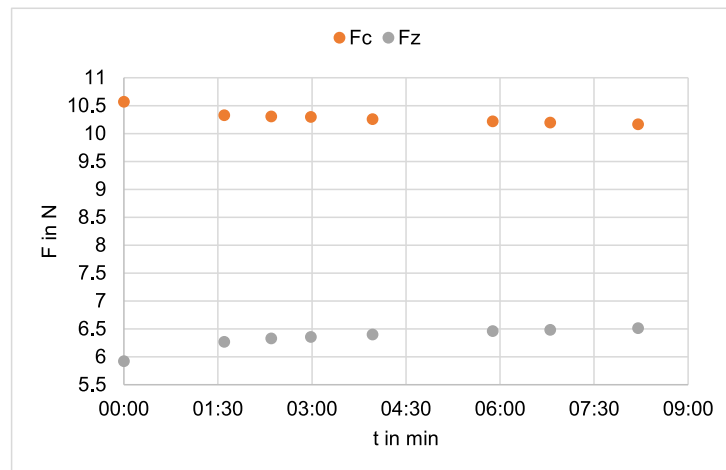


Figure 12.14: Creeping of the calculated force  $F_c$  after a reduction of the normal load from 100 N to 6 N

not permanently glued together to allow a change of the dielectric layer. If there is no load on the sensor the transducer would lift up. That is why a small load was put to hold down the transducer. The ball bearing was used for this purpose as shown in the picture in figure 12.15. The values were recorded for around half an hour and filtered with a FIR median filter with the degree 20. For the normal force measurement one can see clearly the influence of the temperature. The measured force moves all the time in the opposite way as does the temperature. Because of the thin layers the temperature response is surprisingly fast. While the shear force measurement shows a less noticeable influence of temperature. This was expected because the shear force measurement uses the difference of the capacities. The temperature on the other hand influences both capacities in the same way. This influence is canceled by the difference. The normal force nevertheless seems to be more stable. It varies with the temperature but only about a few hundredth of a Newton while the difference between the minimum and the maximum value measured for the shear force is roughly 0.4 N. A possible explanation for this might be that the measurement of the capacitance is also prone to temperature influence. The serial resistance slowing down the charging for example is influenced by temperature. The function for the normal force calculation is the shallowest close to zero. Therefore a varying capacitance has low impact on the output. Most likely the drift would be higher with a greater normal load. The function for the calculation of the shear forces on the other hand is steep at zero. This causes a greater influence of the capacitance measurement.

The sensor itself was really resistant to overload. It was exposed to a normal load of 200%  $F_{max}$  (around 200 N) without any damage or malfunction. This makes it favorable

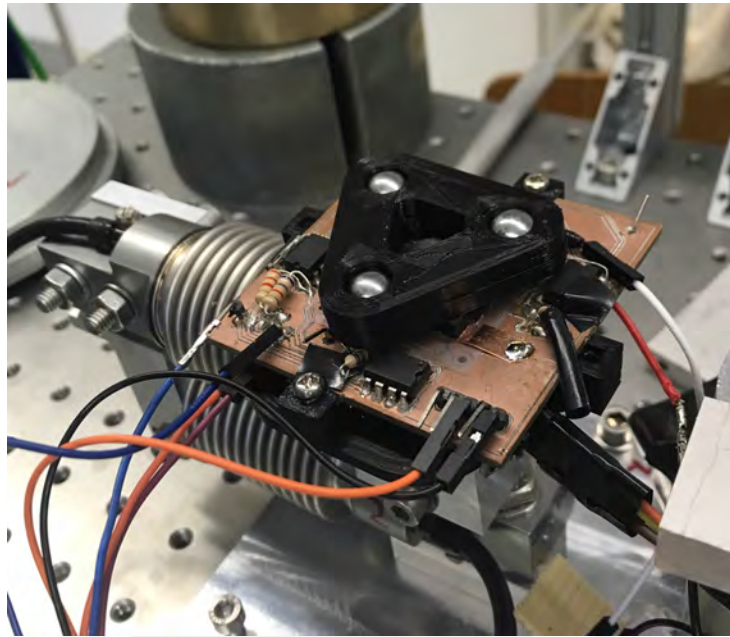


Figure 12.15: Sensor with the ball bearing as weight to prevent the transducer from lifting off

for the use in the prosthesis, where unexpected force peaks could occur during the use in many cases.

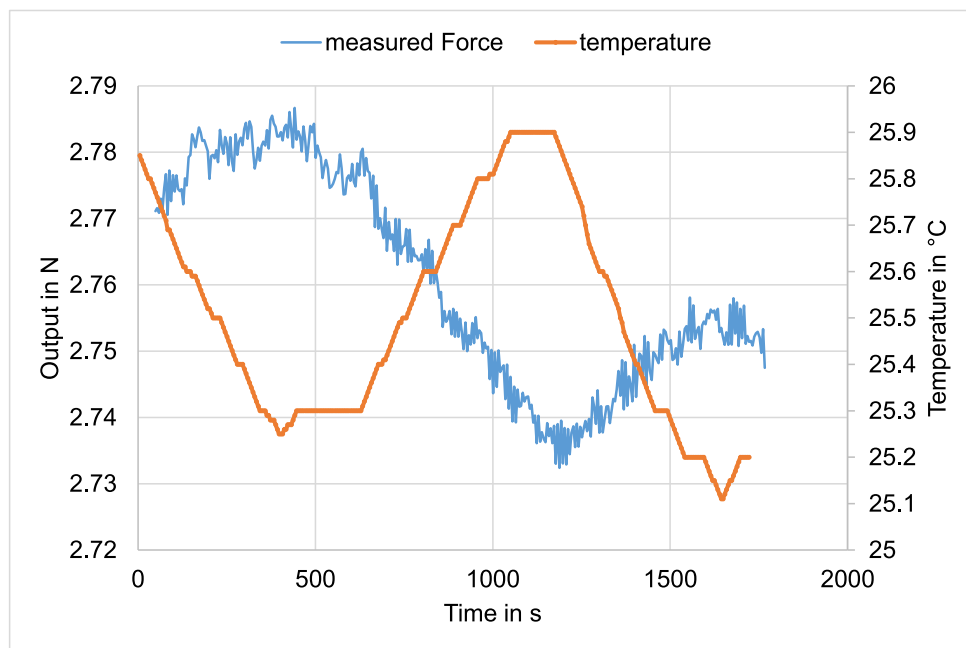


Figure 12.16: Drift of the normal force measurement near the zero point

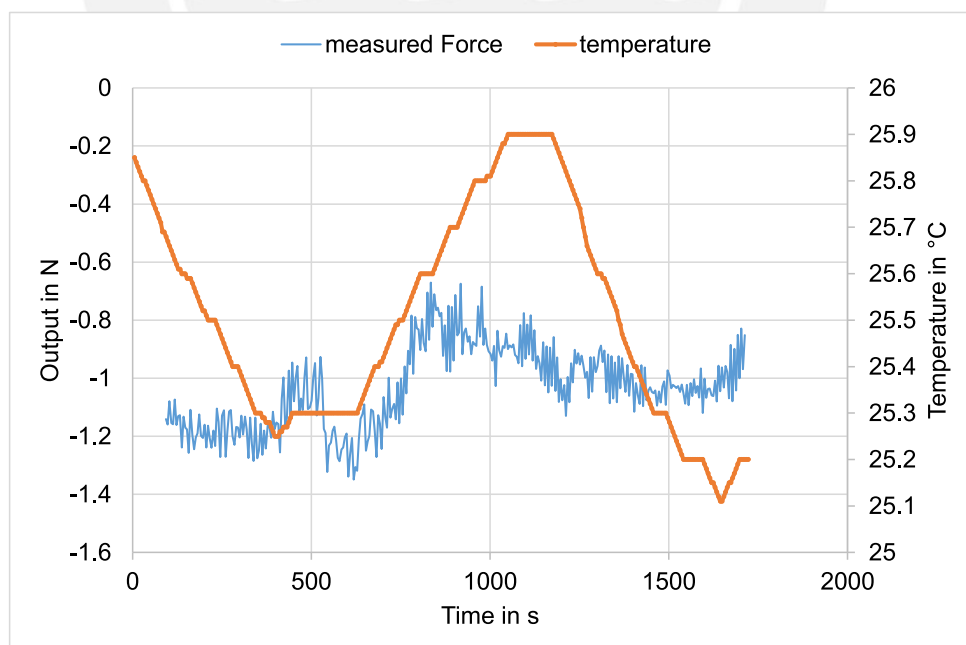


Figure 12.17: Drift of the shear force measurement near the zero point

## 12.3 Characteristics of the resistive sensor

The following tests were conducted to evaluate the second measurement option of using resistive sensors instead of the capacitive ones. The sensors to be used to measure the four reaction forces on the bottom of the transducer are to be placed in the same positions as the capacitive areas are. The goal is to show the basic properties of the Flexiforce A101 sensor in order to lay the foundation of a decision which way of measuring is more promising for future versions. To simplify the procedure the measurement is done with only one element and a force acting in z direction. Again the test stand was used. The sensor was fixed on the adapter plate as shown in figure 12.18. The force was induced by a screw. Its head was filled with hot glue to make a soft and plate surface. For the measurement of the basic behavior tests a precision amplifier was used. The sensor was connected in four wire connection to minimize errors during the measurement.

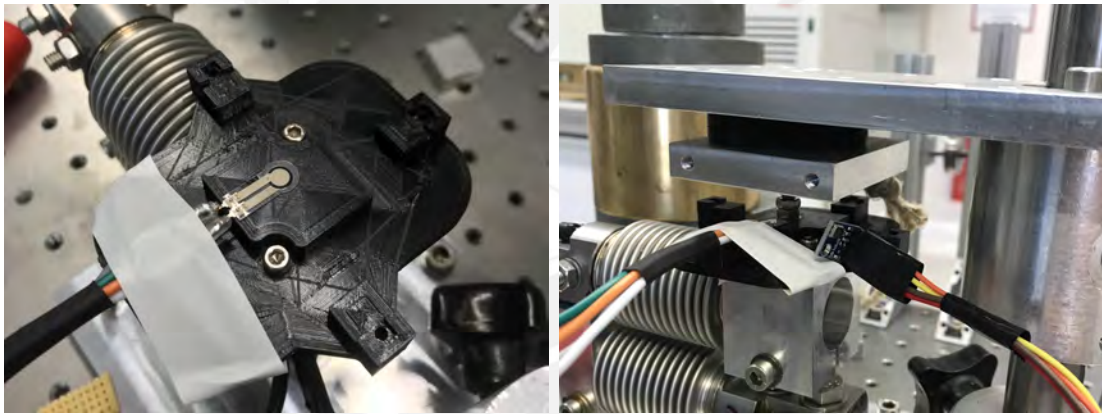


Figure 12.18: The Flexiforce A101 sensor mounted on the test stand

At first the output curve was determined. As previously described different loads were applied and the measured resistance was compared to the force measured by the reference. If the conductivity  $G = 1/R$  is compared to the force, the sensor shows a good linearity (compare to [Data sheet FlexiForce Standard Model A101 2019]).

The output can be mapped to the force using the following linear equation:

$$F_c = 265.464 \frac{\text{N}}{\text{mS}} \cdot G - 2.90 \text{ N} \quad (12.8)$$

To test if there was a hysteresis the force  $F_z$  was increased and reduced again step wise like previously explained. The resulting graph shows that the hysteresis is very small. It can not really be seen because the deviation of the measurement is bigger so the curves merge (see figure 12.20).

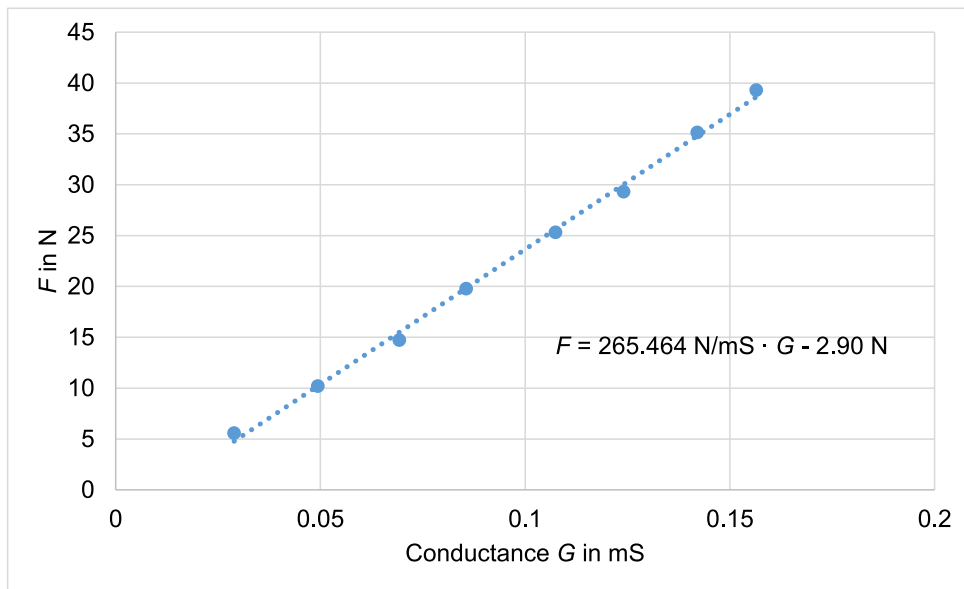


Figure 12.19: Output force relation of the Flexiforce A101

The repeatability for the force measurement with the sensor was tested using the designed circuit to use with the Arduino as described in chapter 8.5. The test was done as explained before by putting and removing the same weight several times and measuring the output. The observation here again was that there is a drifting after the load has risen.

Table 12.4: Repeatability measurement

$G$ in mS	$F_z$ in N	$F_c$ in N	$\Delta F$ in N
0.0890	30.2	20.7	-9.4
0.0876	29.9	20.4	-9.5
0.0875	30.2	20.3	-9.8
0.0831	29.9	19.2	-10.7
0.0911	30.1	21.3	-8.8
0.0872	29.7	20.2	-9.4
0.0801	28.7	18.4	-10.3
0.0864	29.6	20.0	-9.5
0.0785	29.8	17.9	-11.9
0.0803	30.3	18.4	-11.9

The resulting deviation and uncertainty are displayed in table 12.5.

It is interesting to mention that the resistance with low forces varied greatly from one test to another. As seen in table 12.5 the uncertainty does not get better for lower forces as it was the case with the capacitive measurement. Also interesting to see is that there is also an offset of the measured force. This can not be explained at the moment but most likely it is caused by a varying contact between the bolt and the sensor. If that is true this offset



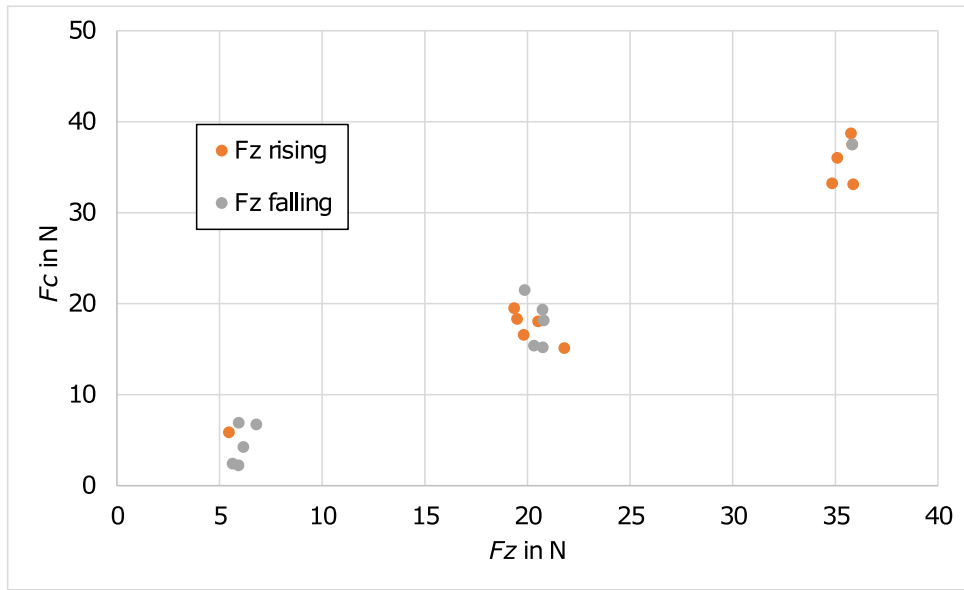


Figure 12.20: Hysteresis test of the flexiforce sensor; A clear hysteresis effect is not visible

Table 12.5: Resulting uncertainties

	$Fz = 30 \text{ N}$	$Fz = 6 \text{ N}$
Mean	-10.14 N	-5.59 N
$S$	1.05 N	1.13 N
$CI_{95\%}$	2.35 N	2.51 N

between measurements will not be seen in the final construction because there the sensors will be glued to the transducer. The contact between them will then not change anymore due to relative movement between the components. The three axis sensor will use four of the Flexiforce A101 sensors analog to the capacitive design. The expected uncertainty can be calculated using the Gaussian uncertainty relation. For a function  $f(x_1 \dots x_n)$  the total deviation can be calculated using the following equation.

$$S_{total}(f) = \text{sqr}t \sum_{i=1}^n \left( \Delta x_i \frac{\delta f}{\delta x_i} \right)^2 \quad (12.9)$$

The calculation of the normal force will be done using the sum of the four sensors.

$$F = F_1 + F_2 + F_3 + F_4 \quad (12.10)$$

For the estimation we assume that all the sensors have a similar behavior and deviation. Only one sensor was tested so the estimated deviation for the sensors will be the same. This way the confidence interval for the combined measurement of all four sensors can be

calculated knowing that  $\frac{\delta F}{\delta F_i} = 1$ .

$$S_{total}(F) = \sqrt{\sum_{i=1}^4 \Delta F_i} = \sqrt{4 \cdot S_{sensor}} = 2S_{sensor} \quad (12.11)$$

The shear force measurement is done using each time the difference of two sensors for each direction. The factor  $a$  represents the ration between height  $h$  and the distance of the sensors from the center  $d$ .

$$F_x = a \cdot (F_2 - F_1) \quad (12.12)$$

Differentiation of the force expression gives:

$$\frac{\delta F_x}{\delta F_i} = \begin{cases} \text{for } i = \{1, 2\} : a \\ \text{for } i = \{3, 4\} : 0 \end{cases} \quad (12.13)$$

The combined uncertainty for both sensors calculating the shear force component is.

$$S_{total}(F) = \sqrt{\sum_{i=1}^s a \Delta F_i} = \sqrt{2a \cdot S_{sensor}} = \sqrt{2a} \cdot S_{sensor} \quad (12.14)$$

The expected uncertainties for the complete sensor using the Flexiforce A101 sensors to measure the single reaction forces are then.

Table 12.6: Expected combined uncertainty for the complete sensor

	$F_z$	$F_x$
$S$	$\approx 2.5 \text{ N}$	$\approx 1.7 \text{ N}$
$CI_{95\%}$	$\approx 5.0 \text{ N}$	$\approx 3.5 \text{ N}$

The calculated values are of course only estimations but they can give an expression of the accuracy to expect. The real values can differ because for the calculation it was supposed that all effects causing the deviation measured for the single sensors are normally distributed and randomly. But one can see that the measurement uncertainty of the resistive design will most likely be similar to the capacitive one.

The drift behavior is shown in figure 12.21. It is clear to see that the sensor has a similar behavior than the capacitive prototype. The values on the maximum load drift for about three newton during around ten minutes. The complete design with four sensors equipped would shown than a drift for about 12 N which is comparable to the behavior of the capacitive design.

During the tests one sensor was damaged. It is not clear why this happened but it is supposed that this happened due to overload. It seems likely that the surfaces between the

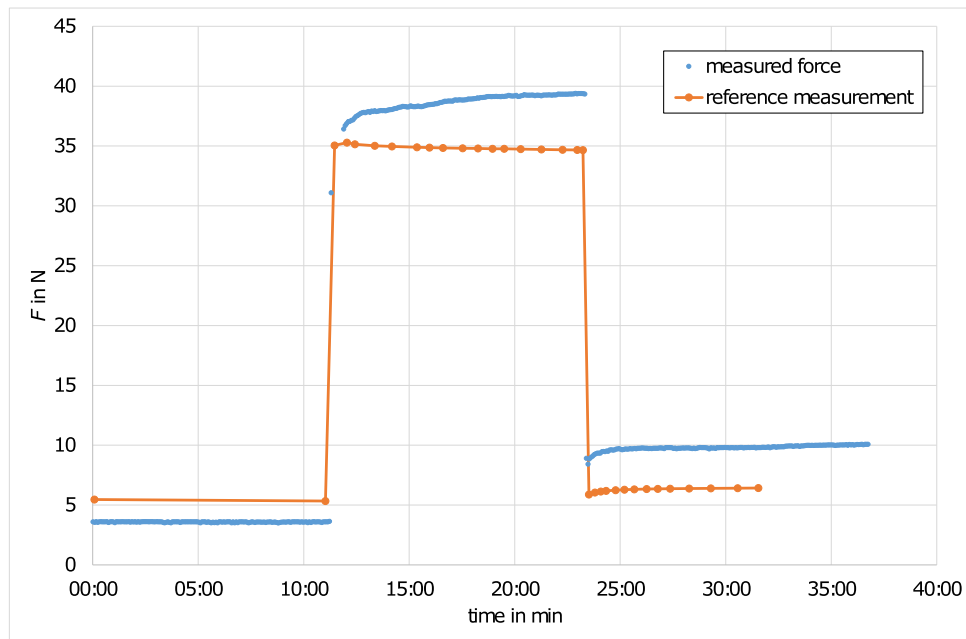


Figure 12.21: Drift test of the Flexiforce A101

conductive layers are very sensible to overload. Once they are damaged the characteristics of the sensor change so that a measurement is not possible anymore. The curve of the damaged sensor was different from before and its repeatability was a lot worse. The capacitive version was better regarding robustness. To achieve a robuster design another sensor would have to be chosen for example the Flexiforce A201 with a way higher force range. This on the other hand would increase the sensor size a lot.

# 13 Sensor array design

Next step in the development will be the design of a sensor array to be placed on the prosthesis. During the creation of this work the design of the prosthesis was not finished yet. Therefore the geometrical requirements for fitting the array to the prosthesis can not be clarified. Thus the following chapter will show the basic ideas of the construction. Most likely the design will change later in order to fit the prosthesis.

## 13.1 Mechanical design

The single sensors need to be integrated onto the foot sole. The easiest way to achieve this is to integrate the sensors into a shoe sole like it is shown for example in [Jacobs and Ferris 2015]. This idea does not match exactly the needs of this work since it will be equipped to a prosthesis but the idea nevertheless could be used. The future sensors can be designed using two separate boards, one to build up the sensor itself containing just the sensing areas and connection pins. The other board contains the electronics. Since the sensor board is double layered the shielding effect is not lost but the electronics do not have to be next to the sensor but can be beneath it on the extra board. The boards are fixed on the up- and on the downside of an elastic rubber layer. The boards are connected through holes (see figure 13.1) with thin flexible connection pins soldered to both boards. The rubber layer permits flexing of the sensor array.

This way the array can adapt to the bending of the prosthesis. The rubber layer also protects the cables and connectors which are on the side of the electronics board between the prosthesis and the rubber layer. Due to the damping properties of the rubber layer the shock of a sudden impact on the sensor can be reduced. In comparison to a stiff base this protects the sensor way better. The connection pins between the boards need to have a S-shape to give them the freedom to bend and to extend to follow the deformation of the rubber layer. The size of the sensor could be reduced by thinning out the gap between the triangular electrodes. This way the sensing areas stay the same while the whole sensor becomes smaller. But the decrease in size should be only a few millimeters because a reduced transducer size leads to higher tension in the dielectric material thus

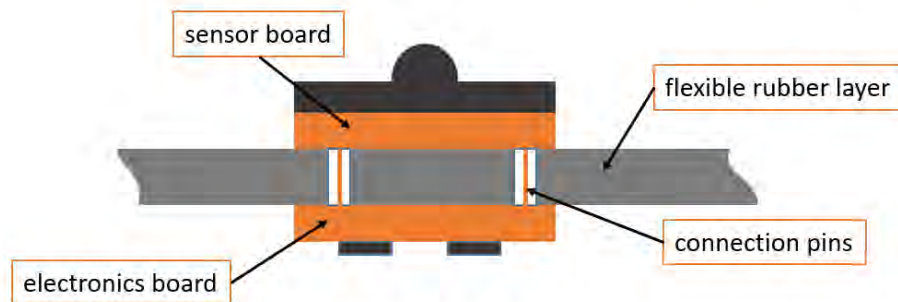


Figure 13.1: The sensor solution with two boards fixed on a rubber layer

producing a narrower output curve and a worse resolution. The rubber equipped with the sensors can then be fixed to the prosthesis. Figure 13.2 shows the suggested distribution of the sensors on the foot sole. The interesting parts are the anterior and posterior region. In the anterior part, there are more sensors because during the stance phase the highest pressures are expected in this region.

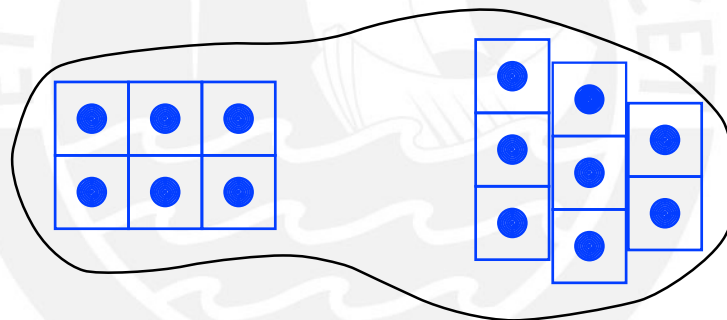


Figure 13.2: Positioning of the sensors on the foot sole

## 13.2 Electrical design

When using more than one sensor the connection of them has to be redesigned because most of the common micro controllers can not handle that much signals at the same time on there inputs. There are basically two options to do the connection schematic. The single sensors can be connected to a grid of connection. The selection of the active sensor happens via multiplexers in this case. In case of resistive sensors this can be easily done by connecting only one sensor each time to the measurement current [see Danilovic 2013]. The capacitive version uses amplifiers to drive the output. In order to use the multiplexing scheme the schematic has to be modified. By changing the connection pins on the input

of the amplifier the voltage levels can be changed. The normal level is than high and when the reference voltage is reached the signal turns to low. By inserting a pull up resistance into the voltage supply of the amplifiers there outputs can be connected to the same line. When one amplifiers turns to low level it tears down the whole line voltage to low level. The multiplexers than only connect the chosen sensor to the excitation signal. The other sensors without an excitation stay in high level output. So the signal on the line is definitively from the active sensor. Using this procedure the number of sensors can easily augmented up to 64 complete sensors with four capacitive sensing elements each by using two 16 channel multiplexers. On the contrary this method only allows to read one element at a time. Making the readout slower the more sensors are involved.

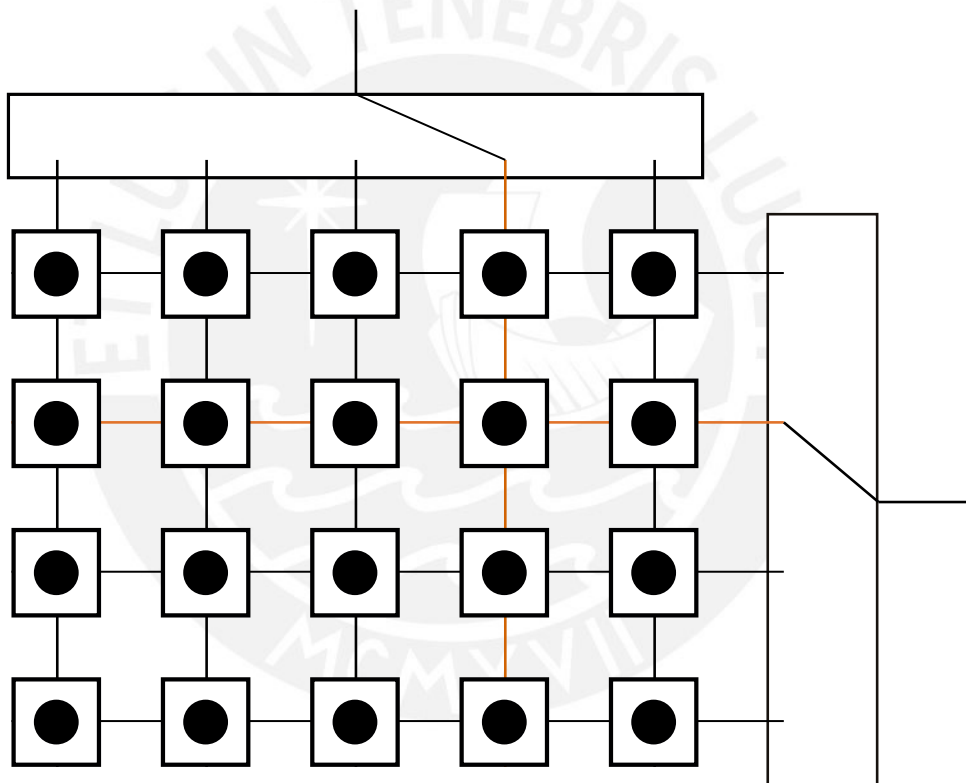


Figure 13.3: Choosing the sensor using multiplexers

Another option would be to integrate a small micro controller on every sensor to do the measurement on board. A common signal line with a clocked signal would give the measurement order causing each chip to start the measurement of its four corresponding capacities at the same time. The results are stored and can than be read out by a central processing unit that could be an Arduino via bus system (I2C for example) addressing each sensor one by one. This method has the advantage that the measurement is done simultaneously on all the sensors. Also it is the better options when the number of

sensors used becomes big because the number of connections does not rise with the rising number of sensors as it does with the multiplexer version. But on the other hand it makes the sensor more expensive because on every board there has to be an additional micro controller. For the presented design the multiplexer version is more favorable because the number of sensors is relatively low. The multiplexers can be placed together with the voltage divider for the reference voltage, the capacitors to filter noise and the micro controller to process the data on an extra board. This way there are only few components on the electronics boards of the single sensors making a very small design possible.



## 14 Conclusion and outlook

During the work a robust and inexpensive force sensor that is capable of measuring normal as well as lateral acting forces in a range up to more than 100 N in normal and 40 N in lateral direction was built up. The designed test stand to produce the forces and conduct the reference measurement was built up and classified. It can measure the acting forces very precisely with a repeatability which is good enough to make solid estimations of the tested sensor prototype. The first prototype already shows a repeatability error of only a few percent although only common materials and low cost electronics were used. There were two options of measurement shown. The capacitive variant was used in the prototype. The resistive measurement alternative was tested using a small Flexiforce A101 force sensor to predict the outcome if the prototype was built up using these elements instead of a capacitive measurement. From the results one can see that both versions are similar in their accuracy. The resistive version would be better regarding the hysteresis which was really low during the tests. And external electrical fields would have a lower impact on this measurement technique. The capacitive measurement on the other hand was more robust and can be adjusted freely to the requirements of the design because the measuring elements are not bought but self-made. The preferred version depends a lot on the requirements which can not be foreseen completely at the moment. The decision which version to prefer should be made in a later state of the total prosthesis project based on the results from this work when there are more specific requirements. After the work presented previously there are still a lot of interesting and useful things to implement in the future. First of all the prototype has to be advanced further according to the details mentioned in chapter 10.2. To verify the changes really brought an improvement parts of the testing have to be repeated. With the built up second version of the sensor a real three axis measurement will be finally possible. The actual prototype was, due to some complications with the electrics, only able to measure the normal load and one shear force component. Anyway it was possible to make assumptions on the behavior of the sensor. Because of its symmetric design the second shear force component is measured the same way. To verify the proper function the sensor could be tested with a force attack angle of  $45^\circ$  which causes the shear force to be measured as the sum of two equal



lateral force components on the measuring axis of the sensor. There are already holes prepared on the adapter of the test stand to mount the sensor with an  $45^\circ$  angle. The transducer itself could be made of an epoxy resin in future versions. A 3D-printed mold could be used to shape it. This would make the transducer stiffer and would therefore help to reduce the influence of the transducer deformation. Also using a casting procedure to produce the transducer would definitively be more practically when multiple sensors have to be produced to build up an array. The future sensor will most likely be made of two boards as mentioned in chapter 13 and equipped with SMD parts. This means the board layout has to be renewed completely. After the new prototype is assembled the output curve needs to be estimated anew. The regression functions will be the same but the factors could have changed. The shear force curve has to be measured various times to get the influence of a varying normal load on the curve exactly. To improve the accuracy for further designs it, should be considered using another micro controller. Using a controller with a higher clock frequency would help increase the sensing rate and the time resolution of the capacitive measurement. Also the used electrical components have to be investigated further on their influence on the measurement. Using highly time stable resistors to charge the capacitors could reduce the influence of temperature for example. The calculation of the PWM parameters described in chapter 9.2 should be repeated with the won knowledge. Most likely the time resolution can be reduced without a big loss in accuracy. Optimizing the timing and maybe reducing the serial resistor on the capacitive sensing areas would enable a higher PWM frequency and therefore a higher measurement rate, too. Another already mentioned point is a shield for electric fields when capacitive sensing is chosen as a concept. If the resistive measurement is chosen one could investigate if a better ADC will improve the measurement. Most likely the performance can be improved by this measures. But due to the nature of polymers which are used as dielectric layer some effects like the hysteresis will never be eliminated completely. To cope with the creeping of the sensor output a software compensation would be very useful [see Phan 2008]. Further investigation could also test a broader range of materials. Using non conductive crystalline materials like silicon could also reduce the hysteresis. But most likely other problems would appear so there would have to be done a lot of basic research. Also the accuracy will not be better than a few percent anyway. The next logical step in the development, after the single sensor design is advanced to a convincing level, will be to build up a complete array prototype with multiple sensors. The sensors have to be integrated on a rubber layer as shown in section 13.1. The shape of the rubber has to be adapted to the needs of the prosthesis. Maybe some extra parts have to be constructed to safely join prosthesis and sensor array. The performance of the built up array has to

be proven. Depending on the task it might be useful to invest some time and effort in a sophisticated programming. Using modern techniques like artificial neural networks stable and surprisingly good results can be achieved [see Jacobs and Ferris 2015]. The tested capacitive sensor showed very good repeatability results for low acting forces. Therefore, it could be interesting also for other fields of application besides the prosthesis project. In areas of lower forces, for example gripping tasks, the sensor could expand its full potential reaching errors below one percent. The design is easy to build and can be adapted to different needs. The sensor is a good choice for low cost prototyping projects specially for tasks where the exact value is not of mayor importance but a qualitative estimation of the acting forces is required with low effort. Further developments implementing the mentioned improvements will reveal the full potential of the sensor.



# 15 Bibliography

## Literature

- Barnett, C.H. (Oct. 1956). “The phases of human gait”. In: *Lancet* 271, pp. 617–21. DOI: 10.1016/S0140-6736(56)92309-1.
- Chuah, M. Y. and S. Kim (May 2014). “Enabling Force Sensing During Ground Locomotion: A Bio-Inspired, Multi-Axis, Composite Force Sensor Using Discrete Pressure Mapping”. In: *IEEE Sensors Journal* 14.5, pp. 1693–1703. DOI: 10.1109/JSEN.2014.2299805.
- Chuah, Meng (Mar. 2013). “Composite force sensing foot utilizing volumetric displacement of a hyperelastic polymer”. In:
- Dahiya, Ravinder S. and Maurizio Valle (2013). *Robotic Tactile Sensing*. Dordrecht: Springer.
- Danilovic, Andrew (2013). “SmartCast Novel Textile Sensors for Embedded Pressure Sensing of Orthopedic Casts”. MA thesis. University of California.
- Data sheet BMP180 Digital pressure sensor* (Apr. 2013). BST-BMP180-DS000-09. Rev. 2.5. Bosch.
- Data sheet BMP280 Digital pressure sensor* (Jan. 2018). BST-BMP280-DS001-19. Rev. 1.19. Bosch.
- Data sheet FlexiForce Standard Model A101* (2019). DS Rev G 062519. Tekscan Inc.
- FSR 400 Series Data Sheet* (2019). PDS-10004-C. Interlink Electronics Inc.
- Guggenheim, Jacob W. et al. (2016). “Robust and Inexpensive 6-Axis Force-Torque Sensors using MEMS Barometers”. In: *IEEE TRANSACTIONS ON MECHATRONICS*.
- Ishido, H. et al. (Feb. 2015). “6-Axis force/torque sensor for spike pins of sports shoes”. In: *Proceedings of the IEEE International Conference on Micro Electro Mechanical Systems (MEMS) 2015*, pp. 257–260. DOI: 10.1109/MEMSYS.2015.7050937.
- Jacobs, Daniel and Daniel Ferris (Dec. 2015). “Estimation of ground reaction forces and ankle moment with multiple, low-cost sensors”. In: *Journal of NeuroEngineering and Rehabilitation* 12. DOI: 10.1186/s12984-015-0081-x.

- Kim, Uikyum et al. (Oct. 2015). “Force Sensor Integrated Surgical Forceps for Minimally Invasive Robotic Surgery”. In: *Robotics, IEEE Transactions on* 31, pp. 1214–1224. DOI: 10.1109/TR0.2015.2473515.
- Leong, Joanne et al. (Oct. 2016). “proCover: Sensory Augmentation of Prosthetic Limbs Using Smart Textile Covers”. In: pp. 335–346. DOI: 10.1145/2984511.2984572.
- Mancillas, Francisco Javier (Oct. 2018). “Analysis of a Micro-scale, Tri-axial, Capacitive-based, Differential Force Sensor for Haptic Feedback System in Robotic Surgery”. MA thesis. University of California.
- Nigg, Benno M., Brian R. Macintosh and Joachim Mester (Jan. 2000). *Biomechanics and biology of movement*. Champaign, United States: Human Kinetics Publishers, p. 488. ISBN: 978-0736003315.
- Perry, Jacquelin and Judith Burnfield (Feb. 2010). *Gait Analysis: Normal and Pathological Function*. ISBN: 978-1556427664.
- Phan, K. L. (Oct. 2008). “Methods to correct for creep in elastomer-based sensors”. In: pp. 1119–1122. ISSN: 1930-0395. DOI: 10.1109/ICSENS.2008.4716637.
- Polster, Tobias and Martin Hoffmann (2009). “Aluminum nitride based 3D, piezoelectric, tactile sensor”. In: *Procedia Chemistry* 1.1. Proceedings of the Eurosensors XXIII conference, pp. 144–147. ISSN: 1876-6196. DOI: <https://doi.org/10.1016/j.proche.2009.07.036>. URL: <http://www.sciencedirect.com/science/article/pii/S1876619609000370>.
- Reeks, Christian et al. (May 2016). “Angled sensor configuration capable of measuring tri-axial forces for pHRI”. In: pp. 3089–3094. DOI: 10.1109/ICRA.2016.7487475.
- Takahashi, Hidetoshi et al. (Sept. 2013). “A triaxial tactile sensor without crosstalk using pairs of piezoresistive beams with sidewall doping”. In: *Sensors and Actuators A: Physical* 199, pp. 43–48. DOI: 10.1016/j.sna.2013.05.002.
- Technical data sheet TPU95A* (May 2017). 3.010. Ultimaker.
- Tenzer, Y., L. P. Jentoft and R. D. Howe (Sept. 2014). “The Feel of MEMS Barometers: Inexpensive and Easily Customized Tactile Array Sensors”. In: *IEEE Robotics Automation Magazine* 21.3, pp. 89–95. DOI: 10.1109/MRA.2014.2310152.
- Tenzer, Yaroslav, Leif P. Jentoft and Robert D. Howe (2012). “Inexpensive and Easily Customized Tactile Array Sensors using MEMS Barometers Chips”. In: *IEEE*.
- Ting, Zhang et al. (Feb. 2013). “Development of a Flexible 3-D Tactile Sensor System for Anthropomorphic Artificial Hand”. In: *Sensors Journal, IEEE* 13, pp. 510–518. DOI: 10.1109/JSEN.2012.2220345.
- Tiwana, MI et al. (Feb. 2011). “Characterization of a capacitive tactile shear sensor for application in robotic and upper limb prostheses”. In: *Sensors and Actuators A-physical*

- *SENSOR ACTUATOR A-PHYS* 165, pp. 164–172. DOI: 10.1016/j.sna.2010.09.012.

VDI2222:1997-06:1997-06. *Methodisches Entwickeln von Lösungsprinzipien*. Verein Deutscher Ingenieure (VDI). Berlin: Beuth Verlag. Konstruktionsmethodik. valid.

VDI2223:2004-01:2004-01. *Systematic embodiment design of technical products*. Verein Deutscher Ingenieure (VDI). Berlin: Beuth Verlag. Konstruktionsmethodik. valid.

## Online

Arduino AG (2019). *Arduino Uno Rev. 3 product page*. URL: <https://store.arduino.cc/arduino-uno-rev3> (visited on 26/10/2019).

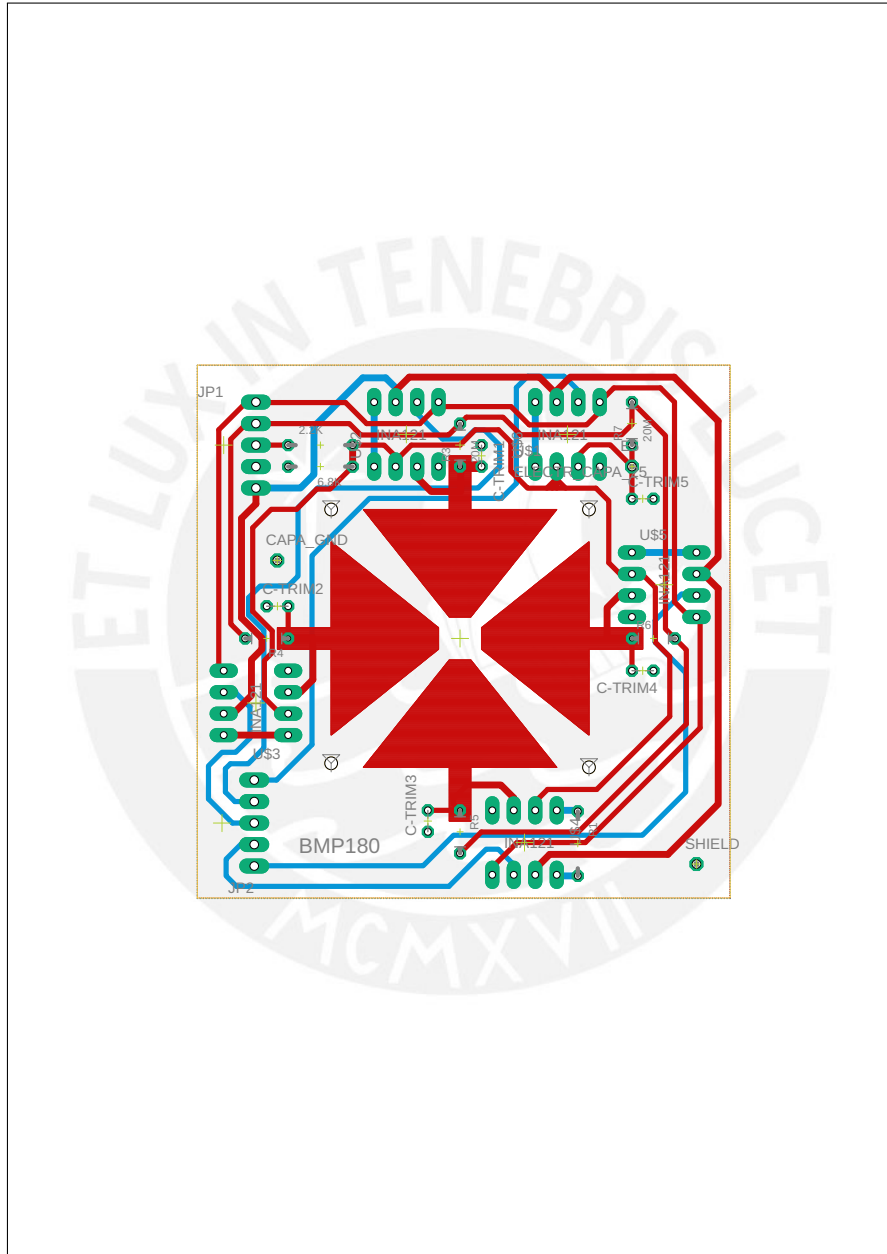
jon (2014). *Capacitance measurement with the Arduino Uno*. URL: <http://wordpress.codewrite.co.uk/pic/2014/01/21/cap-meter-with-arduino-uno/> (visited on 20/07/2019).

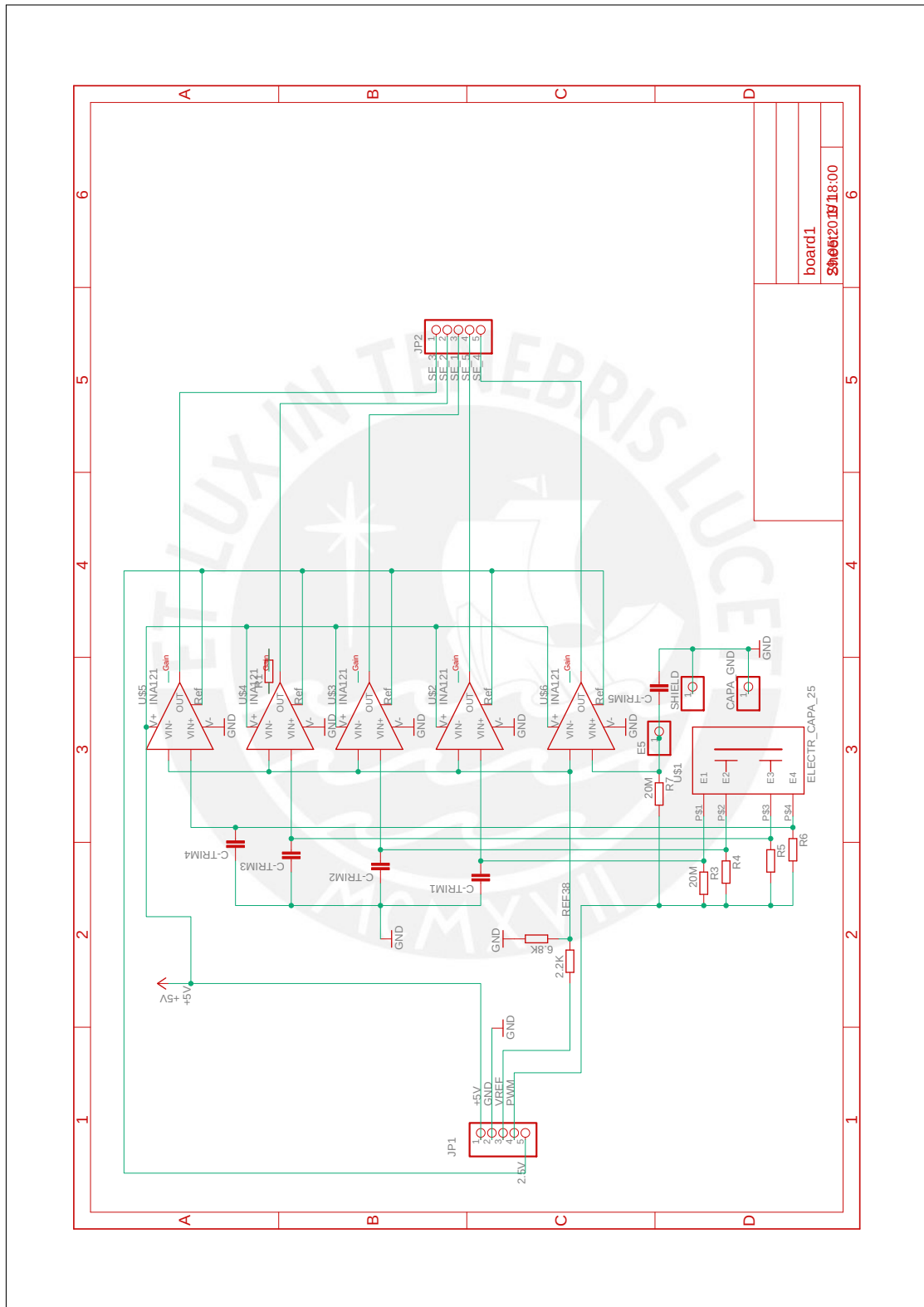
ME-Messsysteme GMBH (2019). *Online Shop ME-Systeme*. URL: <https://www.me-systeme.de/shop/en/sensors/force-sensors/k6d/k6d1752> (visited on 20/10/2019).

plastic-electronic (2019). *Loadskin sensor array*. URL: <https://plastic-electronic.com/de/loadskin-drucksensormatten/> (visited on 30/10/2019).

XSensor Technology Corporation (2019). *Sensor overview*. URL: <https://xsensor.com/sensors/> (visited on 30/07/2019).

# Appendix





## LT-Spice simulation of resistive measurement

